

CLASS VI PERMIT APPLICATION NARRATIVE 40 CFR 146.82(a)

CLEAN ENERGY SYSTEMS MENDOTA



These documents were prepared by Schlumberger Technology Corporation and delivered to
Clean Energy Systems

Schlumberger

January 31, 2020

Contents

1. Project Background and Contact Information	9
1.1. Preconstruction Application Intention	9
1.2. Project Background	11
1.3. Acronyms and Abbreviations	13
2. Site Characterization	15
2.1. Regional Geology, Hydrogeology, and Local Structural Geology [40 CFR 146.82(a)(3)(vi)]	15
2.2. Maps and Cross Sections of the Area of Review (AoR) [40 CFR 146.82(a)(2), 146.82(a)(3)(i)]	18
2.3. Faults and Fractures [40 CFR 146.82(a)(3)(ii)]	25
2.3.1. Geophysical Workflow	25
2.3.2. Fault Seal Analysis	26
2.3.3. Uncertainty	27
2.4. Injection and Confining Zone Details [40 CFR 146.82(a)(3)(iii)]	33
2.4.1. Structural Mapping	33
2.4.2. Petrophysics	34
2.4.3. Geocellular Modeling and Volumetrics	39
2.4.4. Pre-Operational Testing Requirements	50
2.5. Geomechanical and Petrophysical Information [40 CFR 146.82(a)(3)(iv)]	51
2.6. Seismic History [40 CFR 146.82(a)(3)(v)]	53
2.7. Hydrologic and Hydrogeologic Information [40 CFR 146.82(a)(3)(vi), 146.82(a)(5)]	57
2.7.1. Depth to the Deepest USDWs – 40 CFR 146.93(c)(1)(x)	57
2.7.2. Local Near Surface Groundwater	59
2.8. Geochemistry [40 CFR 146.82(a)(6)]	63
2.8.1. Characteristics of Injection Zone Formation Water	63
2.8.2. Mineral Composition of The Injection Zone	64
2.8.3. Composition of the Injectate	64
2.8.4. Geochemical Modeling Setup	65
2.8.5. Simulated Reaction Pathways	66
2.9. Other Information (Including Surface Air and/or Soil Gas Data, if Applicable)	71
2.10. Site Suitability [40 CFR 146.83]	71
3. AoR and Corrective Action	72
4. Financial Responsibility	72
5. Injection Well Construction	73

5.1. Proposed Stimulation Program [40 CFR 146.82(a)(9)]	76
5.2. Construction Procedures [40 CFR 146.82(a)(12)]	76
5.2.1. Surface Well Head Configuration.....	76
5.2.2. Casing	78
5.2.1. Discussion on Well Construction.....	81
5.2.2. Tubing and Packer	82
5.2.3. Cement	83
6. Pre-Operational Logging and Testing.....	85
7. Well Operation.....	85
7.1. Operational Procedures [40 CFR 146.82(a)(10)].....	86
7.2. Proposed Carbon Dioxide Stream [40 CFR 146.82(a)(7)(iii) and (iv)]	87
8. Testing and Monitoring.....	89
9. Injection Well Plugging	89
10. Post-Injection Site Care (PISC) and Site Closure.....	89
11. Emergency and Remedial Response.....	90
12. Injection Depth Waiver and Aquifer Exemption Expansion	90
13. Other Information	90
14. Approval	91
15. References.....	93

List of Figures

Figure 1: The Phases of a Class VI project (EPA, 2018).....	10
Figure 2:Mendota site location and nearby wells (USGS, 2019) (IHS, 2019) (USGS, 2005)	12
Figure 3: San Joaquin basin depositional model showing submarine fan Panoche formations (Starkey sands) (Scheirer, 2003).....	16
Figure 4: Generalized SW-NE cross section showing Blewett and Lathrop (Panoche) sand injection targets (Scheirer, 2003).....	16
Figure 5: Mendota Stratigraphic column with porosity log (left Section Petrophysics 2.4.2)	17
Figure 6: Subsurface geology and legacy wells surrounding the Mendota site NE cross section.	19
Figure 7: Subsurface geology and legacy wells surrounding the Mendota site SE cross section.	20
Figure 8: 10 wells used in petrophysical analysis and well correlation.....	21
Figure 9: N-S Cross section described in Figure 8, which shows 5 out of 10 petrophysical wells used in analysis of injection and confining rock properties. The Mendota_INJ_1 is located between B. B Company 1 and Sterling-Coleman 1 wells, Tracks left to right include: volume clay (VCL), MD, Zone Log, Facies calculated from volume clay (VCL) and zone color fill between wells.	22
Figure 10: W-E Cross section described in Figure 8. Tracks left to right include: VCL, MD, Zone Log, Facies calculated from volume clay (VCL) and zone color fill between wells.	23
Figure 11: W-E 2 Cross-section described in Figure 8. Tracks left to right include: VCL, MD, Zone Log, Facies calculated from volume clay (VCL) and zone color fill between wells.	23
Figure 12: Formation surface maps	24
Figure 13: Formations isochore maps.....	25
Figure 14: CONFIDENTIAL BUSINESS INFORMATION: 2D Seismic line map, shot points and area wells showing the 3 and 5-mile radii from Mendota Plant Site. This image displays (SEI, 2019) data and it is marked as Confidential Business Information.	28
Figure 15: CONFIDENTIAL BUSINESS INFORMATION: Seismic Well Tie: Line W-SJ-202 and SALLABERRY / 1-6 (4019215350000). This image displays (SEI, 2019) data and it is marked as Confidential Business Information.	29
Figure 16: CONFIDENTIAL BUSINESS INFORMATION: W-SJ-202 2D seismic line (depth) with interpreted horizons and faults. This image displays (SEI, 2019) data and it is marked as Confidential Business Information.	30
Figure 17: CONFIDENTIAL BUSINESS INFORMATION: W-SJ-209 2D seismic line (depth) with interpreted horizons and faults. This image displays (SEI, 2019) data and it is marked as Confidential Business Information.	30
Figure 18: CONFIDENTIAL BUSINESS INFORMATION: W-SJ-013W 2D seismic line (in depth) with interpreted horizons and faults. This image displays (SEI, 2019) data and it is marked as Confidential Business Information.	31
Figure 19: CONFIDENTIAL BUSINESS INFORMATION: 3D View (facing SE) of interpreted faults on the 2D seismic lines and Basement surface. Dotted lines are projected faults (color coded by horizon) or projected fault plane. A legacy Gill Ranch field structure map is inserted at the Second Panoche. This image displays (SEI, 2019) data and it is marked as Confidential Business Information.	31
Figure 20: CONFIDENTIAL BUSINESS INFORMATION: 3D perspective of the depth integrated geophysical model. This image displays (SEI, 2019) data and it is marked as Confidential Business Information.	32

Figure 21: Illustration describing different fault displacement scenarios at Mendota_INJ_1 regarding Fault 13.....	33
Figure 22: Fault 13 terminates within the Moreno Shale. Mendote_INJ_1 wellbore which targets the Second Panoche injection sand is shown in green with MD annotated in white text. Fault 13 is colored by Fault Clay Prediction content based on the SGR algorithm, the results of which indicate the Moreno Shale smearing along the fault.....	33
Figure 23: N-S Cross Section showing Petrophysical analysis results and wells nearest to Mendota_INJ_1. The tracks show left to right PIGE (Effective Porosity) KINT (Permeability), MD, Zone log, Sand and Shale Lithologies as calculated from VCL, and Net Lithology values for Sand and Shale per zone.....	36
Figure 24: W-E Cross Section showing Petrophysical analysis results with same tracks as Figure 23.....	37
Figure 25: W-E 2 Cross section showing Petrophysical analysis results with same tracks as Figure 23.	37
Figure 26: Net Thickness maps of Moreno Shale and First and Second Panoche Sands calculated based on VCL greater than or less than 30%, white diamond denotes Mendota_INJ_1.....	38
Figure 27: Porosity histograms of well logs, upscaled cells and model cells.....	41
Figure 28: Modeled average porosity maps for each formation	42
Figure 29: Permeability histograms of well logs, upscaled cells and model cells.....	43
Figure 30: Porosity permeability cross plot of upscaled cells and model cells (left) and upscaled cells colored by formation	44
Figure 31: Modeled permeability thickness (KH) maps for each formation.....	45
Figure 32: CONFIDENTIAL BUSINESS INFORMATION: Injection well cross-section traverse map, N-S an E-W. This image displays (SEI, 2019) data and it is marked as Confidential Business Information.	46
Figure 33: CONFIDENTIAL BUSINESS INFORMATION: 3D Perspective of N-S and E-W porosity cross-sections at Mendota_INJ_1. This image displays (SEI, 2019) data and it is marked as Confidential Business Information.	47
Figure 34: Effective Porosity Model Cross-section (N-S).....	47
Figure 35: Volume clay model cross-section (N-S)	48
Figure 36: Permeability model cross-section (N-S).....	48
Figure 37: Effective porosity model cross-section (E-W)	49
Figure 38: Volume Shale Model Cross-section (E-W).....	49
Figure 39: Permeability Model Cross-section (E-W)	50
Figure 40: Density, acoustic, and elastic properties in Moreno Shale.....	52
Figure 41: Relative earthquake risk (left) and earthquake map from the CEMA GIS unit (Right). The red star is the location of the Mendota site. (CEMA, 2010).....	54
Figure 42: Regional faulting from the Department of Conservation (left) (USGS, U.S. Quarternary Faults, 2019) and Regional USGS Earthquake History (right) - quakes with magnitudes greater than 2.5 since 1900. (USGS, Earthquake Hazards Program, 2019).....	55
Figure 43: Historical earthquakes near AoR greater than 2.5 since 1900.	56
Figure 44: Wells used to calculate the depth to the deepest USDW	58
Figure 45: CONFIDENTIAL BUSINESS INFORMATION: USDW estimated using resistivity measured in wells near the Mendota site. This image displays (IHS, 2019) data and it is marked as Confidential Business Information.	59
Figure 46: Water well and surface water	61

Figure 47: Potentiometric map of the approximate shallowest groundwater surface.....	62
Figure 48: Changes of the amount of the minerals from the addition of CO ₂ and O ₂ in geochemical modeling	67
Figure 49: Aqueous composition after the addition of CO ₂ and O ₂ in geochemical modeling	68
Figure 50: Mineral volume and mass after the addition of CO ₂ and O ₂ in the geochemical modeling	70
Figure 51: Mendota_INJ_1 well construction diagram	74
Figure 52: Pore and fracture gradients used for well construction	75
Figure 53: Temperature gradient used for well construction.....	75
Figure 54: Surface well head configuration.....	77

List of Tables

Table 1: Well Control Points for Structural model of injection and confining formations.	34
Table 2: Wells used to characterize petrophysical properties within the AoR	35
Table 3: Average porosity and permeability of injection and confining zones - average porosity and permeability of injection and confining zones	39
Table 4: Mineralogy summary from core XRD – NAPA AVE A 1	39
Table 5: Historical earthquakes near AoR greater than 2.5 since 1900.	56
Table 6: Salinity of the formation waters from the oil and gas fields near the proposed Mendota site (California Department of Conservation, 1998).	63
Table 7: Estimated mineral composition (wt. %) for the Panoche Formation used in geochemical modeling	64
Table 8: Composition of the injectate (Mass Fractions)	65
Table 9: Chemical composition of the initial solution for geochemical modeling	66
Table 10: Casing design factors	78
Table 11: Casing design loads	78
Table 12: Mendota_INJ_1 open hole diameters and intervals.	79
Table 13: Mendota_INJ_1 casing specifications	80
Table 14: Mendota_INJ_1 casing details.	80
Table 15: Mendota_INJ_1 tubing specifications	82
Table 16: Mendota_INJ_1 packer specifications.	82
Table 17: Surface section fluid placement in annulus	83
Table 18: Intermediate section fluid placement in annulus	83
Table 19: Long string section fluid placement in annulus	84
Table 20: Proposed operational procedures.	88
Table 21: Approval	92

Disclaimer

Any interpretation, research, analysis, data, results, estimates, or recommendation furnished with the services or otherwise communicated by Schlumberger to Clean Energy Systems at any time in connection with the services are opinions based on inferences from measurements, empirical relationships and/or assumptions, which inferences, empirical relationships and/or assumptions are not infallible, and with respect to which professionals in the industry may differ. Accordingly, Schlumberger cannot and does not warrant the accuracy, correctness or completeness of any such interpretation, research, analysis, data, results, estimates or recommendation. Clean Energy Systems acknowledges that it is accepting the services "as is", that Schlumberger makes no representation or warranty, express or implied, of any kind or description in respect thereto. Specifically, Clean Energy Systems acknowledges that Schlumberger does not warrant that any interpretation, research, analysis, data, results, estimates, or recommendation is fit for a particular purpose, including but not limited to compliance with any government request or regulatory requirement. Clean Energy Systems further acknowledges that such services are delivered with the explicit understanding and agreement that any action taken based on the services received shall be at its own risk and responsibility and no claim shall be made against Schlumberger as a consequence thereof.

To the extent permitted by applicable law, Clean Energy Systems shall not provide this report to any third party in connection with raising finance or procuring investment (other than pursuant to an equity capital raising on a public market) without a No Reliance Letter first being completed and signed by the third party and provided to Schlumberger. The form of the No Reliance Letter being agreed to by both Clean Energy Systems and Schlumberger. Subject to this requirement and upon full payment of applicable fees, copyright ownership in this report shall vest with Clean Energy Systems. Schlumberger grants no title or license or right to Clean Energy Systems to use Schlumberger's Intellectual Property except as necessary for Clean Energy Systems to use the report.

Copyrights

Copyright © 2020, Schlumberger

All rights reserved.

Trademarks

All companies or product names mentioned in this document are used for identification purposes only and may be trademarks of their respective owners.

1. Project Background and Contact Information

GSDT Submission - Project Background and Contact Information

GSDT Module: Project Information Tracking

Tab(s): General Information tab; Facility Information and Owner/Operator Information tab

Please use the checkbox(es) to verify the following information was submitted to the GSDT:

Required project and facility details **[40 CFR 146.82(a)(1)]**

1.1. Preconstruction Application Intention

Clean Energy Systems (CES) has contracted Schlumberger to complete the technical analysis required to prepare a Class VI (GS) preconstruction permit application (EPA, Class VI Guidance Documents, 2019) for the Clean Energy Systems Mendota Site. An evaluation of the geologic, hydrogeologic, and Area of Review (AoR) delineation has been developed using available public data, purchased well data and purchased 2D seismic. CES is seeking conditional approval of this Class VI preconstruction permit application from the Environmental Protection Agency (EPA).

The (EPA, 2018), outlined five phases of a Class VI Project (Figure 1). Based on the descriptions of each phase, CES is in the preconstruction phase. The Environmental Protection Agency (EPA) understands that there will be uncertainties regarding the evaluation of the proposed Mendota site. (EPA, Underground Injection Control , 2019) states *“Because all of the information needed to evaluate the suitability of a proposed GS site will not be available at the time the permit application is submitted, there will likely be uncertainties regarding some aspects of the proposed site or the injection operation”*. Because of this uncertainty, CES plans to acquire site specific data (characterization well, 3D seismic, groundwater etc.) to reduce the uncertainty necessary for EPA approval of future phases of the project. Before CES makes a large financial investment in acquiring these site-specific data, CES has two primary objectives for submitting this preconstruction application:

1. In this early phase of the project, CES intends to make the EPA aware of the intention to develop a CCS project at the Mendota site.
2. CES requests that the EPA review this pre-construction application and if the site characteristics and development plan are suitable, grant CES conditional approval pending the acquisition of the site-specific data necessary to validate all aspects of the Mendota site suitability and USDW non-endangerment. If this conditional approval is granted, CES will acquire the site-specific data and submit this application again with a more detailed site characterization and development plan.

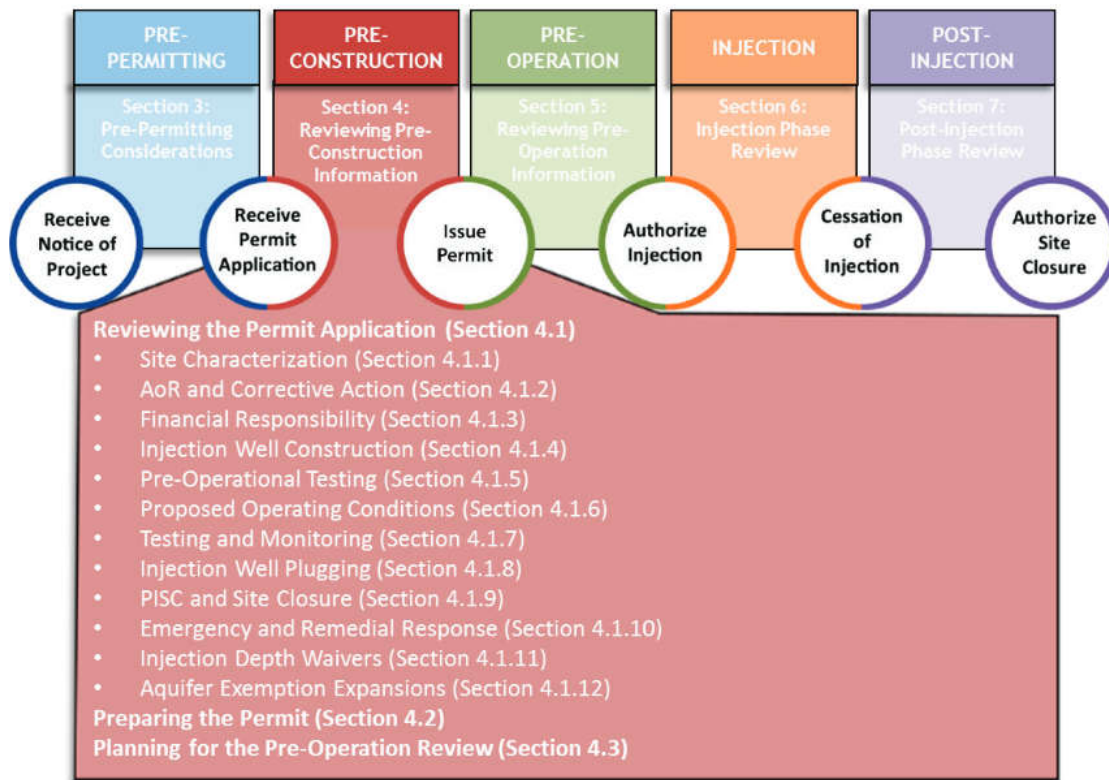


Figure 1: The Phases of a Class VI project (EPA, 2018)

This narrative document summarizes the detailed information provided the following supplemental document templates provided by the EPA. This document is one of the several documents listed below that was prepared by Schlumberger and delivered to Clean Energy Systems. These documents were prepared to support the Clean Energy Systems preconstruction application to the EPA.

- (Schlumberger, Attachment A: Summary of Requirements Class VI Operating, 2020)
- (Schlumberger, Attachment B: Area of Review and Corrective Action Plan, 2020)
- (Schlumberger, Attachment C: Testing and Monitoring Plan, 2020)
- (Schlumberger, Attachment D: Injection Well Plugging Plan, 2020)
- (Schlumberger, Attachment E: Post-Injection Site Care and Site Closure Plan, 2020)
- (Schlumberger, Attachment F: Emergency and Remedial Response Plan, 2020)
- (Schlumberger, Attachment G: Construction Details Clean Energy Systems Mendota, 2020)
- (Schlumberger, Attachment H: Financial Assurance Demonstration, 2020)
- (Schlumberger, Class VI Permit Application Narrative, 2020)
- (Schlumberger Quality Assurance and Surveillance Plan, 2020)

1.2. Project Background

Clean Energy Systems (CES) is developing a series of Carbon Negative Energy (CNE) plants in California. The CNE plants use biomass as feedstock to produce syngas which passes through a gas separation unit to produce renewable hydrogen for transportation fuel. The hydrogen depleted syngas then passes through a CES proprietary gas generator to produce a pure stream of high-pressure CO₂. CES plans to compress this CO₂ to a supercritical state and inject it deep into the subsurface for geologic sequestration (GS). This process is also known as carbon capture and sequestration (CCS). CES is submitting this pre-construction phase application for the Mendota Site located near Mendota California in Fresno County. This pre-construction application was prepared by Schlumberger and delivered to CES.

Figure 2 is a site map that summarizes the location of the Mendota Site and the proposed Mendota_INJ_1 CO₂ injection well. The figure illustrates the Mendota_INJ_1 location relative to known public data such as other wells, the town of Mendota, county lines, rivers and known faults (USGS, U.S. Quarternary Faults, 2019). There are no nearby tribal lands within the area on interest and no state contact available at this time.

The anticipated CO₂ mass to be captured and injected is 350,000 tons/year over the next twelve (4,200,000 tons total) to twenty years (7,000,000 tons total). The injection of CO₂ into the subsurface is regulated by the EPA via the Underground Injection Control Program.

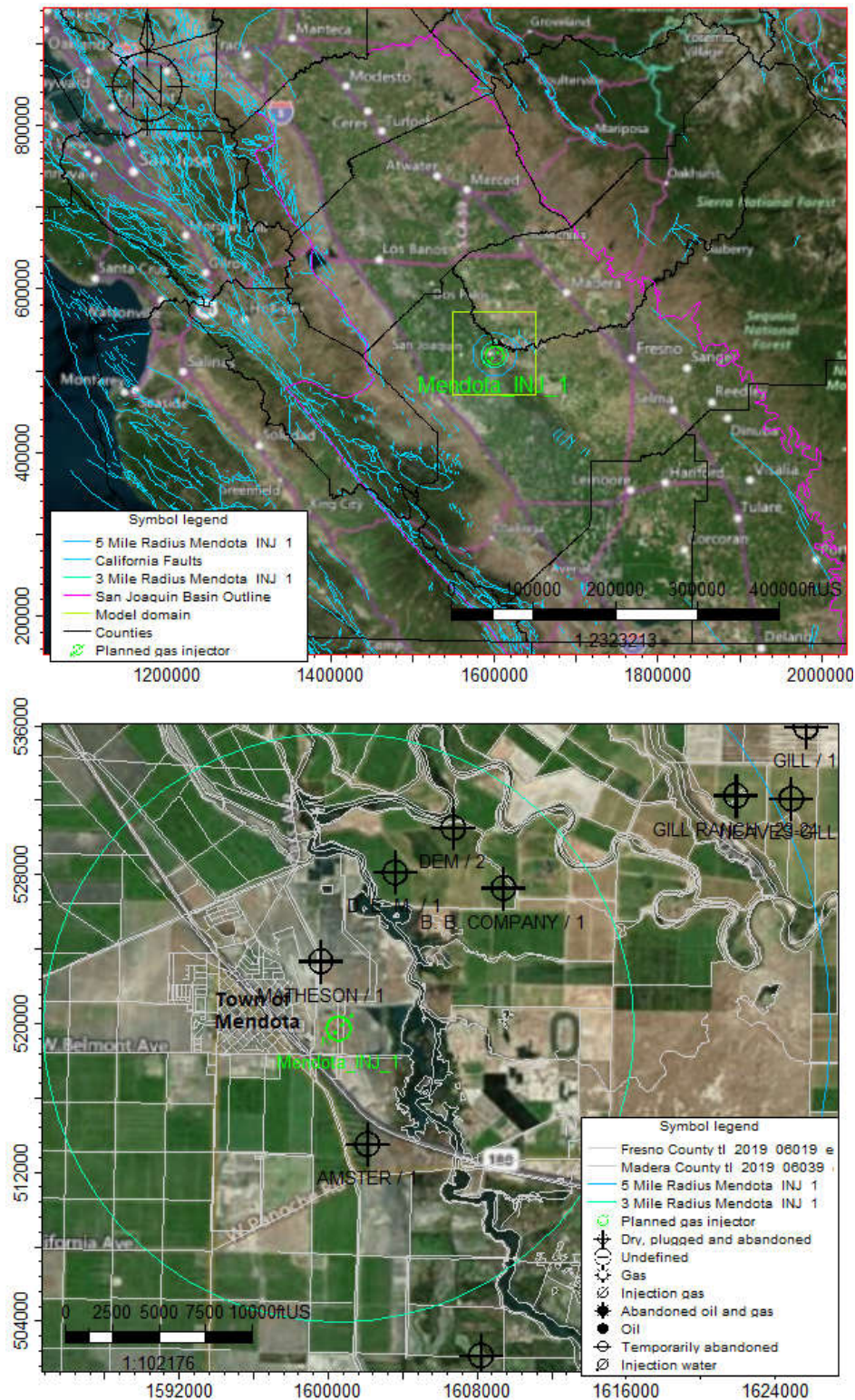


Figure 2: Mendota site location and nearby wells (USGS, 2019) (IHS, 2019) (USGS, 2005)

1.3. Acronyms and Abbreviations

*: Denotes a Mark of Schlumberger

AoR: Area of review

BFS: Base of fresh water

BGS: Below ground surface

CCS: Carbon capture and storage

CEMA: California Emergency Management Agency

CES: Clean Energy Systems

CNE: Carbon negative energy

DFN: Discrete fracture network

DST: Drill stem test

DT: Compressional slowness

DTS: Distributed temperature sensing

EPA: Environmental Protection Agency

FMI: Formation microimager

GRFS: Gaussian random function simulation

GR: Gamma ray

GS: Geological sequestration

KH: Permeability thickness

KINT: Permeability

Mendota_INJ_1: Proposed CO₂ Injection Well

MIT: Mechanical integrity test

MWD: Measurement while drilling

NPHI: Neutron porosity

PISC: Post injection Site Care

PHIT: Total porosity

PIGE: Effective porosity

RHOB: Bulk density

Rwa: Formation water resistivity

SGR: Shale gouge ratio

Shmax: maximum horizontal stress

Shmin: minimum horizontal stress

SP: Spontaneous potential

USDW: Underground sources of drinking water

VCL: Volume clay

VSP: Vertical Seismic profile

Vp/Vs: Compressional to shear velocity ratio

XRD: X-Ray diffraction analysis

2. Site Characterization

2.1. Regional Geology, Hydrogeology, and Local Structural Geology [40 CFR 146.82(a)(3)(vi)]

The Mendota site is in the central San Joaquin Basin in Fresno county, California (Figure 2). The proposed site is situated along the deepest axis of San Joaquin Basin. The San Joaquin Basin formed between a subduction zone in the west and the Sierra Nevada to the east accumulating 25,000 ft of sediment overlying basement rocks capturing the last 100 million years of sedimentary and tectonic history. The San Joaquin Basin forms the southern half of California's Great Valley and is a major petroleum providence. Mapping depositional settings in this basin is challenging because of the changing sea level along with evolving tectonic settings; from forearc margin to strike slip to transpressional regimes (USGS, 2003).

Injection and confinement zones include the Cretaceous Panoche sandstones and shale formations (8000-12000 ft below ground surface (bgs)), with the overlying Moreno shale (7000-8000 ft bgs). The Panoche formation consists of deep-marine shale and submarine fan intervals which were deposited over high and low-stand periods of sea level change (McGuire, 1988). The Panoche and Moreno formations are coeval with Great Valley deposits in the east and pinch out against basement rock to the east as shown in Figure 3 and Figure 4 (Bartow, 1990) (Scheirer, 2003). Sand deposits pinch out along the basins NW-SE structural trend aligning with the Sierra Nevada source materials at the east edge of the basin (Scheirer, 2003). Interbedded shales within the Panoche formation deposited during increases of sea level, as well as the overlying Moreno shale, provide regional geological traps and a caprock seal to contain injected CO₂. Alternating sand and shale layer targets pose an interesting challenge for GS storage assessment because multiple reservoirs can be considered for injection based on their geologic and geochemical properties. This also means multiple caprock seals need to be evaluated as trapping mechanisms to contain CO₂. The lateral heterogeneity of turbidite deposits is also favorable as deposition forms stratigraphic traps.

Figure 5 is a site specific stratigraphic column which describes the geology of this part of the basin at the proposed CO₂ injection well (Mendota_INJ_1). Near the proposed Mendota site, there are two known faults (USGS, 2019) located approximately 5 miles away; there are no other major geological features.

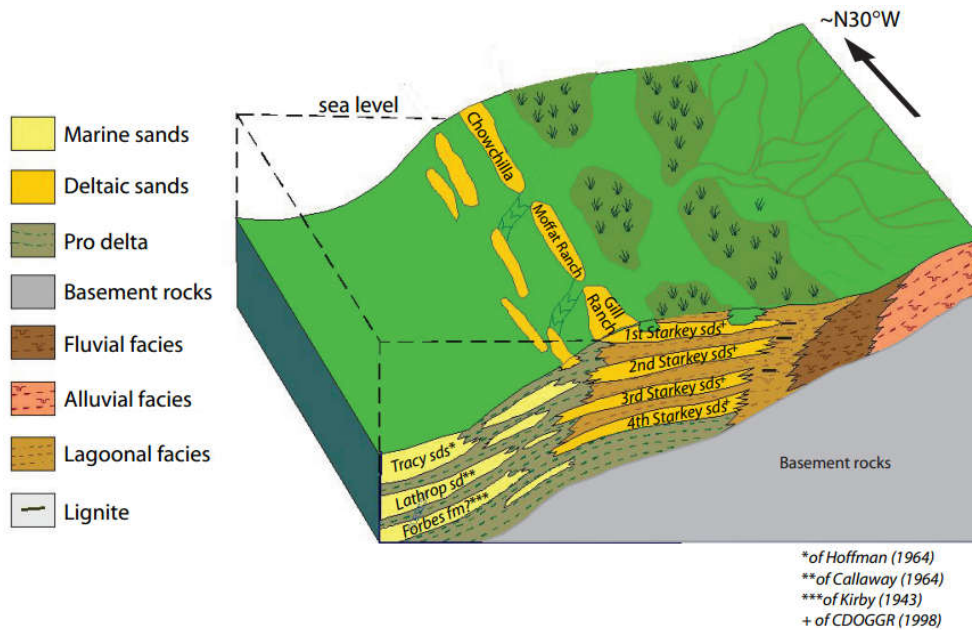


Figure 3: San Joaquin basin depositional model showing submarine fan Panoche formations (Starkey sands) (Scheirer, 2003)

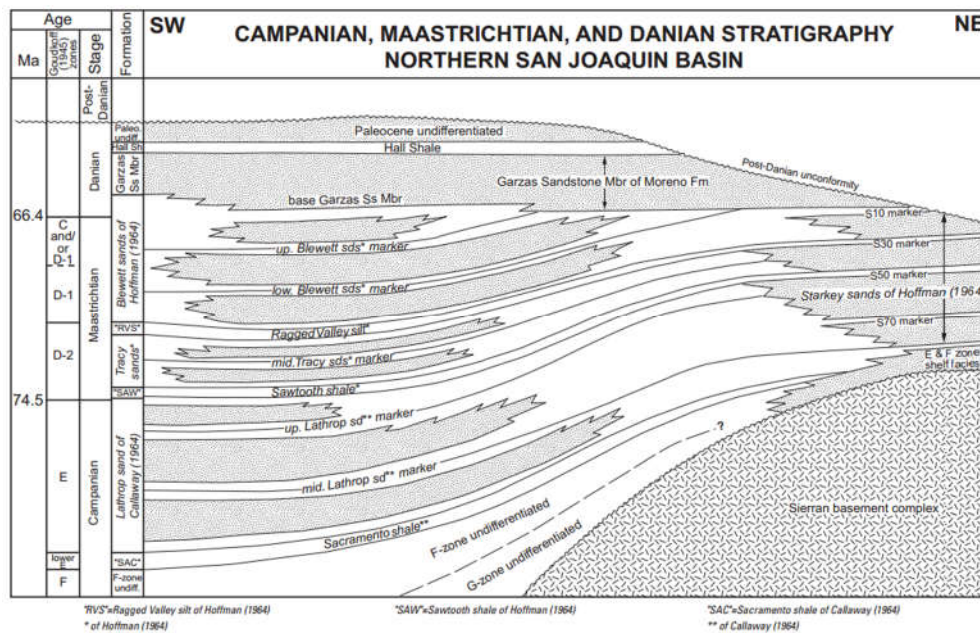


Figure 4: Generalized SW-NE cross section showing Blewett and Lathrop (Panoche) sand injection targets (Scheirer, 2003).

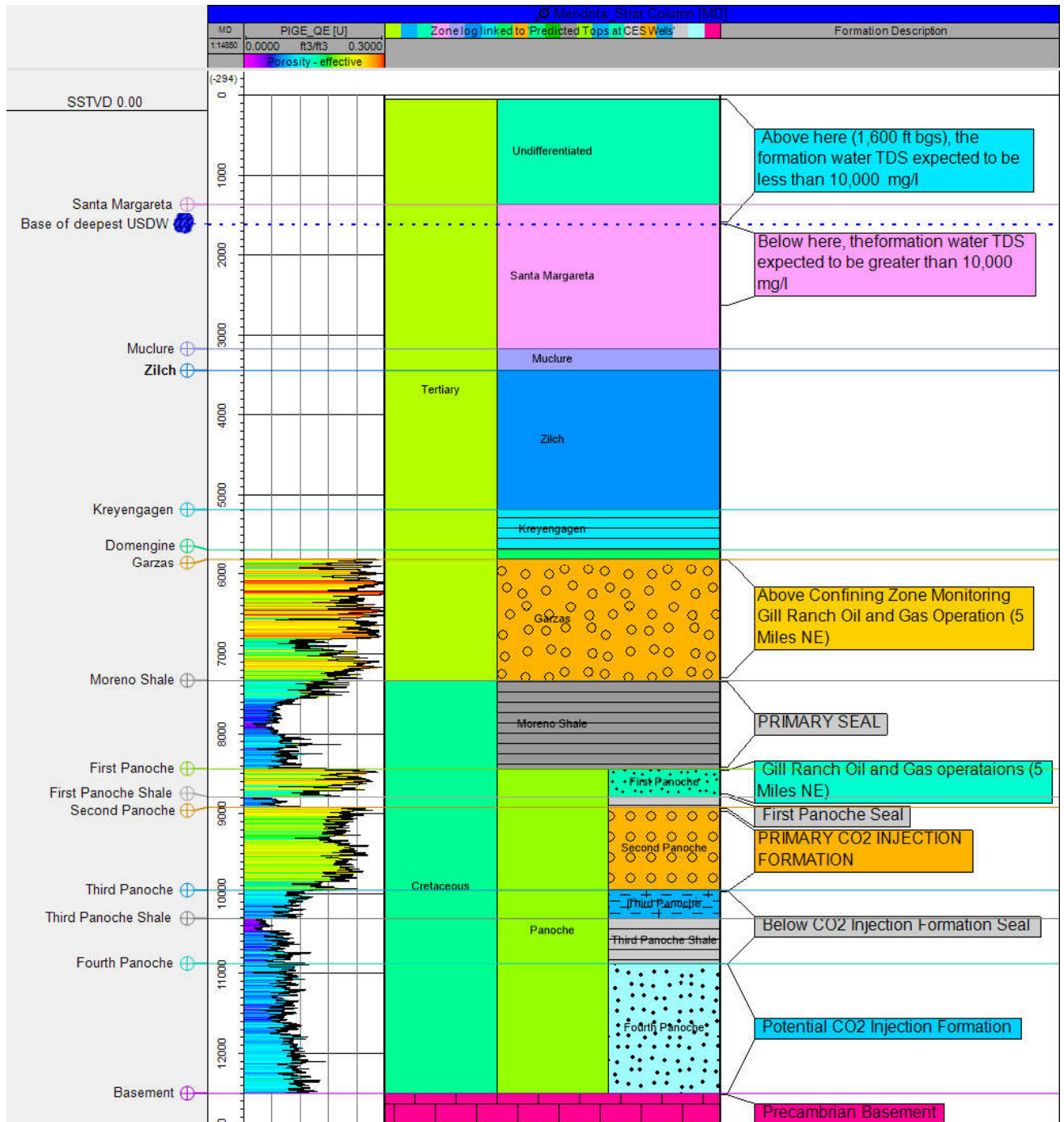


Figure 5: Mendota Stratigraphic column with porosity log (left Section Petrophysics 2.4.2)

2.2. Maps and Cross Sections of the Area of Review (AoR) [40 CFR 146.82(a)(2), 146.82(a)(3)(i)]

2D seismic and well data, including tops, logs, and core, were assembled from various sources in order to assess the feasibility of GS at the Mendota site. Using these data, structural maps and cross sections were generated in Petrel* encompassing the AoR. Figure 6 and Figure 7 show that in this part of the San Joaquin basin the subsurface dip is approximately 4° to the SW, with the closest known faults 5 miles away. The lowermost underground source of drinking water (USDW) is estimated around 1600 ft bgs (Section 2.7.1). The proposed injection targets, the First and Second Panoche sands, are estimated to be at a depth of 8437 ft and 8918 ft bgs, with the overlying Moreno shale estimated at 7332 ft at Mendota_INJ_1 (Figure 5).

Well and 2D seismic data show the Panoche sand targets are continuous through the model domain. Wells used for geological top interpretation and petrophysics are shown in Figure 8 and will be discussed further in Section 2.4.2. Figure 9, Figure 10 and Figure 11 log sections show that the target sands and confining shales appear continuous and laterally extensive; however, the extents are uncertain because of the current lack of available seismic and well data. Literature indicates the Maastrichtian age sand and shale sub-marine fan facies vary in thickness and lateral extent (Suchsland, 1997) (Bartow, 1990) (Scheirer, 2003), and as more data become available after acquisition of 3D seismic and a characterization well is drilled, the extents and thickness of injection and confining zones will be reassessed. Formation surface maps and formation thickness maps are presented in Figure 12 and Figure 13. These maps incorporate the 2D seismic and fault interpretation discussed below in Section 2.3

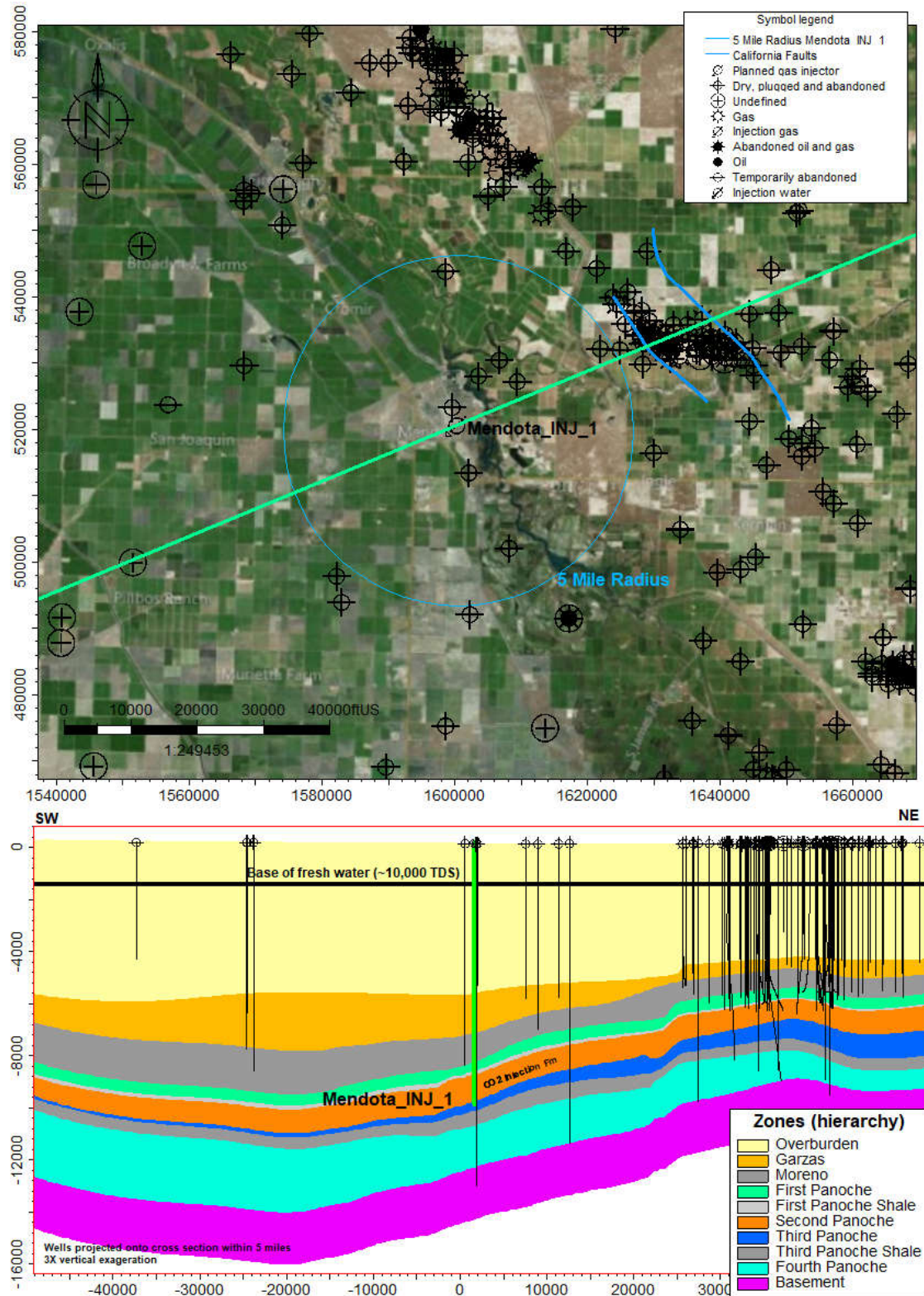


Figure 6: Subsurface geology and legacy wells surrounding the Mendota site NE cross section.

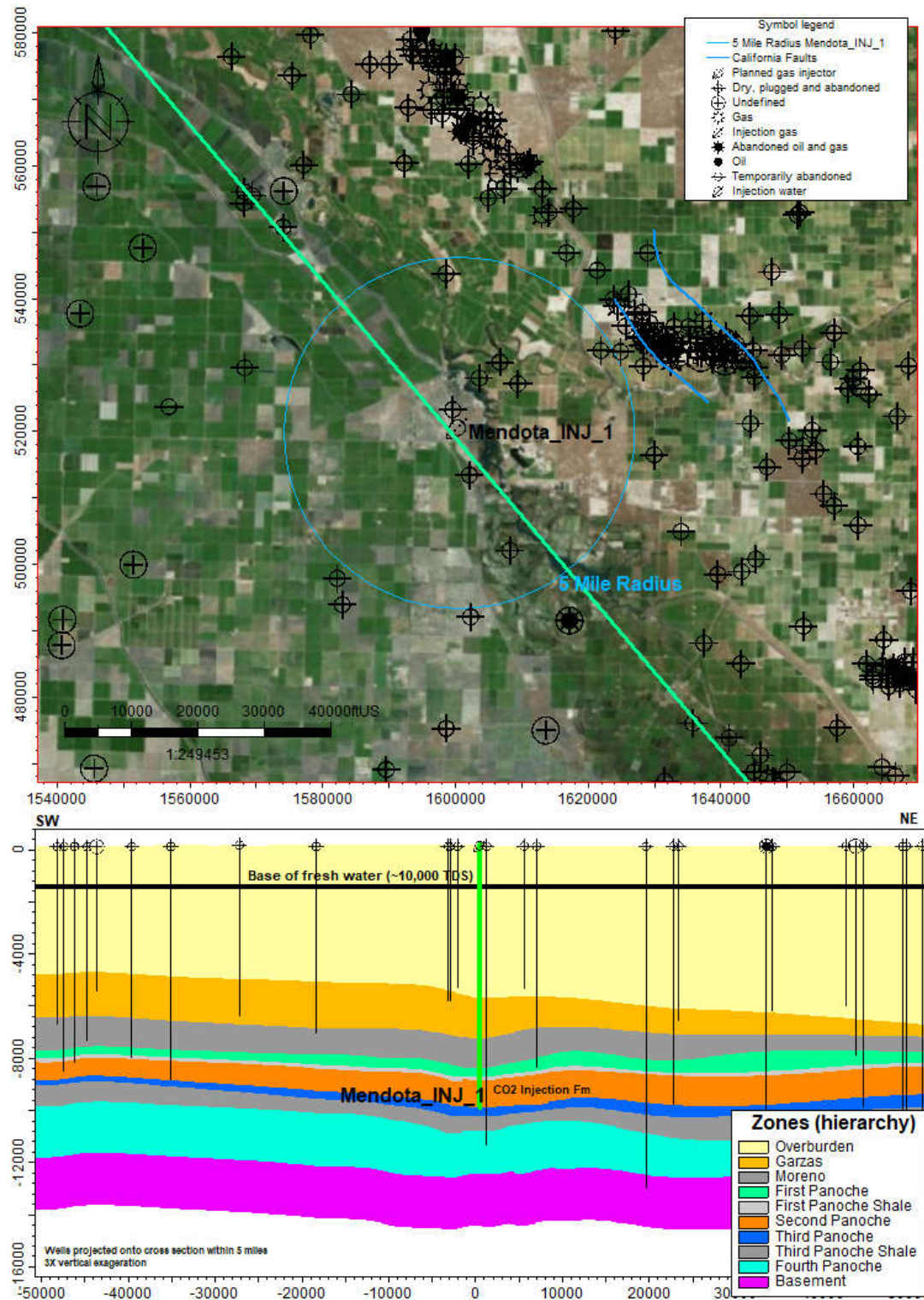


Figure 7: Subsurface geology and legacy wells surrounding the Mendota site SE cross section.

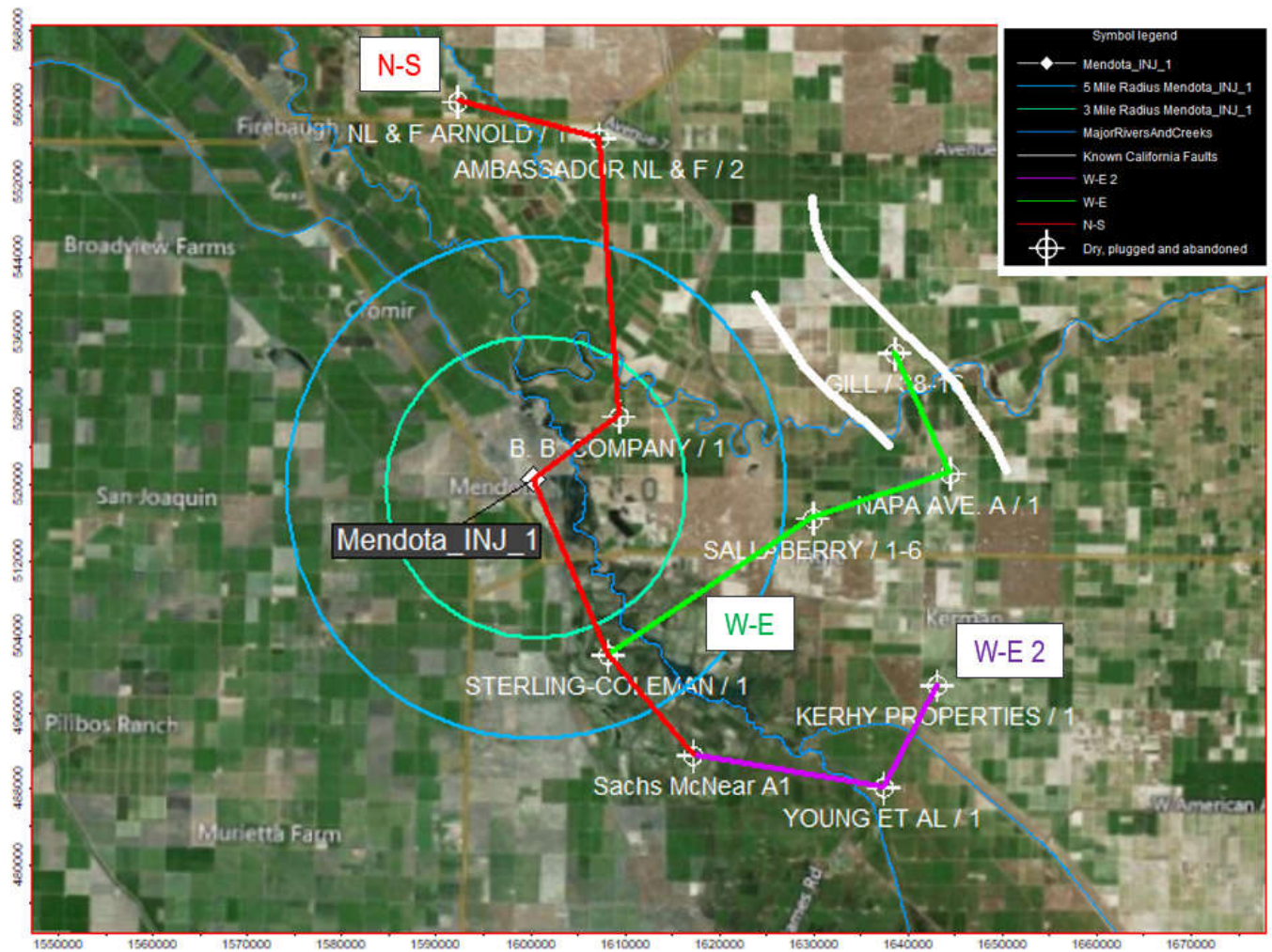


Figure 8: 10 wells used in petrophysical analysis and well correlation.

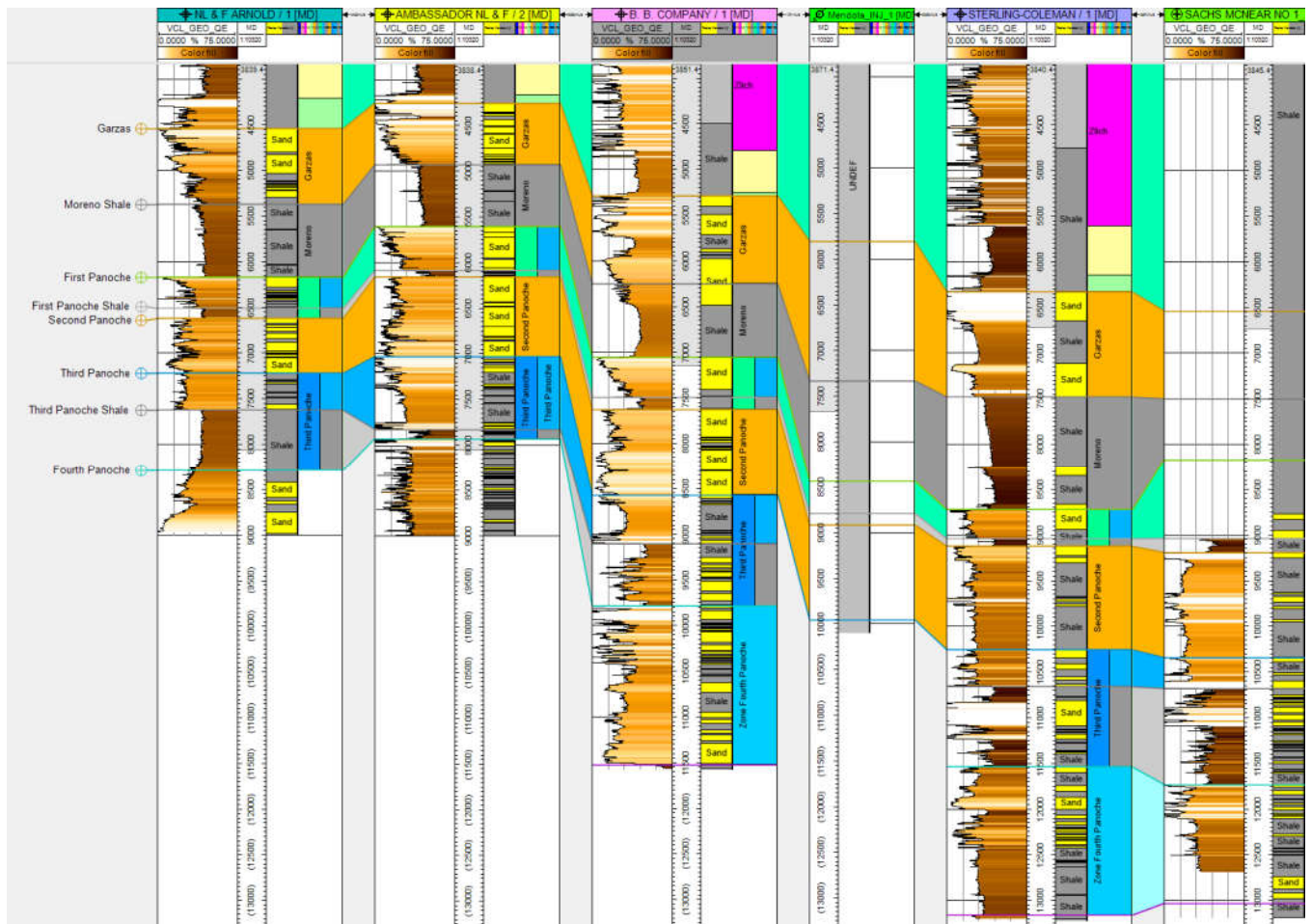


Figure 9: N-S Cross section described in Figure 8, which shows 5 out of 10 petrophysical wells used in analysis of injection and confining rock properties. The Mendota_INJ_1 is located between B. B Company 1 and Sterling-Coleman 1 wells, Tracks left to right include: volume clay (VCL), MD, Zone Log, Facies calculated from volume clay (VCL) and zone color fill between wells.

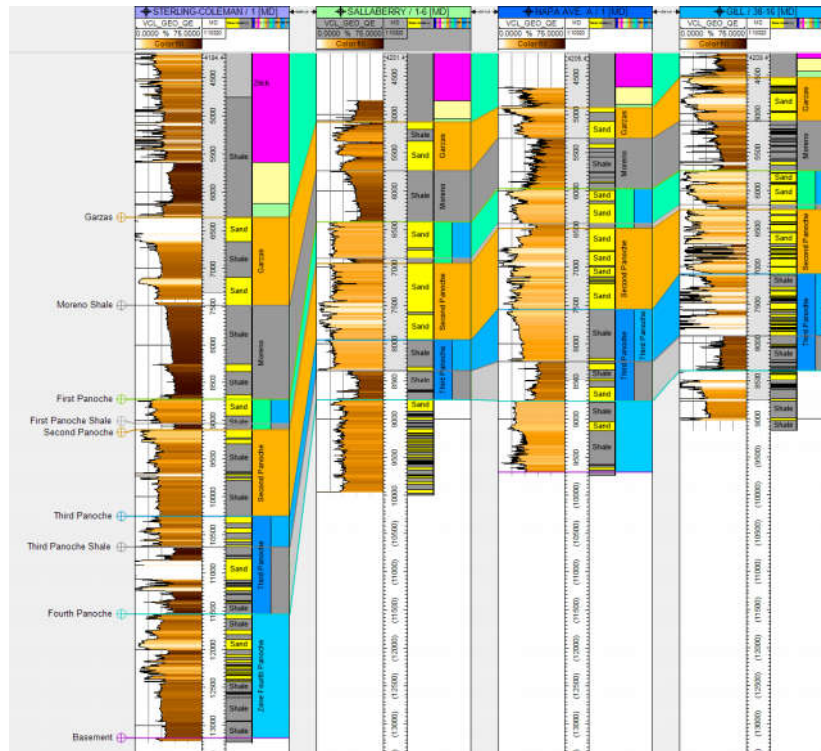


Figure 10: W-E Cross section described in Figure 8. Tracks left to right include: VCL, MD, Zone Log, Facies calculated from volume clay (VCL) and zone color fill between wells.

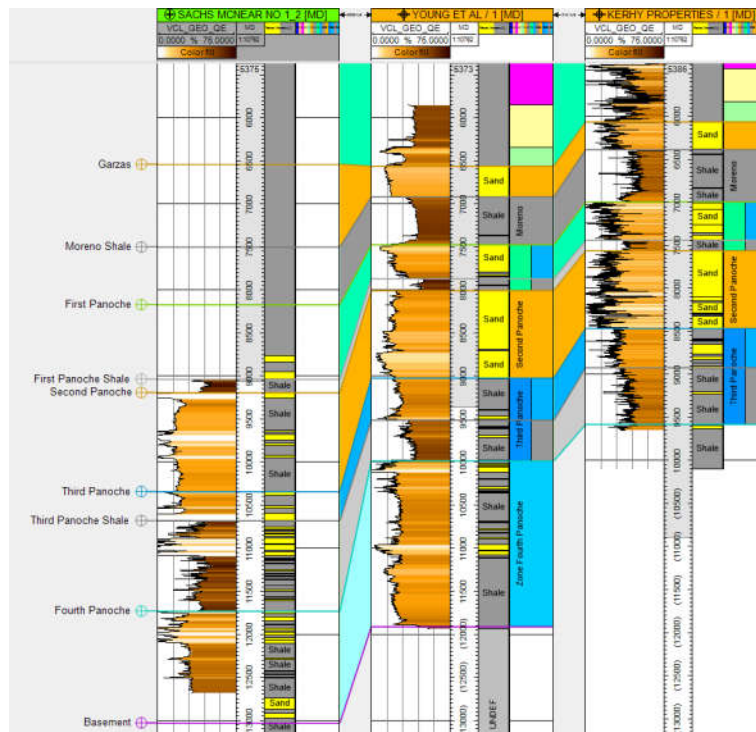


Figure 11: W-E 2 Cross-section described in Figure 8. Tracks left to right include: VCL, MD, Zone Log, Facies calculated from volume clay (VCL) and zone color fill between wells.

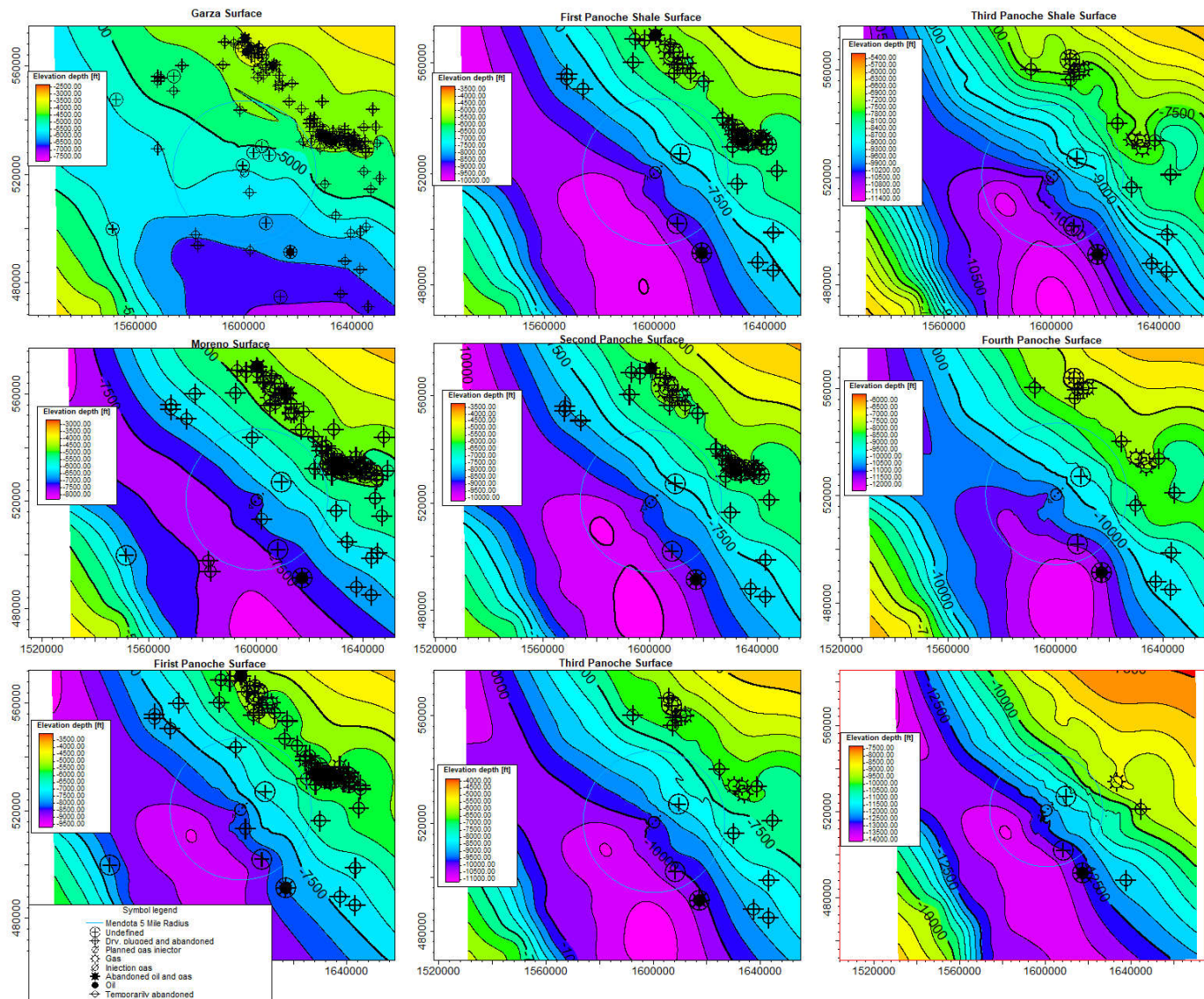


Figure 12: Formation surface maps

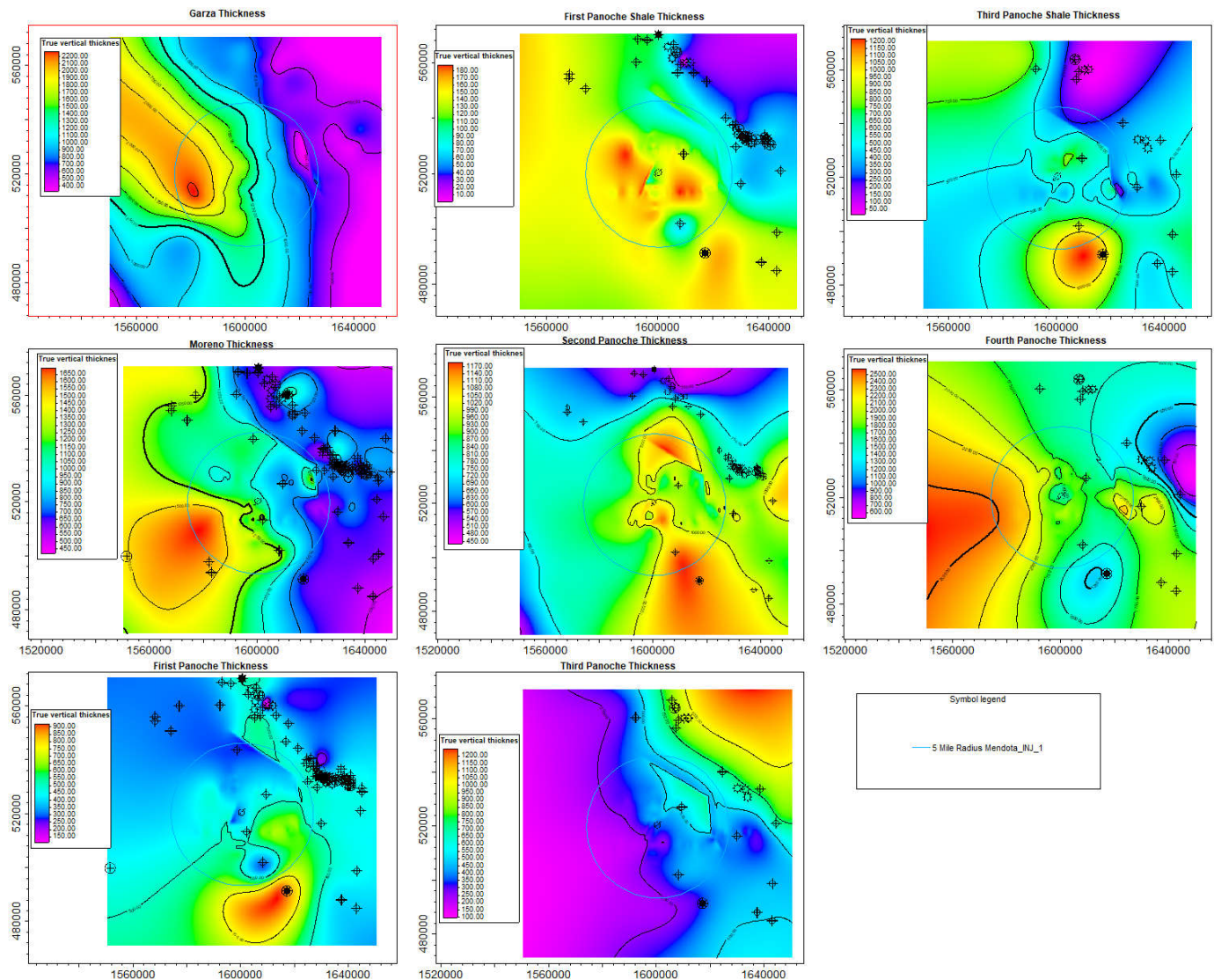


Figure 13: Formations isochore maps

2.3. Faults and Fractures [40 CFR 146.82(a)(3)(ii)]

2.3.1. Geophysical Workflow

In order to evaluate faulting regionally and locally fault data was gathered from public sources (USGS, U.S. Quarternary Faults, 2019) and interpreted locally across three 2D seismic lines which encompass the AoR (SEI, 2019) (Figure 14). Faults were interpreted in the time domain and converted to depth using a regional velocity model derived from synthetic seismic-well ties, horizon interpretations and well formation tops. Well tie analysis was completed in order to calculate the time depth relationship between 2D seismic interpretations in time and well tops interpreted in depth. SALLABERRY / 1-6 was used to complete the seismic-well tie analysis which is shown in Figure 15. The depth converted seismic lines with horizon and fault

interpretations are shown in Figure 16, Figure 17 and Figure 18. The seismic interpretations and well tops provided the structural framework which was calibrated in depth to geologic formation tops and integrated into the geologic model.

The 3D perspective view in Figure 19 provides an overview of the interpreted faults. Most of the interpreted faults are small throw features except for two northerly trending faults that separate the Gill Ranch Field from the Mendota AoR area nearly 4 miles east of the proposed Mendota_INJ_1. These faults can be seen in Figure 16 as Fault 1 and Fault 2 near shot point 1650 and in Figure 19 associated with the step shown on the basement surface. Also, Fault 1 is projected northwest in Figure 19, parallel to the faults shown in the legacy Gill Ranch field Second Panoche structure map; however, sufficient control is missing for accurate positioning of this significant fault. A few minor faults are projected in 3D, but most are small and cannot be projected between the seismic lines. Faulting deeper in the Panoche formation, Fault 3 and Fault 4, are observed near the proposed injection well as shown on 2D seismic line W-SJ-209 which traverses the Mendota site (Figure 17). These normal faults are subtle, have small displacement and do not appear to extend higher than the Third Panoche.

The seismic interpretations provided the structural framework which was calibrated in depth to geologic formation tops and integrated into the geologic model shown in Figure 20.

A preliminary fault evaluation of the 2D seismic data indicates a low-angle feature, Fault 13 (Figure 22), which appears to dip approximately 30° SE (from horizontal) below the planned Mendota_INJ_1. This dip orientation is nearly perpendicular regional principal stress direction of ~N45E. Thus, there is insufficient supporting evidence to suggest this is a thrust fault; rather, it is more plausible that the fault (as interpreted) may result from of strike slip stress, wrenching or differential settlement in the basin. Based on current mapping Fault 13 appears to be present below Mendota_INJ_1 at a depth of 9850 TVDSS. The Mendota_INJ_1 well injection target is the Second Panoche sand interval; which is shallower (9718-9757 TVDSS) at the current planned well location.

2.3.2. Fault Seal Analysis

Fault 13 was incorporated into a geocellular model to analyze injection and confining zonal facies juxtaposition and conduct clay smear analysis. Preliminary analysis of fault seal capacity was completed using a VCL modeled property derived from petrophysical analysis (discussed in Section 2.4.2) and extrapolated using a facies model for bias (discussed in Section 2.4.3). Using the VCL modeled property fault seal properties such as Facies juxtaposition and Shale Gouge Ratio (SGR) were calculated. Facies juxtaposition analysis is necessary to understanding if fault displacement poses a risk to confinement of injected CO₂. If sediment displacement across the fault is high, then an injection target could be juxtaposed against a shallower sand facies posing leakage risk to another zone. Figure 21 illustrates the difference between low and high fault displacement, using the highest risk scenario for leakage in which Fault 13 is not sealing. Based on interpretation of Fault 13 across all three seismic lines (Figure 16, Figure 17, Figure 18) it is likely that sediment displacement across Fault 13 is low, indicating that the right illustration of Figure 21 is most accurate. This indicates that injected CO₂ will be confined to the Second

Panoche injection zone. At this time, it is unknown if the fault is sealing as discussed further in Section 2.3.3 below.

If the more unlikely case that Fault 13 does not seal, the risk of upwards migration via Fault 13 is still possible but limited to zones below the Moreno shale. Clay smeared along the fault zone above the injection zone could provide a seal. To assess this risk, fault clay content prediction was calculated across Fault 13. Fault Clay content prediction uses SGR to estimate the amount of clay smear along the fault using a clay smear factor and clay thickness (Yielding e. a., 1997) (Yielding, 2002). The results of this analysis (Figure 22) show high clay smear in the Moreno zone indicating that there is enough clay in the Moreno zone and the Moreno zone is thick enough to smear along the fault as displacement occurs.

2.3.3. Uncertainty

Uncertainty regarding the extent of fracturing and faulting within the AoR include elements of seismic imaging, depth calibration and availability of deep well control and physical measurements (well logs) near the proposed site. In future phases of this project, 3D seismic and a characterization well's core and image logs will be used in a discrete fracture model to determine the intensity of fractures and provide more precise mapping and clearer understanding of the faulting complexity and connectivity.

Due to poor imaging, the exact location of Fault 13 is unknown. On Figure 17, a projection of this fault is partially imaged on this 2D line. The image quality is diminished possibly because of 'out of plane' interference. The trace of the projected fault is inferred with better imaging on the E-W seismic lines W-SJ-202 and W-SJ-013W (Figure 16 and Figure 18). Fault 13 does not appear to reach the Garzas and has little offset; this implies that the fault has been relatively stationary over time. This also suggests that the Moreno Shale interval likely provides an adequate seal to the terminating fault in the Moreno. Simulation results shows CO₂ migration will occur up-dip in the NE direction (Schlumberger, Attachment B: Area of Review and Corrective Action Plan, 2020), away from Fault 13.

There have been no hydrocarbons identified in the exploration wells from the region to indicate if faults are sealing, i.e., if hydrocarbons were contained by the fault in this area the faults are likely sealing. Further there is insufficient information at this time to assess fault transmissibility of Fault 13. CO₂ plume simulations show the plume migration to the N-E, in the up-dip direction of injection sand, away from Fault 13.

A 3D geomechanical model using well logs, geomechanical core analysis, and well test data combined with 3D seismic data will provide a better characterization of the in-situ stress field, pore pressure, rock strength and 3D fault characterization for fault stability analysis and sealing capacity of these faults (Chiaramonte, 2008). A more comprehensive analysis of faults and potential associated risks will be performed once additional site-specific data are collected. The final location of the injection and monitoring wells will consider all identified faults to mitigate any risk of interaction with the pressure AoR based on the updated AoR delineation and geomechanical models.

Image Removed because it contains Confidential Business Information. This image will be sent directly to the EPA.

*Figure 14: **CONFIDENTIAL BUSINESS INFORMATION:** 2D Seismic line map, shot points and area wells showing the 3 and 5-mile radii from Mendota Plant Site. This image displays (SEI, 2019) data and it is marked as Confidential Business Information.*

Image Removed because it contains Confidential Business Information. This image will be sent directly to the EPA.

*Figure 15: **CONFIDENTIAL BUSINESS INFORMATION:** Seismic Well Tie: Line W-SJ-202 and SALLABERRY / 1-6 (4019215350000). This image displays (SEI, 2019) data and it is marked as Confidential Business Information.*

Image Removed because it contains Confidential Business Information. This image will be sent directly to the EPA.

*Figure 16: **CONFIDENTIAL BUSINESS INFORMATION:** W-SJ-202 2D seismic line (depth) with interpreted horizons and faults. This image displays (SEI, 2019) data and it is marked as Confidential Business Information.*

Image Removed because it contains Confidential Business Information. This image will be sent directly to the EPA.

*Figure 17: **CONFIDENTIAL BUSINESS INFORMATION:** W-SJ-209 2D seismic line (depth) with interpreted horizons and faults. This image displays (SEI, 2019) data and it is marked as Confidential Business Information.*

Image Removed because it contains Confidential Business Information. This image will be sent directly to the EPA.

*Figure 18: **CONFIDENTIAL BUSINESS INFORMATION:** W-SJ-013W 2D seismic line (in depth) with interpreted horizons and faults. This image displays (SEI, 2019) data and it is marked as Confidential Business Information.*

Image Removed because it contains Confidential Business Information. This image will be sent directly to the EPA.

*Figure 19: **CONFIDENTIAL BUSINESS INFORMATION:** 3D View (facing SE) of interpreted faults on the 2D seismic lines and Basement surface. Dotted lines are projected faults (color coded by horizon) or projected fault plane. A legacy Gill Ranch field structure map is inserted at the Second Panoche. This image displays (SEI, 2019) data and it is marked as Confidential Business Information.*

Image Removed because it contains Confidential Business Information. This image will be sent directly to the EPA.

Figure 20: **CONFIDENTIAL BUSINESS INFORMATION:** 3D perspective of the depth integrated geophysical model. This image displays (SEI, 2019) data and it is marked as Confidential Business Information.

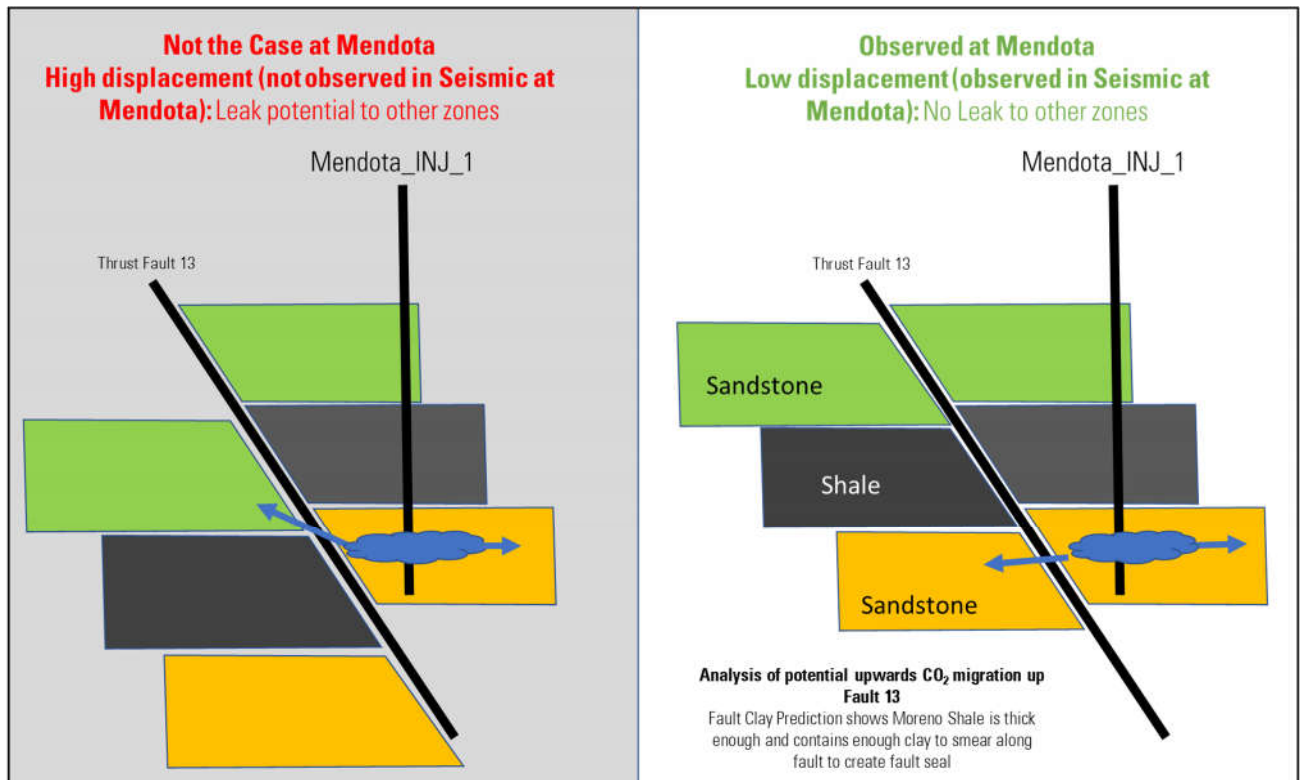


Figure 21: Illustration describing different fault displacement scenarios at Mendota_INJ_1 regarding Fault 13.

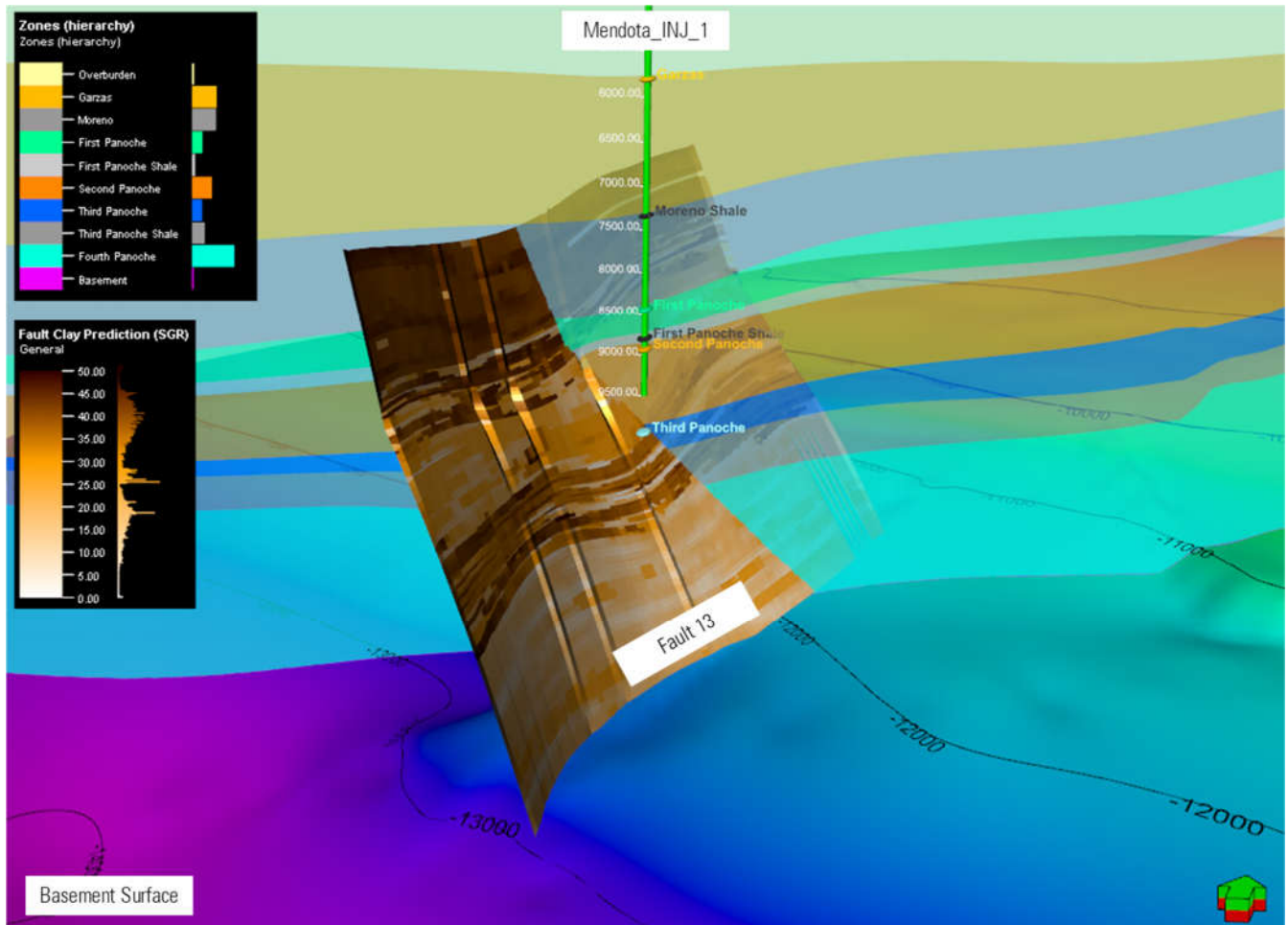


Figure 22: Fault 13 terminates within the Moreno Shale. Mendote_INJ_1 wellbore which targets the Second Panoche injection sand is shown in green with MD annotated in white text. Fault 13 is colored by Fault Clay Prediction content based on the SGR algorithm, the results of which indicate the Moreno Shale smearing along the fault.

2.4. Injection and Confining Zone Details [40 CFR 146.82(a)(3)(iii)]

2.4.1. Structural Mapping

Well and 2D seismic data was incorporated into a geomodel in Petrel* to determine depth, areal extent, and thickness of the injection and confining zones. Well tops were re-interpreted when necessary, but otherwise imported from (DOGGR, 2019) or (IHS, 2019) data sources. Surface gridding was completed using a combination of convergent and conformal interpolation mapping algorithms. Seismic horizon interpretation data was used as a secondary input for surface gridding. Table 1 shows the number of well top control points used in surface gridding. Figure 12 Section 2.2 highlights the structure maps. illustrates the 3D structural model built from seismic and well tops, and domain converted from time to depth.

Table 1: Well Control Points for Structural model of injection and confining formations.

Formation	Well Control
Moreno	31
First Panoche	23
Second Panoche	11
Third Panoche	11
Fourth Panoche	10

2.4.2. Petrophysics

Petrophysical analysis (Figure 8) for 10 wells was completed using the Techlog* Wellbore Software Platform and the Quanti.Elan* multicomponent inversion solver to estimate porosity and permeability of the injection and confining zones targeted for carbon storage. Raw log data in both raster and LAS form were acquired from (IHS, 2019) and (DOGGR). The log basic log data were from wells drilled between 1942 and 1987 (Table 2). Logs were imported into the Techlog* software and normalized. Petrophysical properties such as effective porosity (PIGE), permeability (KINT) and volume of clay (VCL) were calculated and used to determine sand and shale facies. These properties were later used to populate the geologic model discussed in Section 2.4.3. Petrophysical results show a reasonable estimate of total porosity and permeability; however, there is uncertainty on the effective porosity because an empirical relationship was used to estimate irreducible water.

The petrophysical workflow involved building a model using well log data from NAPA AVE A/1 calibrated to core data for the same well (TGS, 2019). This workflow was applied to the other wells within the geologic model in which only well data was available to determine the porosity and permeability. As shown in Table 2, some of the wells have a limited set of well log data. The petrophysical property uncertainty around these wells was reduced by calibrating parameters and multi-well comparisons across different formations. The petrophysical evaluation focused on the formations included in the geological model from the Garzas formation to the Precambrian Basement. Petrophysical calculation results are illustrated in cross section Figure 23, Figure 24, Figure 25.

The mineralogy around the Mendota site is assumed to be like that from the well – NAPA AVE A/1 which is approximately 9 miles from the site and penetrates similar formations; however, there is uncertainty in the lateral continuity of the formations which could result in differences in the reservoir properties and mineralogy. This uncertainty will be significantly reduced by acquiring 3D seismic, logging a comprehensive suite of wireline tools and core data as detailed in (Schlumberger, Attachment G: Construction Details Clean Energy Systems Mendota, 2019) from a characterization well drilled in future phases of this project.

VCL logs derived from petrophysical modeling were used to generate a simple lithology log of sand and shale. VCL log values greater than 30% were considered shale and anything less than 30% VCL was flagged as sand. The resulting facies log is shown in Figure 23, Figure 24, Figure 25 cross sections. Facies definition will be re-evaluated and refined as new well data is added to

the petrophysical model. Figure 26 shows facies thickness maps of the Moreno shale caprock and First and Second Panoche sand intervals. At Mendota_INJ_1, the estimated thickness of the First Panoche sand is 325 ft and the second Panoche sand 1000 ft. The Moreno shale caprock seal thickness is estimated at 1000 ft. Within the AoR the thickness of the injection target varies from approximately 1000-2000 ft. There are multiple overlaying shale formations. The Moreno shale main seal reaches thicknesses around 500-1700 ft, as show in Figure 26. Regional well data show Panoche sand targets to be continuous across the modeled area based on well log data as discussed in Section 2.2 Figure 8 and Section 2.4.2.

Table 2: Wells used to characterize petrophysical properties within the AoR

Well Name	UWI	Latitude (deg)	Longitude (deg)	Spud Date	Data Available ¹
AMBASSADOR NL & F/2	4039001440000	36.85492	-120.34239	09-23-1962	SP, DT and Resistivity
B B COMPANY /1	4019207520000	36.774431	-120.334662	04-12-1973	SP, DT and Resistivity
GILL / 38-16	4039000460000	36.79396	-120.23433	12-02-1942	SP and Resistivity
KERHY PROPERTIES / 1	4019216070000	36.86941	-120.21743	01-14-1978	GR, DT, RHOB, NPHI, Resistivity
NAPA AVE A /1	4019225380000	36.75919	-120.21387	01-24-1987	GR, DT, RHOB, NPHI, Resistivity and Core
NL & F ARNOLD / 1	4039200320000	36.86496	-120.39371	03-07-1982	SP, DT and Resistivity
SACHS MCNEAR NO 1_2	4019060420000	36.6767	-120.30546	08-18-1965	SP, DT and Resistivity
SALLABERRY / 1-6	4019215350000	36.74573	-120.26308	07-27-1981	GR, DT, RHOB, NPHI, Resistivity
STERLING COLEMAN /1	4019203700000	36.70535	-120.337582	07-14-1969	SP and Resistivity
YOUNG ETAL / 1	4019204110000	36.66817	-120.23627	12-19-1969	DT, RHOB, Resistivity

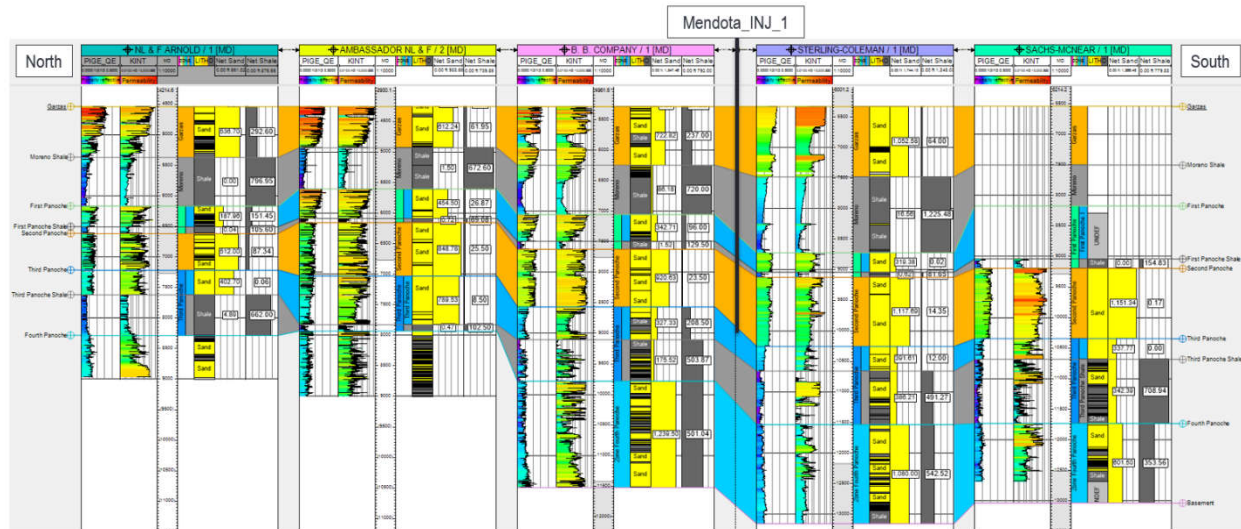


Figure 23: N-S Cross Section showing Petrophysical analysis results and wells nearest to Mendota_INJ_1. The tracks show left to right PIGE (Effective Porosity) KINT (Permeability), MD, Zone log, Sand and Shale Lithologies as calculated from VCL, and Net Lithology values for Sand and Shale per zone.

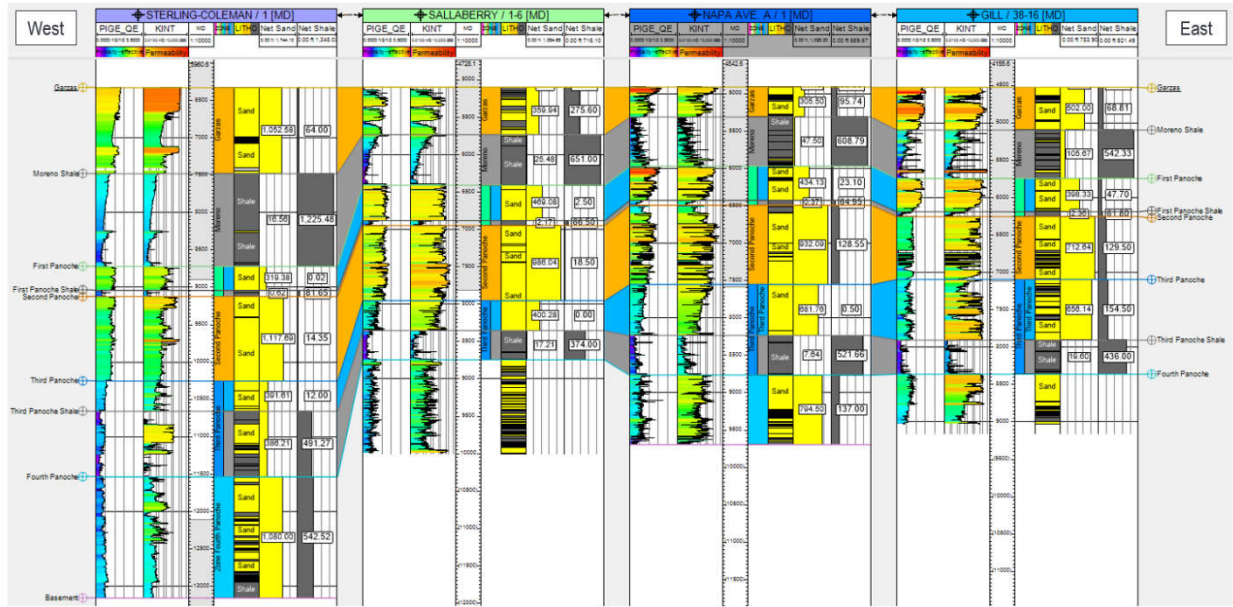


Figure 24: W-E Cross Section showing Petrophysical analysis results with same tracks as Figure 23.

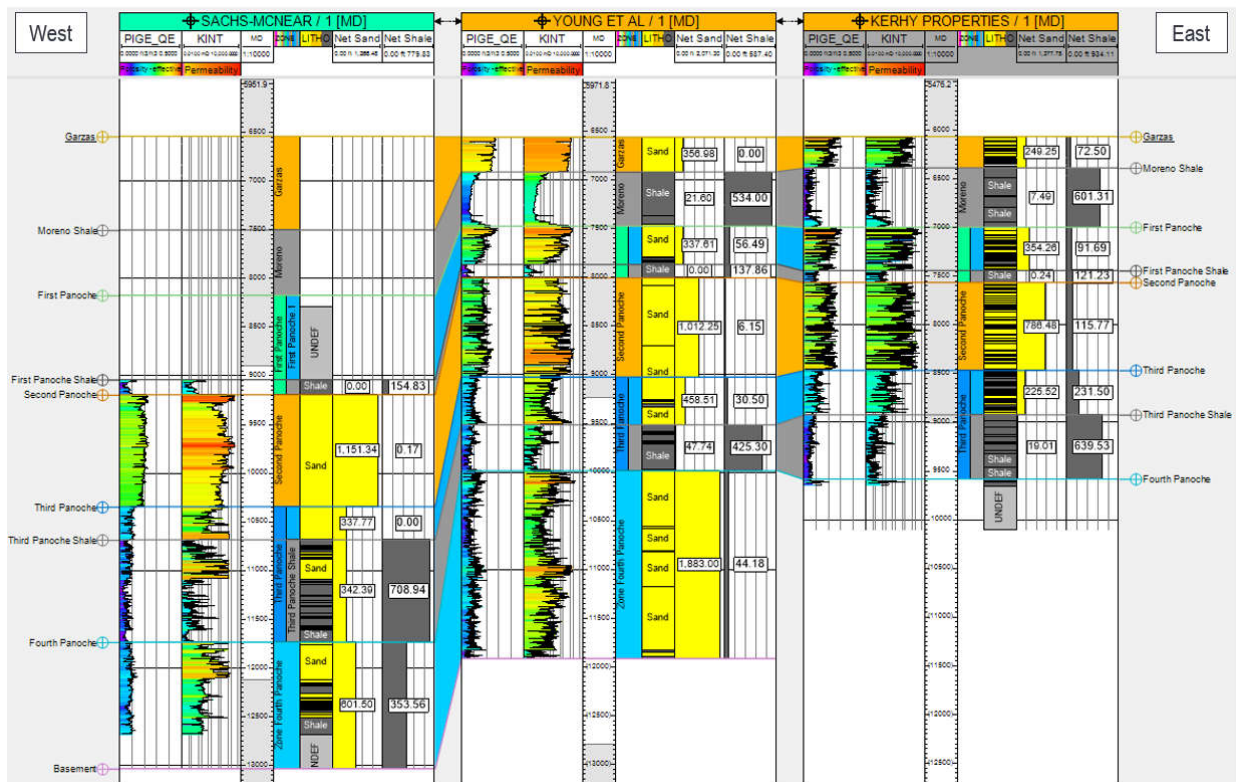


Figure 25: W-E 2 Cross section showing Petrophysical analysis results with same tracks as Figure 23.

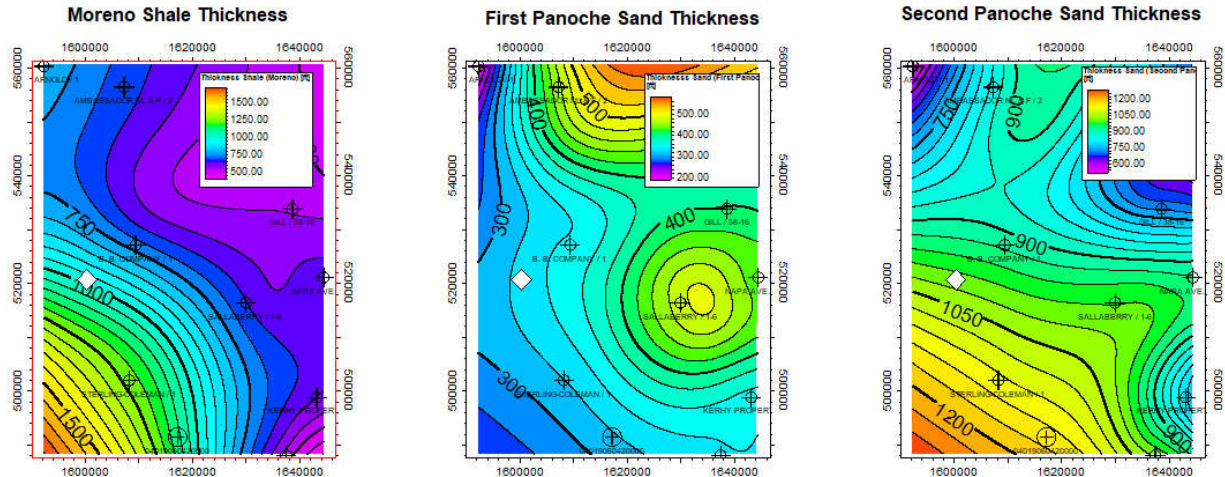


Figure 26: Net Thickness maps of Moreno Shale and First and Second Panoche Sands calculated based on VCL greater than or less than 30%, white diamond denotes Mendota_INJ_1.

2.4.2.1. Porosity

The total porosity of the injection zone was determined from either the bulk density or compressional slowness depending on data availability (Figure 27). The porosity of the Third and Fourth Panoche sands is lower than that of the First and Second Panoche sands as evident by the denser, faster log responses seen on the raw logs from all the wells within the geologic model. Clay volume was estimated from the spontaneous potential or gamma ray log to derive the clay bound water and with an empirical estimate of irreducible water gave an estimation of the effective porosity. This effective porosity was distributed into the geomodel. Figure 28 shows the spatial distribution of the effective porosity across both the injection and confining zones. The average effective porosity for the injection and confining zones is as shown in Table 3.

2.4.2.2. Permeability

The intrinsic permeability was estimated based on the porosity and lithology of the formation (Herron, 1987) using the wells around Mendota_INJ_1 (Figure 29). The lithology model consisted primarily of Quartz, Clay and Feldspars based on the core from NAPA AVE A/1. The relationship of porosity vs permeability is shown in (Figure 30). The average permeability of both the injection and confining zones is shown in Table 3 and Figure 31 shows the spatial variations in permeability thickness (KH) for the different formations.

Table 3: Average porosity and permeability of injection and confining zones - average porosity and permeability of injection and confining zones

Formation	Average Porosity (%)	Average Permeability (mD)
Moreno Shale	8	4.7
First Panoche	20	300
Second Panoche	18	290
Third Panoche	12	140
Fourth Panoche	10	87

2.4.2.3. Mineralogy and Geochemistry Analysis

The mineralogy around the Mendota site is assumed to be similar to that from the well – NAPA AVE A/1. The core X-Ray Diffraction (XRD) report indicates the presence of Quartz, K-Feldspar, Plagioclase, Pyrite, Clay and Calcite stringers as shown in Table 4 (California Department of Conservation, 1998). Expected geochemical reactions to the injected CO₂ stream are discussed in sections 2.8.2 Mineral Composition of The Injection Zone through 2.8.5 Simulated Reaction Pathways of this narrative. A more comprehensive analysis is planned using core and geochemical logs from a characterization well in a future phase of this project.

Table 4: Mineralogy summary from core XRD – NAPA AVE A 1

Depth ft	Quartz %	K-Feldspar %	Plagioclase %	Calcite %	Ankerite %	Siderite %	Pyrite %	Barite %	Clay %
8200	32	22	35				4		7
8208	15	10	22	1			7		45
8222	19	13	20				5	3	33
8612	36	20	33						9
8618	20	12	16	25	3	11			9
8751	36	20	33					1	10

2.4.3. Geocellular Modeling and Volumetrics

In order to estimate the spatial distribution of rock properties between wells, structural surfaces discussed in Section 2.4.1 were used to build the skeleton for a 3D geocellular model. The lateral grid resolution (cell size) was defined as 400 ft by 400 ft. A finer resolution grid will be considered for future modeling after incorporation of 3D seismic data. The 3D model was divided into 4 ft layer increments, and log data from the 10 petrophysical wells (Figure 8) was upscaled into the cells along the wellbore. The upscaled log data (discussed in section 2.4.2) provides the basis for populating the geomodel properties which include effective porosity, permeability, clay volume and pore volume. Petrophysical properties were distributed through the model domain using the Gaussian Random Function Simulation (GRFS) algorithm. This kriging based algorithm was used because it can generate multiple equiprobable realizations,

which is preferred when working with sparse well data. Before running this simulation, it is necessary to define vertical, major and minor variograms to guide property distribution. Variogram modeling based on petrophysical logs shows a NE-SW depositional trend, with a vertical resolution of roughly 20 ft. 20 ft is likely representative of larger depositional changes (for example from high-stand to low-stand sea level). To capture smaller changes within each depositional cycle, 4 ft layer increments were defined for each zone. Because modeled zones are based on estimated facies changes, facies logs were not used as bias in the porosity or permeability models at this time. Facies biasing and Kriging to 3D seismic data will be considered in future model iterations.

Histograms for porosity and permeability comparing petrophysical logs to upscaled (averaged based on layer increment) and to full-field simulated properties are illustrated in Figure 27 and Figure 29. The relationship between porosity and permeability are shown in the Figure 30 cross plots. Once colored by zone and facies, the distributions show distinguishable separation; therefore, estimated porosity and permeability ranges can be predicted for the injection and confining zone. Figure 28 and Figure 31 show the simulated average porosity and simulated permeability thickness (KH) for each modeled zone is consistent with regional geology and predicted lithology type. The Moreno shale formation has low porosity and low permeability which is required to act as an effective seal. The Second Panoche injection zone has high porosity and permeability throughout the model domain area. Figure 32 shows a 2D view with Mendota_INJ_1 at the center and North-South, East-West transverses. Figure 33 shows this same view in 3D, along with simulated effective porosity N-S and E-W transverses. This 3D view shows the confining and injection zone to be continuous within the model domain, and confining zones with low porosity are present above and below the Second Panoche target injection zone. Spatial distributions for porosity, permeability and clay volume are illustrated in Figure 34 through Figure 39.

The storage capacity of the injection zone was measured in bulk volume ft³. The integrity of the confining zone is measured based on the thickness of Moreno shale and available core data. Within a 2.5-mile radius of the Mendota_INJ_1, the total pore volume of the Second Panoche injection zone is calculated using the 3D geocellular model; for each model cell, the porosity was multiplied by the cell volume. The total pore volume was calculated to be 3.74×10^{11} ft³. Given the high porosity and permeability of the Second Panoche, this formation is suitable to receive the forecasted 350,000 tons/year of CO₂.

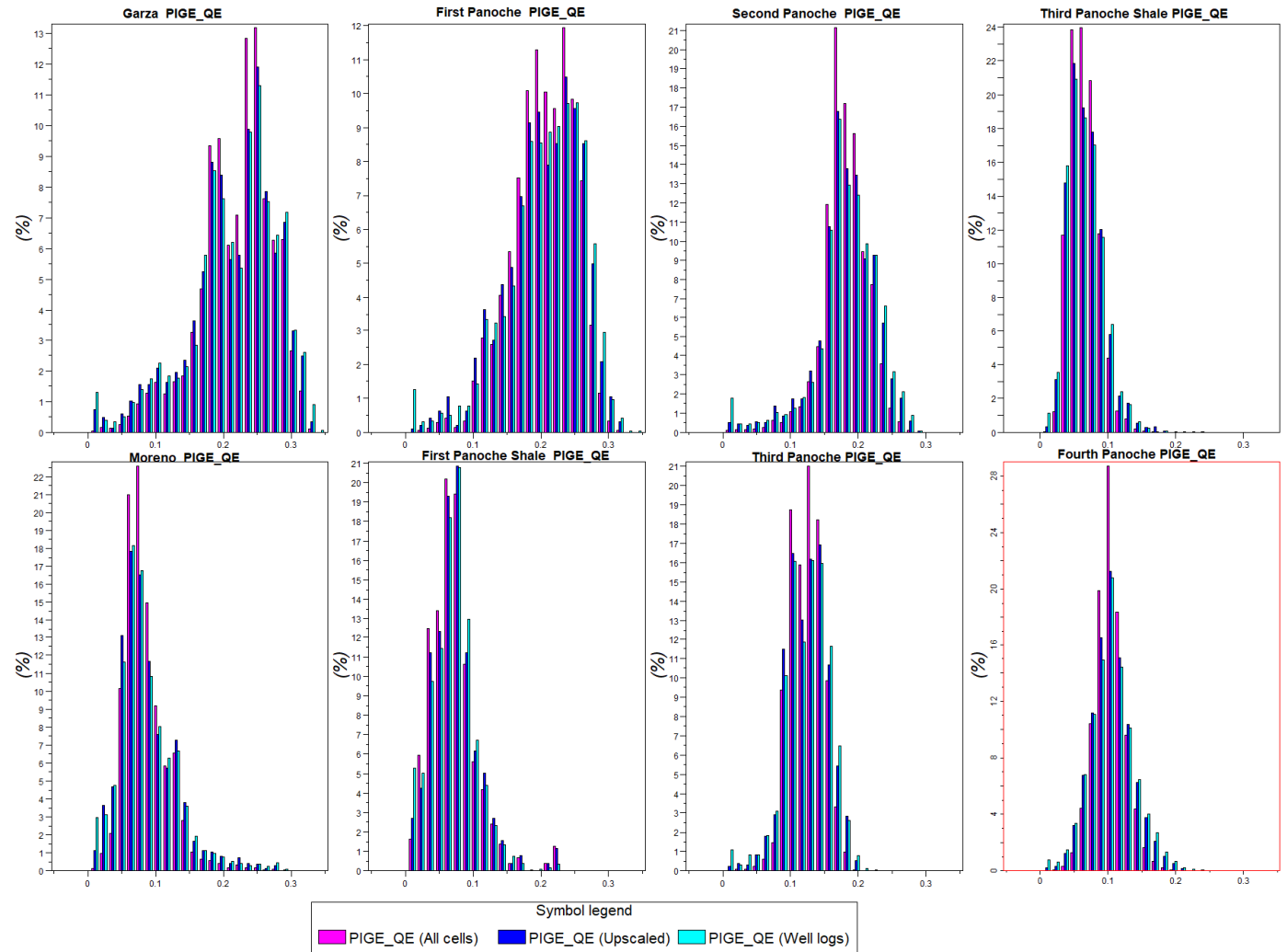


Figure 27: Porosity histograms of well logs, upscaled cells and model cells

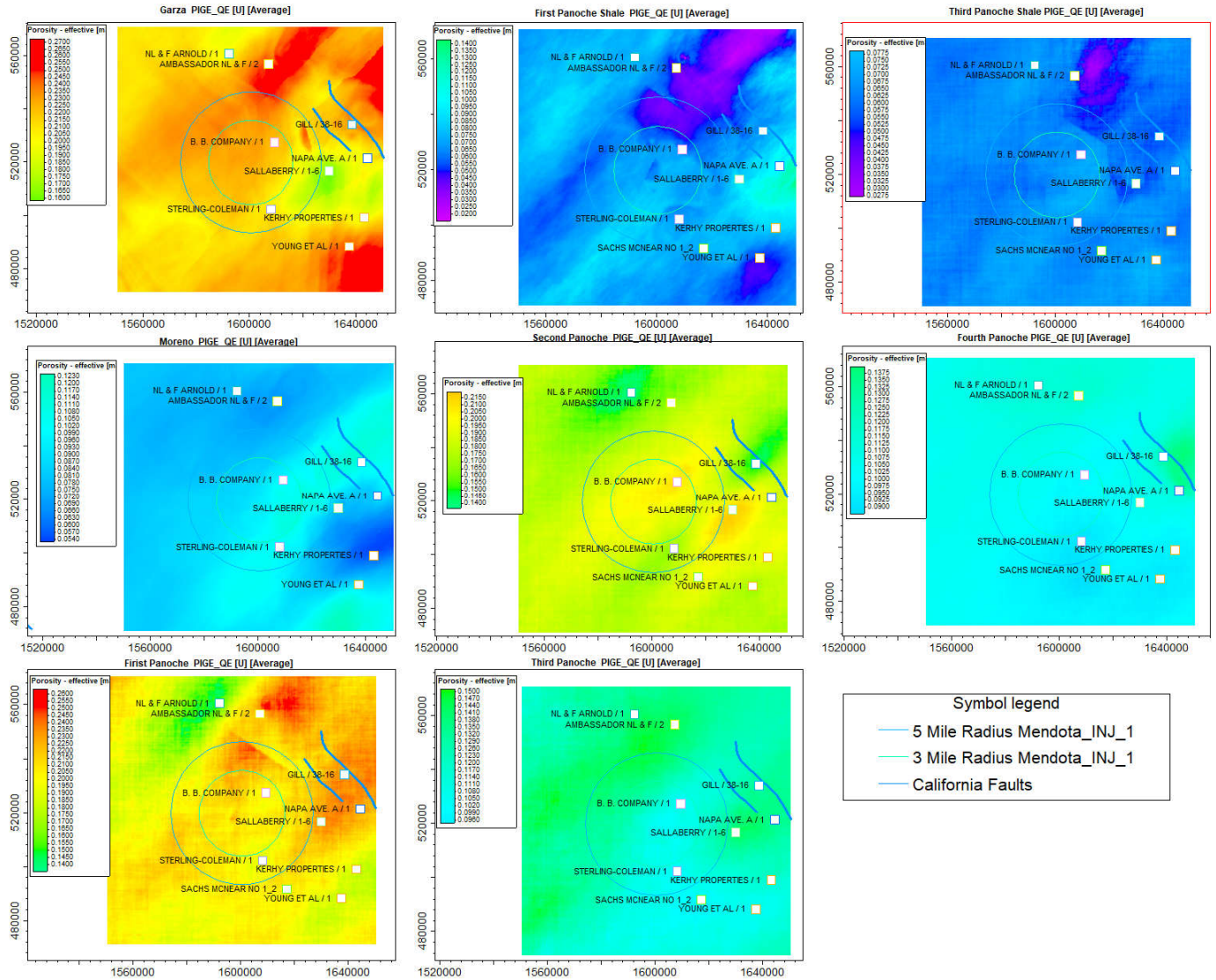


Figure 28: Modeled average porosity maps for each formation

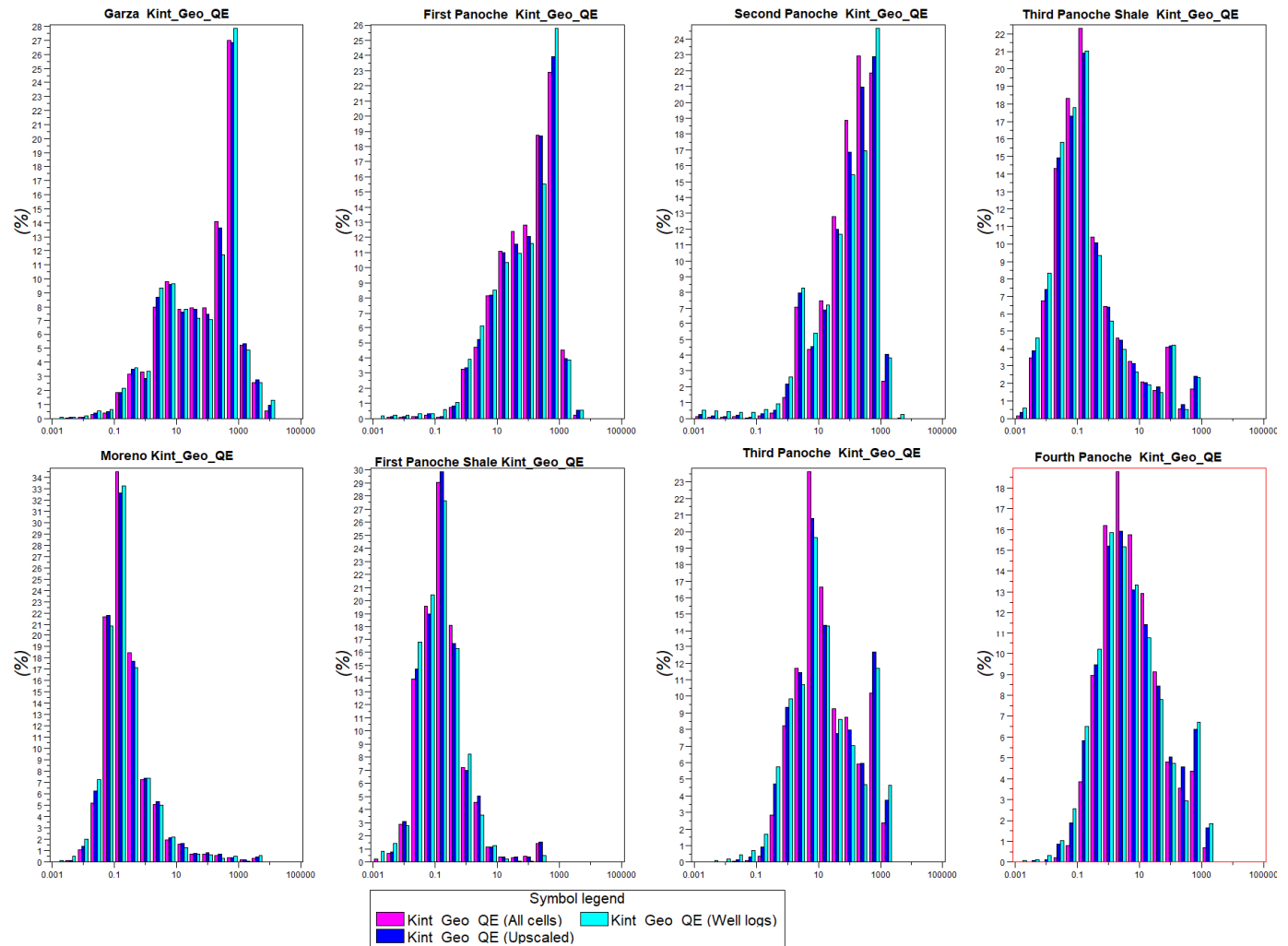


Figure 29: Permeability histograms of well logs, upscaled cells and model cells

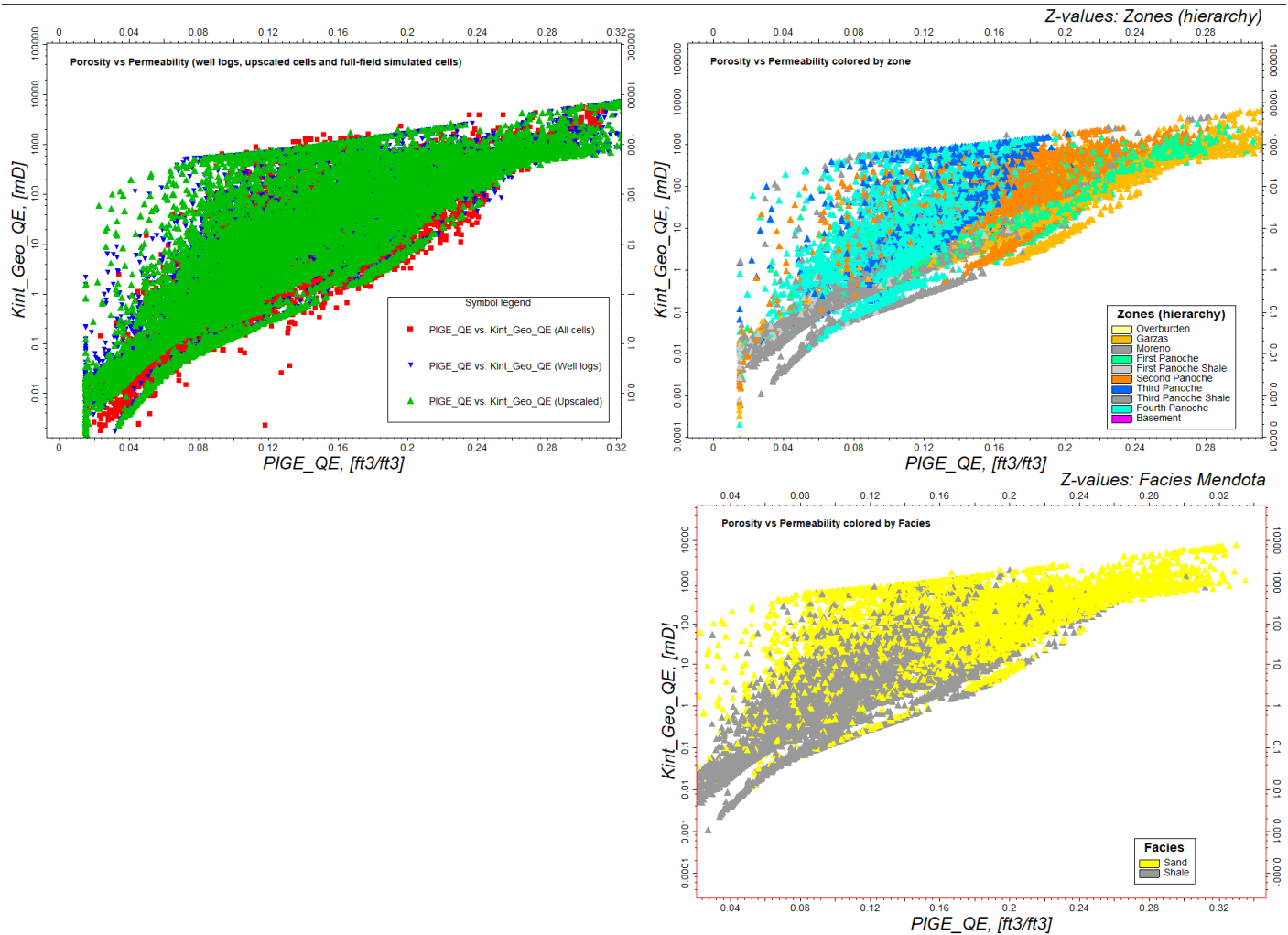


Figure 30: Porosity permeability cross plot of upscaled cells and model cells (left) and upscaled cells colored by formation

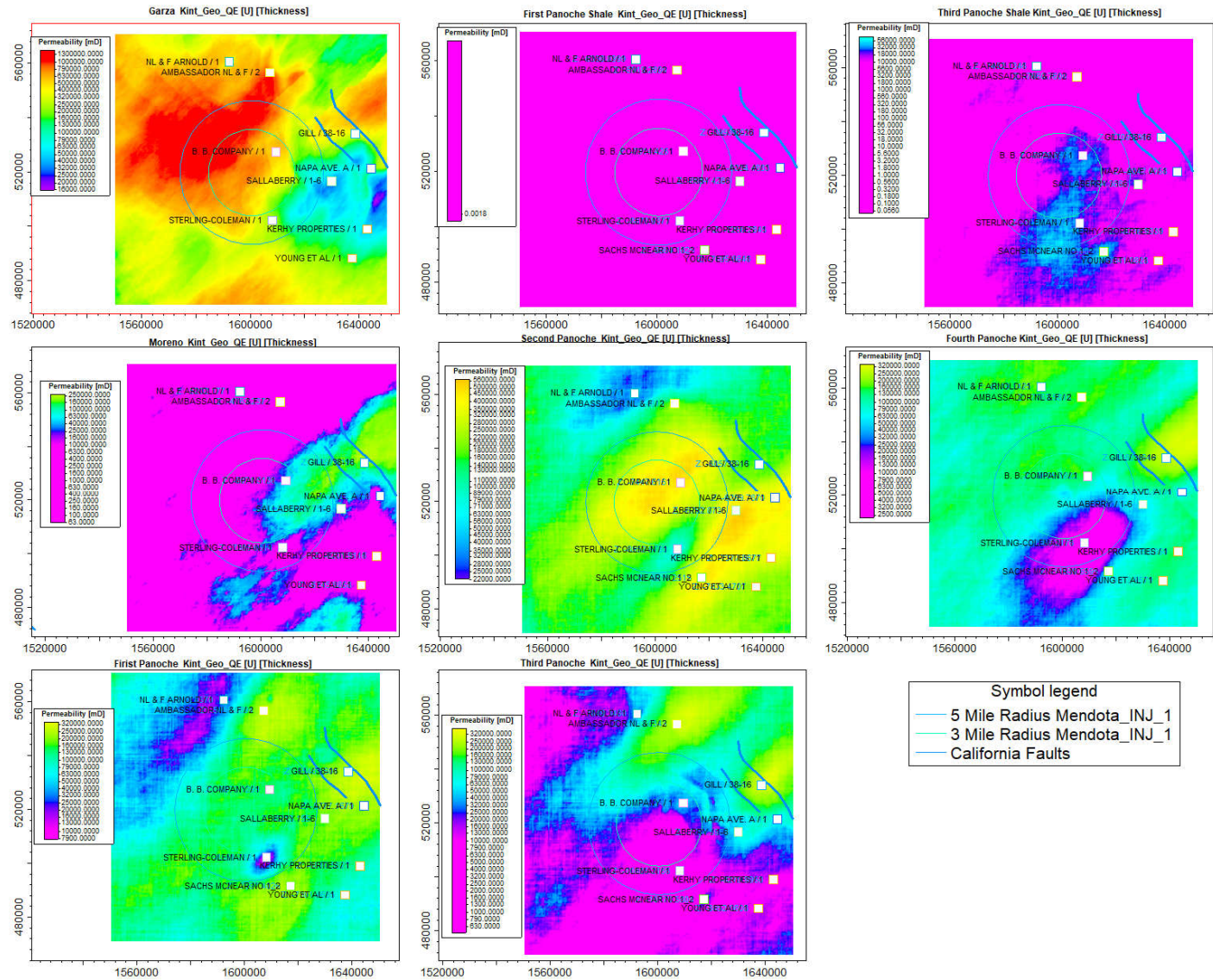


Figure 31: Modeled permeability thickness (KH) maps for each formation

Image Removed because it contains Confidential Business Information. This image will be sent directly to the EPA.

*Figure 32: **CONFIDENTIAL BUSINESS INFORMATION:** Injection well cross-section traverse map, N-S an E-W. This image displays (SEI, 2019) data and it is marked as Confidential Business Information.*

Image Removed because it contains Confidential Business Information. This image will be sent directly to the EPA.

Figure 33: **CONFIDENTIAL BUSINESS INFORMATION:** 3D Perspective of N-S and E-W porosity cross-sections at Mendota_INJ_1. This image displays (SEI, 2019) data and it is marked as Confidential Business Information.

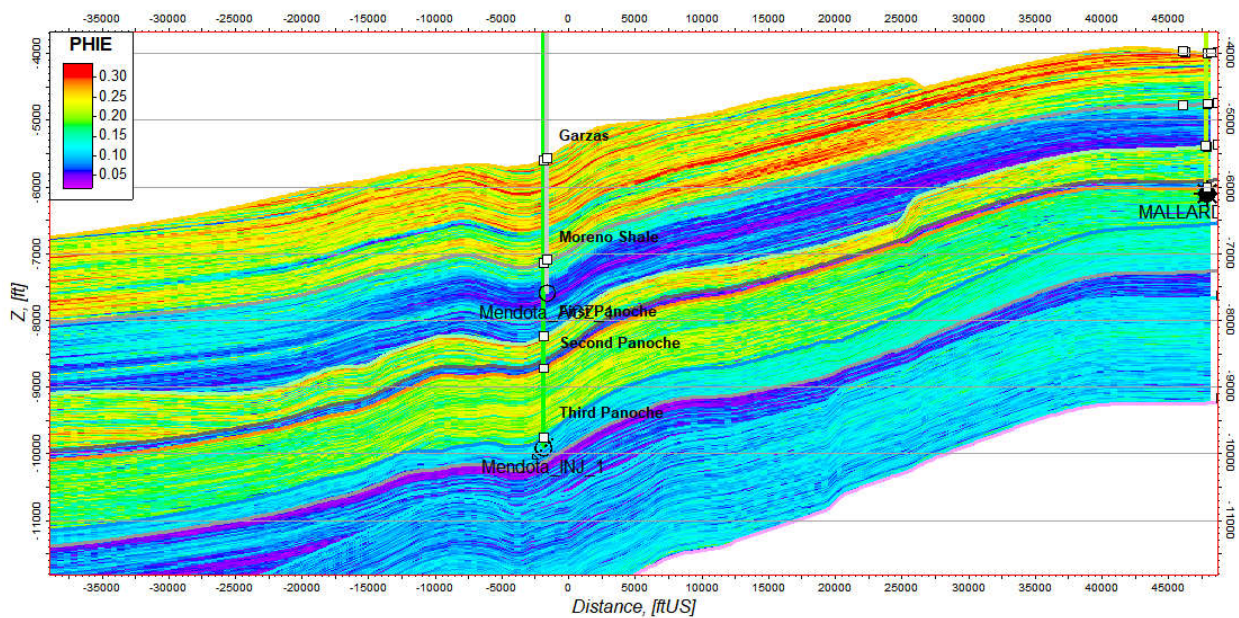


Figure 34: Effective Porosity Model Cross-section (N-S)

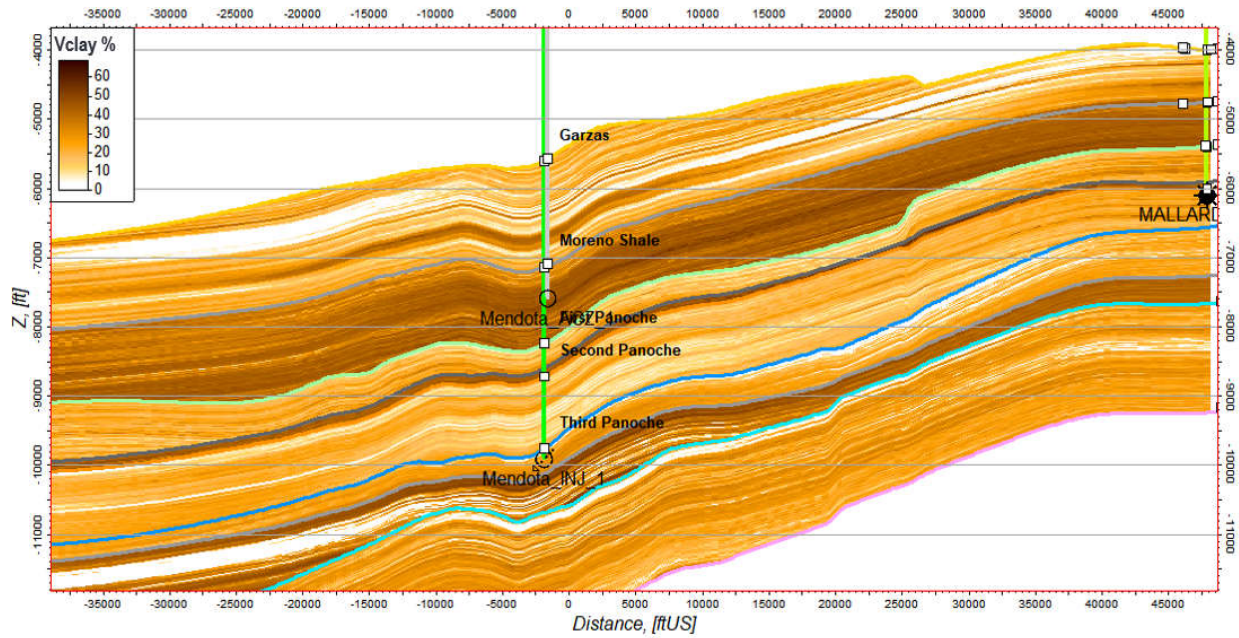


Figure 35: Volume clay model cross-section (N-S)

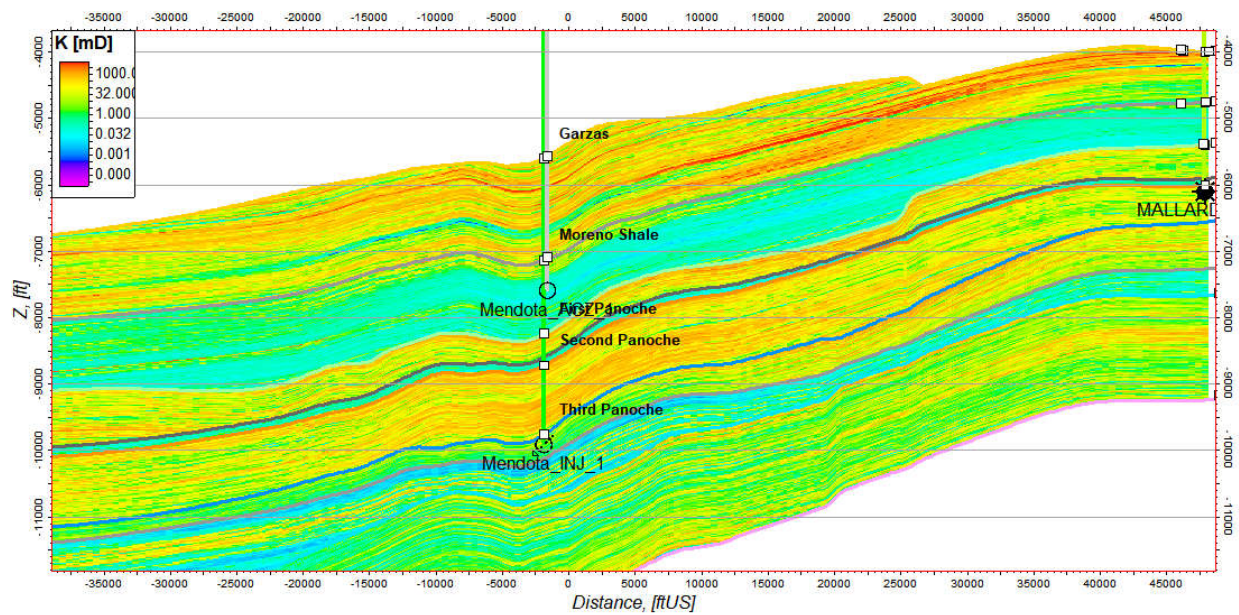


Figure 36: Permeability model cross-section (N-S)

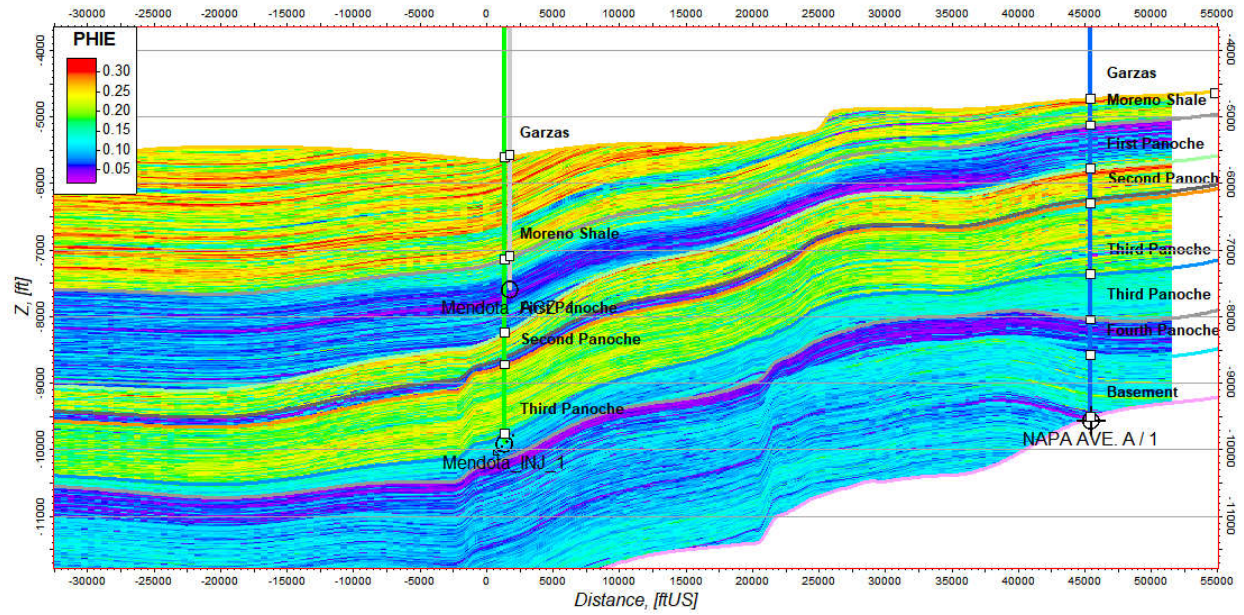


Figure 37: Effective porosity model cross-section (E-W)

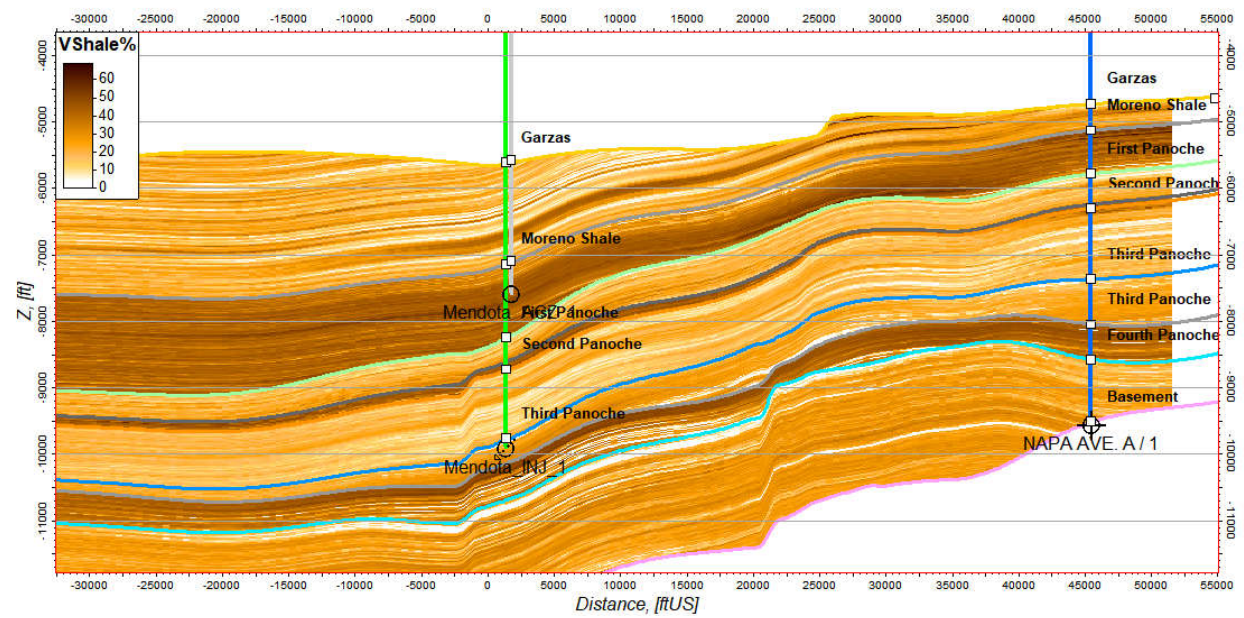


Figure 38: Volume Shale Model Cross-section (E-W)

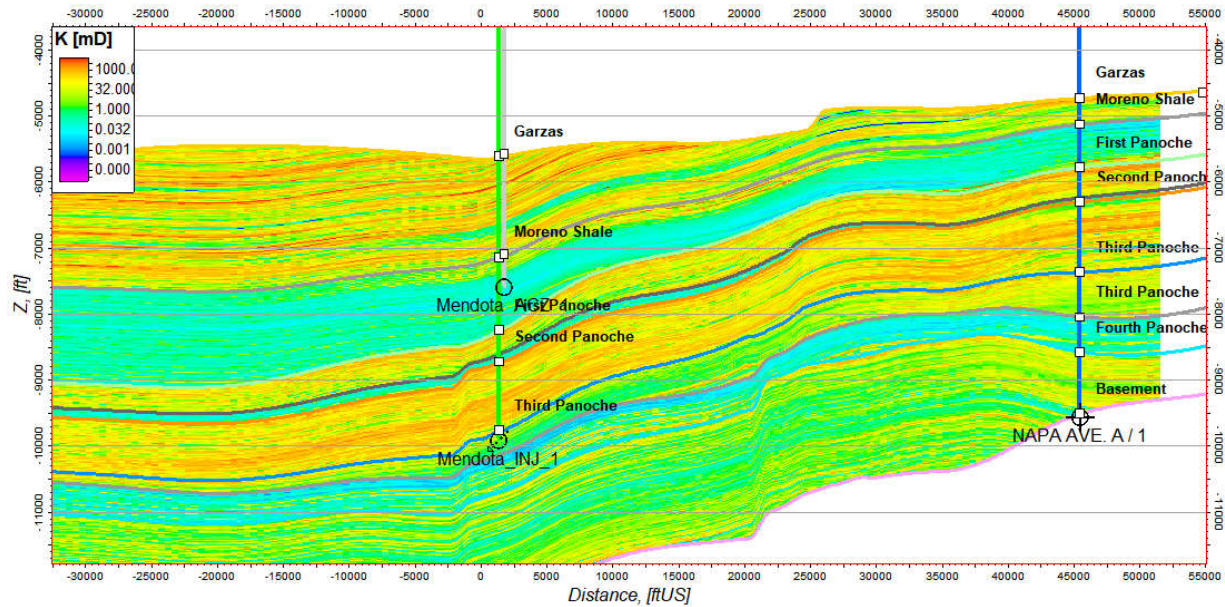


Figure 39: Permeability Model Cross-section (E-W)

2.4.4. Pre-Operational Testing Requirements

Because a characterization well has not yet been drilled, and 3D seismic was not included in this evaluation, there are many areas of uncertainty to be considered. The largest uncertainty is lateral thickness and homogeneity of injection targets. Additionally, without 3D seismic data the spatial extents and distribution of faulting is uncertain. Uncertainties can be better addressed in future iterations of modeling when newly acquired 3D seismic and 3D seismic inversion products become available, they will be integrated into the geomodel. Seismic elastic properties (Poisson's Ratio or V_p/V_s) and seismic inversion products (acoustic impedance and porosity) can be co-kriged to well data to guide extrapolation of petrophysical properties in the model domain where well data does not exist. Moreover, geomechanical log properties should be acquired in the new well to include anisotropic shear sonic for geomechanical analysis and for 3D stress analysis. This sonic data would also provide the basis for prestack seismic inversion to derive Poisson's Ratio or V_p/V_s from the 3D seismic. Further, fracture logs from wellbore images (FMI) can be used to calibrate parameterization of seismic discontinuity analysis for detailed fault and fracture delineation for developing a discrete fracture network (DFN).

Because of the absence of laboratory measurement currently, capillary pressure in the confining zone (shale) was determined using the Van Genuchten model. Detailed description of capillary pressure model and parameters applied to the model is found in (Schlumberger, Attachment B: Area of Review and Corrective Action Plan, 2020). Additional data that could help measure confinement zone integrity would include image log measurements (FMI) and drill stem test (DST) or Modular Dynamics Tester (MDT) stress testing information.

2.5. Geomechanical and Petrophysical Information [40 CFR 146.82(a)(3)(iv)]

The petrophysical properties of the confining Moreno shale is summarized in Section 2.4.2. The elastic properties at Mendota_INJ_1 were evaluated using the existing acoustic and density logs of nearby wells show in Figure 8. The average density in the Moreno Shale is 2.13 g/cc, and the average compressional slowness is 107 μ s/ft (Figure 40) based on well logs from NAPA AVE A 1. An empirical correlation (Han, 1986) was applied to derive the shear slowness due to the lack of shear measurements in available log data. The dynamic elastic properties including Young's Modulus and Poisson's Ratio are computed based on the density, compressional, and modeled shear slownesses. The average dynamic Young's Modulus and Poisson's Ratio in Moreno Shale is 1.9 Mpsi and 0.29 (Figure 40). Due to the lack of core measurements from laboratory, there is no specific core data for the rock strength and ductility. (Chanchani, 2003) has measured rock mechanical properties of the Antelope Shale in Buena Vista Hills field with unconfined compressive strength in the range of 92 to 126 MPa (13-18kpsi). Shales are typically more ductile than sand or limestone at the same confining pressure. (Winters, 1987) shows that the ductility in Shale can be 1.5% at a confining pressure of 5000psi. The geomechanical properties of the confining zone including the elastic properties, rock strength, and ductility can be measured in the laboratory using the triaxial compressional test.

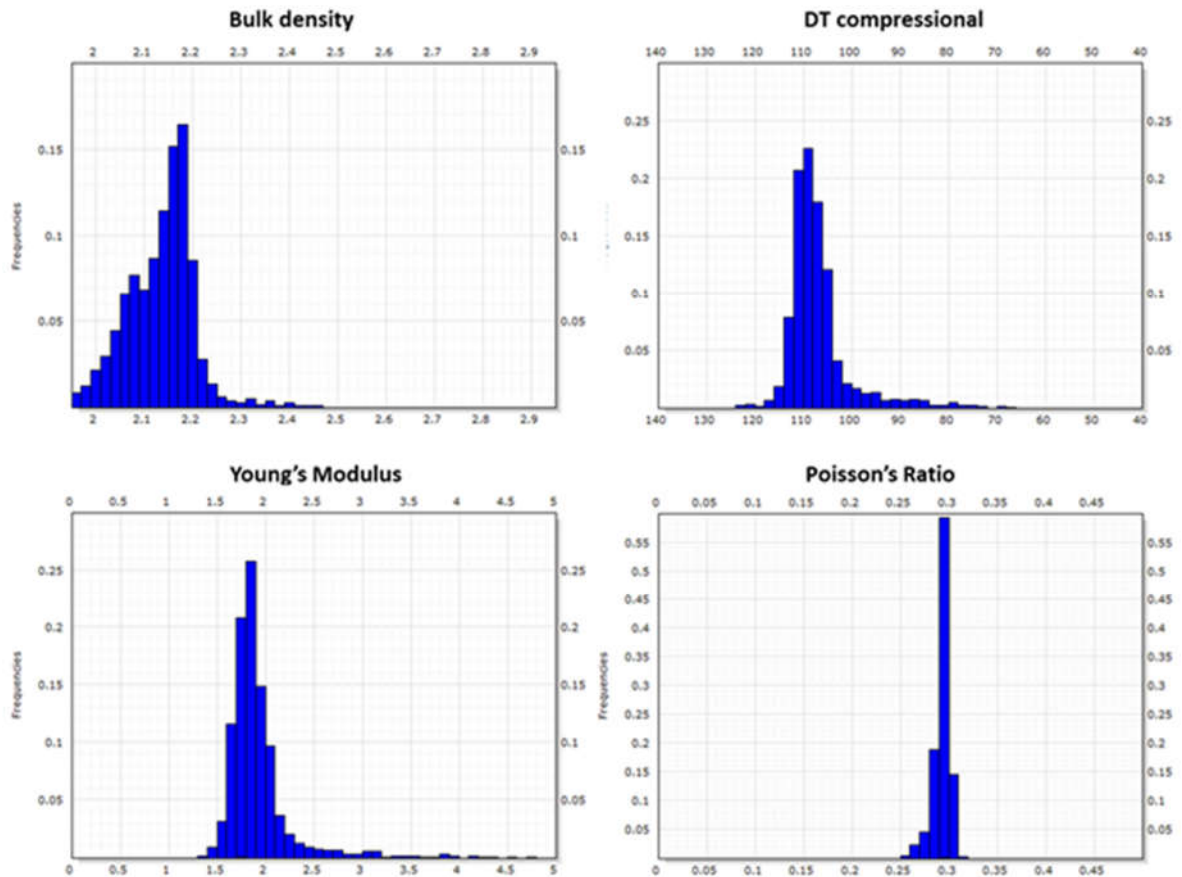


Figure 40: Density, acoustic, and elastic properties in Moreno Shale

The amount of fracturing in the injection formation is not known at this time because of the lack of borehole image logs and 3D seismic. In future phases of this project, borehole image logs will be acquired and used with 3D seismic to determine the intensity of fractures in a discrete fracture model (see Faults and Fractures [40 CFR 146.82(a)(3)(ii)]).

There are no direct measurements for in-situ stress. The in-situ stress field consists of three components: vertical stress, minimum horizontal stress, and maximum horizontal stress. The vertical stress can be determined by integrating the density of the rock above the depth of interest. Based on the available density logs in the area, the average density of the overburden rock is estimated to be 2.18 g/cc (or 0.94 psi/ft). The minimum horizontal stress (S_{hmin}), which is typically the minimum principal stress, can be measured using minifrac or extended leak-off tests. The maximum horizontal stress (S_{hmax}) can be obtained using different methods including the modeling of wellbore failure features such as drilling induced tensile fractures or borehole breakout and the breakdown pressure from hydraulic fracture (Zoback, 2003; Vernik, 1989). In addition to the stress magnitude, the orientation of the maximum horizontal stress can be determined from the borehole image logs based on the drilling induced fracture and/or breakout. The world stress map indicated a maximum horizontal stress direction of north 40 to 57° east based on earthquake focal mechanism and wellbore failure features. The in-situ stress field will

be better characterized in the next phase of this project after collecting the pilot hole logs and well tests data.

The stability and sealing capacity of the faults is also not clearly understood at this time because of limited site-specific data. A characterization well planned for the pre-operation phase of this project will include collecting important geomechanical information. These data will include geomechanical core analysis, pilot hole logs, and well test data. These data will be combined with 3D seismic data to build a 3D geomechanical model and to provide a better characterization of the in-situ stress field, pore pressure, rock strength and 3D fault characterization for the fault stability analysis and sealing capacity of these faults (Chiaramonte, 2008). The analysis will be conducted at this time.

A normal pore pressure gradient was assumed at this point without additional well test data. Initial reservoir pressure was collected from nearby oil and gas field (<20 mile) reported in (California Department of Conservation, 1998). Pressure gradient of 0.4339 psi/ft is estimated based on the data (Schlumberger, Attachment B: Area of Review and Corrective Action Plan, 2020).

2.6. Seismic History [40 CFR 146.82(a)(3)(v)]

Because California is situated along the Pacific and North American plate boundary, the region experiences a significant earthquake activity. Figure 41 shows general earthquake activity and risk in relation to the Mendota site (CEMA, 2010). The relative risk of the proposed site is low compared with the active zones associated with major faulting.

Historical earthquake data was obtained from the USGS Earthquake Hazards database and imported into Petrel for analysis (USGS, Earthquake Hazards Program, 2019). All area earthquakes with a magnitude greater than 2.5 occurring since 1900 were taken into consideration for risk analysis.

Figure 42 shows the major fault systems in the region associated with primary earthquake activity and a map showing the USGS earthquake data highlighting the position of earthquake locations by relative strength in relation to the AoR. A narrow lineament of quake activity is associated with the San Andreas Fault located approximately 40 miles Southwest of Mendota_INJ_1.

A cluster of smaller quakes less than 5.0 magnitude (denoted in by the red circle in Figure 42) occur historically along an extension of the San Joaquin and Ortigalita fault systems trending NW-SE offset approximately 15 to 20 miles south and west of the AOR. The largest proximal quake in the area was the Coalinga Quake with a magnitude 6.7 on May 2nd, 1983 located approximately 36 miles south of the AoR (USGS, 1983).

The AoR is positioned in a comparatively tectonically quiet area near the center of the San Joaquin Basin. Most activity occurs along the margins of the basin and principally associated with tectonically induced faulting. The local earthquake activity near the AoR is shown in

Figure 43 with the magnitude, depth and date annotated. Only very low magnitude quakes have occurred near the AoR (none within 3 miles) and three on the 5-mile radius periphery. A summary of the local quakes shown in this map is shown in Table 5.

The exact magnitude and proximity required for an earthquake to have disruptive impacts on CO₂ plume containment is unknown at this time. Various factors such as local stresses and fracture networks will need to be considered and are a source of uncertainty. Future iterations of modeling should integrate newly acquired geomechanical information (dipole sonic logs), FMI image logs (Section 8) and possibly micro-seismic monitoring to better address uncertainties regarding local tectonics and stress. The historical earthquake activity near the Mendota site is sparse with low magnitude (the largest of which is ~3.52). Given to the relatively distal proximity to major fault and earthquake activity a low risk of quakes is inferred within the AoR.

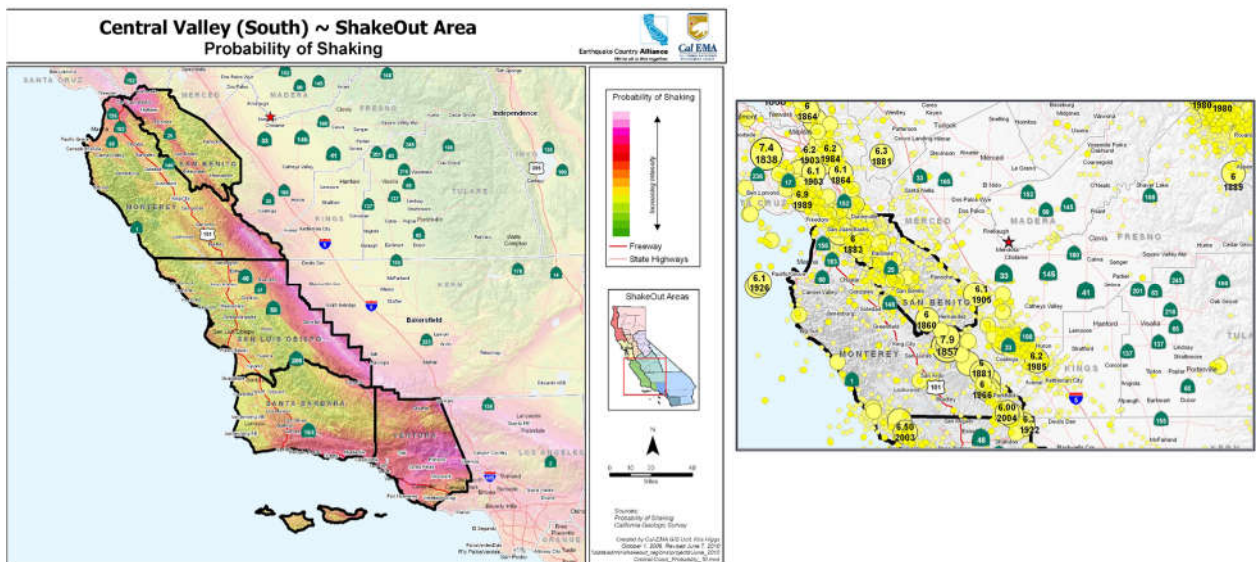


Figure 41: Relative earthquake risk (left) and earthquake map from the CEMA GIS unit (Right). The red star is the location of the Mendota site. (CEMA, 2010)

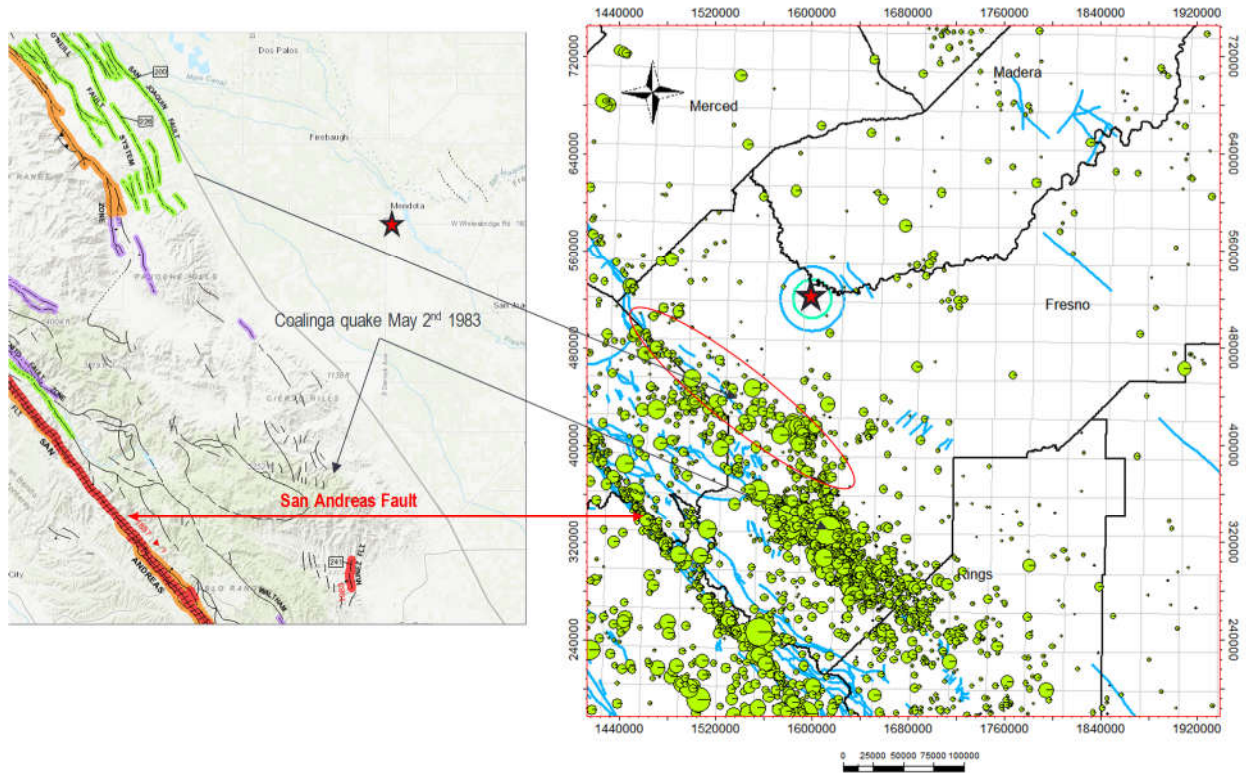


Figure 42: Regional faulting from the Department of Conservation (left) (USGS, U.S. Quarternary Faults, 2019) and Regional USGS Earthquake History (right) - quakes with magnitudes greater than 2.5 since 1900. (USGS, Earthquake Hazards Program, 2019)

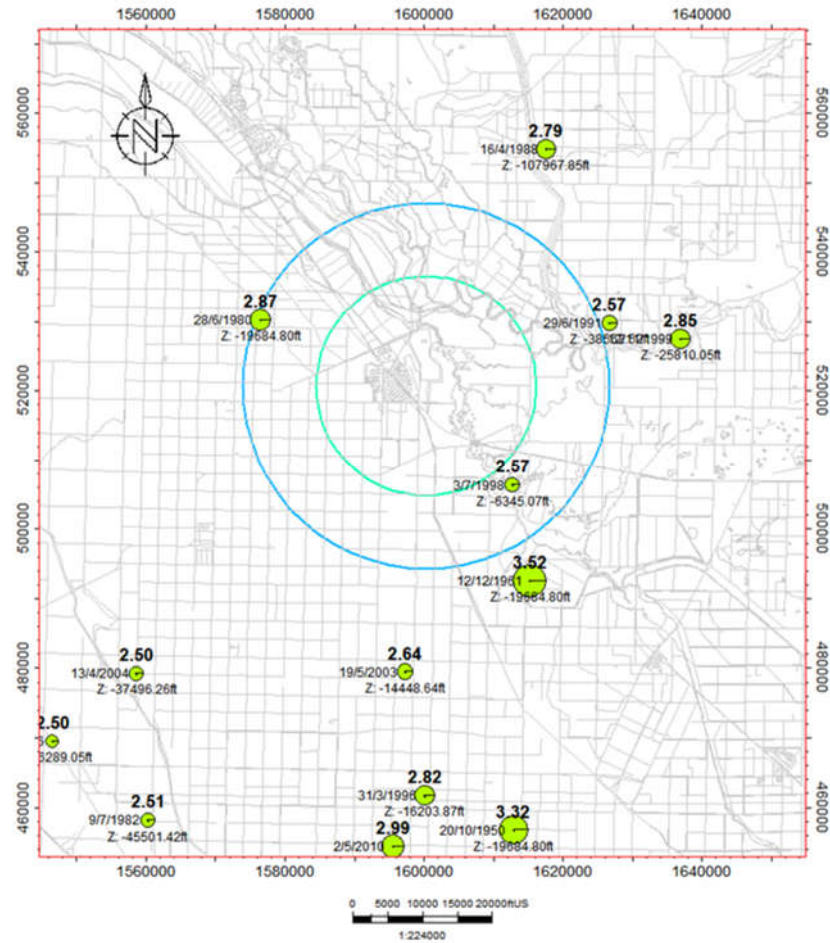


Figure 43: Historical earthquakes near AoR greater than 2.5 since 1900.

Table 5: Historical earthquakes near AoR greater than 2.5 since 1900.

Time	Z (ft)	latitude	longitude	depth (Km)	mag	mag Type	nst	gap	dmin	rms	horiz Error	depth Error	mag Error	mag Nst
2010-05-02T17:37:00.250Z	-38857.8	36.5735	-120.377	11.844	2.99	ml	168	36	0.1937	0.29	0.26	0.6	0.25	17
2006-05-04T16:35:36.810Z	-26289.1	36.613	-120.545	8.013	2.5	md	60	86	0.2063	0.22	0.51	0.84	0.08	35
2004-04-13T11:00:56.760Z	-37496.3	36.6402	-120.504	11.429	2.5	md	84	67	0.2333	0.2	0.23	0.77	0.12	60
2003-05-19T01:33:32.960Z	-14448.6	36.6423	-120.373	4.404	2.64	md	5	195	0.5649	0.08	3.44	10		1
1999-11-12T04:29:08.860Z	-25810.1	36.7758	-120.24	7.867	2.85	md	6	206	0.5333	0.53	8.95	18.84	0.07	4
1998-07-03T12:59:44.310Z	-6345.07	36.7168	-120.321	1.934	2.57	md	5	164	0.3829	0.04	1.25	8.06	0.11	5
1996-03-31T17:39:22.390Z	-16203.9	36.5937	-120.362	4.939	2.82	md	6	138	0.4117	0.15	4.14	14.13	0.19	3
1991-06-29T23:26:16.560Z	-38562.5	36.7817	-120.275	11.754	2.57	md	21	127	0.4333	0.67	5.18	9.4	0.07	8
1988-04-16T16:30:51.830Z	-107968	36.8502	-120.307	32.909	2.79	md	4	188	0.4243	0.1	1.96	11.41	0.26	9
1982-07-09T03:56:31.870Z	-45501.4	36.5823	-120.498	13.869	2.51	md	58	119	0.2514	0.16	0.25	0.91	0.12	42
1980-06-28T06:40:16.010Z	-19684.8	36.781	-120.446	6	2.87	mh	3	236		0.6	12.68	31.61	0.124	8
1961-12-12T20:38:34.060Z	-19684.8	36.679	-120.312	6	3.52	ml	8	275	1.425	0.7	4.49	31.61	0.188	9
1950-10-20T08:23:20.370Z	-19684.8	36.5805	-120.319	6	3.32	ml	4	332	2.191	0.5	4.57	31.61	0.041	7

2.7. Hydrologic and Hydrogeologic Information [40 CFR 146.82(a)(3)(vi), 146.82(a)(5)]

2.7.1. Depth to the Deepest USDWs – 40 CFR 146.93(c)(1)(x)

The protection of USDW is a primary objective of any CCS project; in order to protect the USDWs, it is important to know how deep they are in the AoR. A USDW is defined as any formation that has formation water with less than 10,000 ppm TDS. At Mendota, this depth is estimated to be at 1,415 ft TVDSS. This depth was calculated by using the resistivity logs of 5 wells near the Mendota site. The resistivity image logs were digitized, and Archie's equation was used to estimate the resistivity of the water (R_{wa}) using standard parameters and a porosity of 0.35 pu. R_{wa} was then converted to an estimated water salinity.

Matheson 1 and Amstar 1, 0.5 miles and 1.5 from the Mendota site respectively, had resistivity logs above the estimated Base of Fresh Water (BFW) recorded in the California Division of Oil, Gas and Geothermal Resources (DOGGR) well data sheets (Figure 44) (DOGGR, 2019). California DOGGR define BFW as less than 3,000 ppm salinity. There is reasonable agreement of water salinity around 3,000 ppm for the estimated BFW of Matheson 1 and Amstar 1. The calculated water salinity indicates the base of USDW for the five wells near Mendota between 1,200 to 1,450 feet TVDSS. The largest uncertainties in the water salinity estimate are formation porosity, Archie equation parameters and the effect of clay that may be present. Using a lower estimated porosity would raise the estimated water salinity where clay may reduce the estimate. The USDW will need to be verified by sampling in the characterization well. The wells used and estimated water salinity for the five wells used are shown in Figure 45 below.

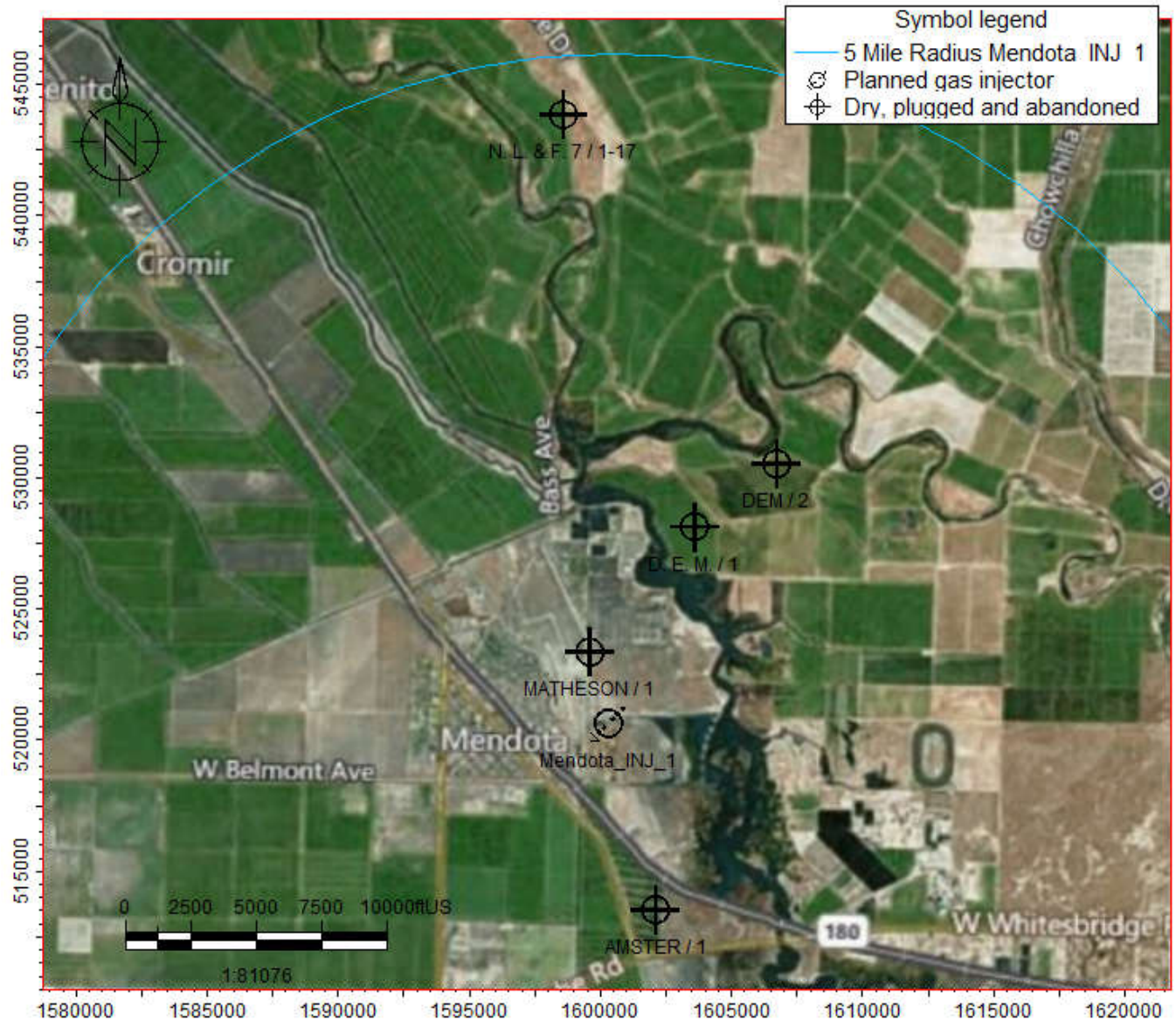


Figure 44: Wells used to calculate the depth to the deepest USDW

Image Removed because it contains Confidential Business Information. This image will be sent directly to the EPA.

*Figure 45: **CONFIDENTIAL BUSINESS INFORMATION:** USDW estimated using resistivity measured in wells near the Mendota site. This image displays (IHS, 2019) data and it is marked as Confidential Business Information.*

Additionally, the California Oil & Gas Fields field data sheets published for nearby fields show information of formation water salinity for some formations and estimated BFW for the field. The published water salinity for the Eocene and Cretaceous formations generally range between 17,100 and 26,500 ppm. The exceptions were the Jergins formation at Cheney Ranch and Blewett formation at Merrill Ave. The Jergins and Blewett formations are in the Moreno formation and have published salinities of 8,500 and 15,000 ppm respectively. The wells near Mendota do not show lower water salinities based on the resistivity response for sands in the Moreno formation but have been identified as a potential risk. The salinities for permeable formations near the Moreno formation will need to be verified by sampling in the characterization well.

2.7.2. Local Near Surface Groundwater

The characteristics of water wells and the piezometric elevation of the near surface shallow groundwater was evaluated. Figure 46 shows the location of all active and non-active water wells in the area. These wells include water supply well, monitoring wells, water wells and abandoned wells. At the Mendota_INJ_1, the depth to the deepest USDW is estimated to be ~1609 ft bgs (~1411 ft SSTVD; Section 2.7.1); this is 7,165 ft above the top of the Second Panoche injection formation.

These public data were downloaded from (California Department of Water Resources, n.d.). The surface elevation of these wells was not available; therefore, the surface elevations were

estimated from the digital elevation model of the area. The location of these wells is not accurate because they were originally reported in a legal land description format; therefore, they all plot in the middle of a section and line up in an organized grid pattern. In future phases of this project, accurate locations of these water wells will be provided. There were 525 of these water wells within a 5 mile radius of Mendota_INJ_1. These wells range in depth from approximately 50 feet to 500 feet. The recorded water levels were filtered to determine the piezometric elevation of the shallowest groundwater zone within a 5-mile radius of Mendota_INJ_1. These recoded water levels were the water levels at the time of drilling; therefore, they do not take into account seasonal or annual variations in water levels. It does provide a reasonable representation of shallow groundwater elevation and flow direction (Figure 47). At the Mendota site, the shallowest groundwater is ~32 ft bgs (~114 ft SSTVD). The San Joaquin River flows north south and is 0.6 miles east of the site. In future phases of this project, a more detailed evaluation of surface groundwater will be completed. Within the AoR as defined in (Schlumberger, Attachment B: Area of Review and Corrective Action Plan, 2020), there are 67 groundwater wells (monitoring wells, water wells etc.) 7 of which are domestic water supply wells, 27 are water wells used for irrigation.

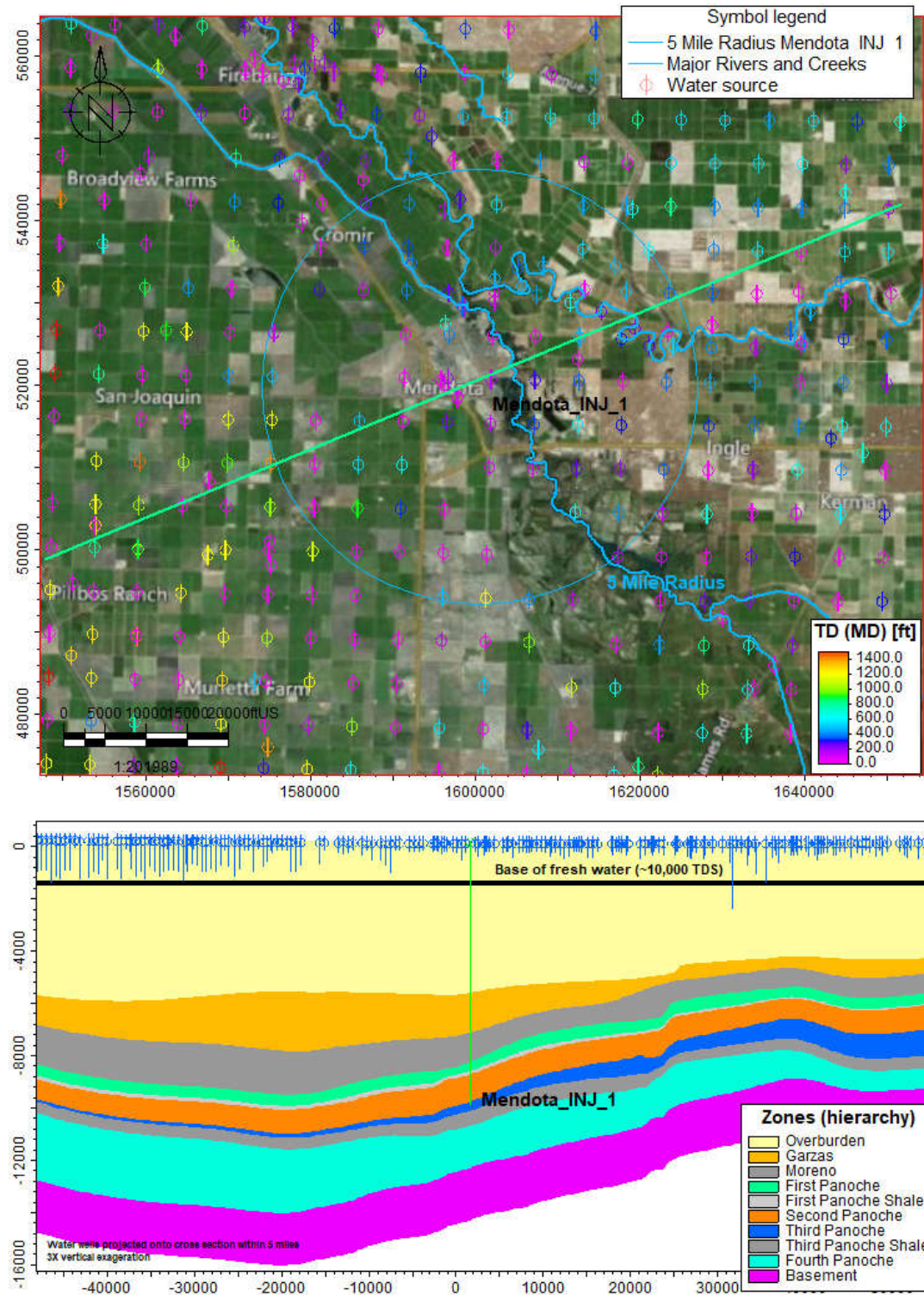


Figure 46: Water well and surface water

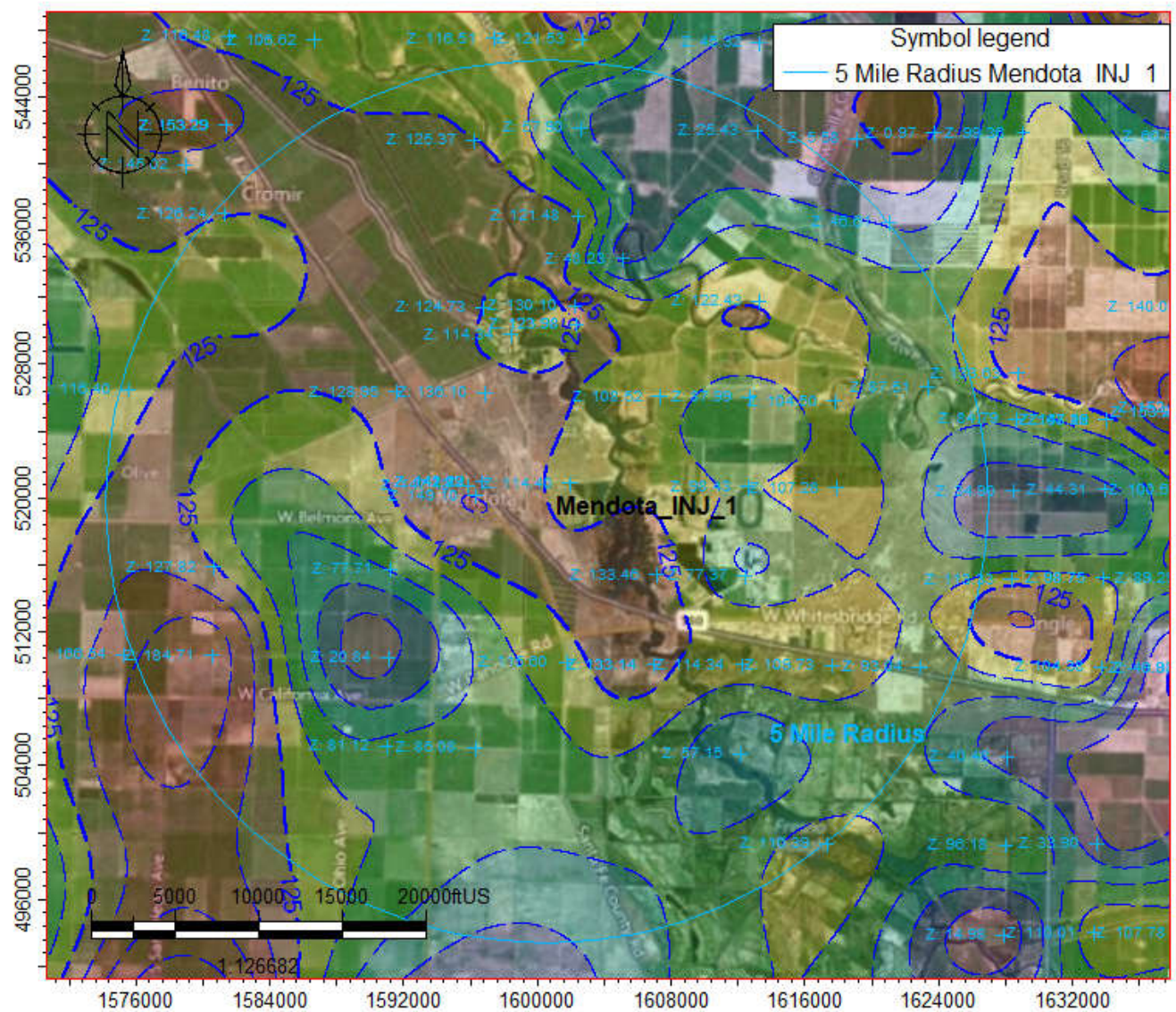


Figure 47: Potentiometric map of the approximate shallowest groundwater surface

2.8. Geochemistry [40 CFR 146.82(a)(6)]

2.8.1. Characteristics of Injection Zone Formation Water

There was no available formation water information in the target Panoche sands at the proposed storage site; however, several oil and gas fields nearby produced from the Cretaceous Panoche Formation and overlying formations and provide salinity of the brine and related information. Available data on water quality from the wells near the proposed site are listed in Table 6.

Table 6: Salinity of the formation waters from the oil and gas fields near the proposed Mendota site (California Department of Conservation, 1998)

County	Field	Formation	Depth (ft)	Salinity (ppm)	TDS (ppm)
Fresno	Raisin City	Miocene	5,080	44,000	44,200
Fresno	Moffat Ranch	Eocene	3,900	26,500	
Fresno	Gill Ranch	Eocene	4,430	25,700	42,000
Fresno	Raisin City	Eocene	8,450	22,300	22,500
Fresno	San Joaquin	Eocene	7,000	21,100	
Fresno	Cheney Ranch	Moreno	7,000	8,500	14,000
Fresno	Gill Ranch	Panoche	5,850	20,000	20,900

The Gill Ranch gas field is approximately 6.5 miles northeast to Mendota. There are wells penetrated through the Fourth Panoche sand and the basement at about 9000 ft bgs. Salinity of the water from the First Panoche sand is 20,000 ppm (NaCl). Total dissolved solids (TDS) is at 20,900 ppm, close to salinity, suggesting Na-Cl dominated water chemistry. Salinity from the rest of the Upper Cretaceous is similar to the Panoche Formation. The Panoche Formation is also penetrated at the Moffat Ranch gas field 8.5 miles north to Mendota; however, no water chemistry data is available. The salinity tends to increase to the west away from the recharge area (Gillespie, 2017). A slightly higher salinity around 25,000 ppm is expected in the Panoche Formation at the proposed site.

Salinity in the Eocene at the Gill Ranch field is reported as 25,700 ppm and 26,500 ppm at Moffat Ranch field somewhat higher than the Panoche formation water in those fields. TDS in the Eocene is much higher at 42,000 ppm at the Gill Ranch, suggesting significant change of water chemistry.

The Miocene Zilch Formation has higher salinity 44,000 ppm (NaCl) at the Raisin City oil field which is 16 miles southeast to Mendota. TDS is reported at 44,200 ppm, suggesting Na and Cl-dominated water composition.

The Cheney Ranch gas field approximately 12 miles southwest to Mendota reports formation water in the Jergins Sand at the bottom of the Moreno Formation overlying the Panoche Formation with salinity of 8,500 ppm and TDS of 14000 ppm. Review of the resistivity logs from wells in the AoR do not indicate a sand with formation water fresher than the Panoche Formation, but it has been recognized as a potential risk. The planned testing program for the characterization well includes formation water sampling for the Panoche and overlying sands (Schlumberger, Attachment G: Construction Details Clean Energy Systems Mendota, 2020).

2.8.2. Mineral Composition of The Injection Zone

The Cretaceous Panoche Formation sandstones are the target CO₂ sequestration storage zones (between 7000 and 10000 ft), with the overlying Moreno shale acting as a confining seal. The Panoche formation consists of deep-marine shale and submarine fan deposit intervals (McGuire, 1988). A core description was available for the interval 11,422 to 11,471 ft corresponding to the 4th Panoche sand in the B.B. Co 1 well, which is within 2.5 miles of the proposed storage site. Conglomerate and sandstones are identified in the core. The sandstones are mostly composed of fine to coarse grained, poorly sorted quartz and feldspar grains and locally well cemented by calcite. Biotite is abundant with small amounts of chlorite and muscovite. Trace amounts of pyrite are also present. Both tuff interbeds and tuffaceous matrix is noted in the sandstone below 11,430 ft. Weathered volcanic rock fragments are also noted and likely contain abundant feldspar minerals and quartz. Based on the core description, a generalized mineral composition of the sandstones is proposed for geochemical modeling (Table 7).

Table 7: Estimated mineral composition (wt. %) for the Panoche Formation used in geochemical modeling

Quartz	K-feldspar	Plagioclase	Calcite	Pyrite	Muscovite	Chlorite	Illite	Kaolinite
60	10	15	4.5	0.5	2	2	6	Trace

2.8.3. Composition of the Injectate

The gas stream for injection will contain 96.78% CO₂ with some impurities (Table 8). O₂ is the most notable impurity at 1.15% because it is reactive when redox sensitive minerals are present in the formation. It also requires surface and well components which are resistant to that environment. To understand its effect, O₂ is included in the geochemical models.

Table 8: Composition of the injectate (Mass Fractions)

H ₂ O	0.002245
O ₂	0.011536
H ₂	0.000164
N ₂	0.001475
CO	0.005322
CO ₂	0.967834
Ar	0.01119
NO	9.01E-05
NO ₂	9.03E-08
H ₂ S	0.000144
NH ₃	1.93E-10

2.8.4. Geochemical Modeling Setup

Geochemical modeling is conducted using the React module of Geochemist's Workbench version 12 software and the resident thermo database to predict the reaction paths between the rock-forming minerals, the formation water, and injectate. A solution of TDS 25,154 mg/kg was constructed by equilibrating a NaCl solution with minerals (quartz, K-feldspar, albite, calcite, illite, kaolinite, muscovite, and chlorite) in the React module of Geochemist's Workbench (Table 9). Initial pH in models is set to be at neutral (Table 9). Mineral composition used in the models is estimated from the core description of the B.B. Co. 1 well (Table 7). The mineral reaction rate constants from Palandri and Kharaka (2004) are applied to the models. CO₂ and O₂ with a ratio of 100:1 are added into the system. The modeling is set at 70°C and run for 5 years. The simulation duration can be changed in the model, but it does not alter reaction paths.

Table 9: Chemical composition of the initial solution for geochemical modeling

Element	Concentration (mg/kg)
Al	0.00553
Ca	0.183
Cl	13,300
Fe	0.0355
H	1.09
HCO ₃	2,340
K	63.8
Mg	0.839
Na	9,440
SO ₄	20
SiO ₂ (aq)	29.1
TDS	25,154

2.8.5. Simulated Reaction Pathways

CO₂ dissolving into the brine produces carbonic acid which dissociates into bicarbonate and carbonate ions, HCO₃⁻ and CO₃²⁻ and lowers the brine pH. A series of mineral reactions are initiated from the drop of pH. The results show several minerals (e.g. calcite, pyrite, albite, K-feldspar, and illite, in a decreasing order in the amount of dissolution) are dissolved, while others (e.g. anhydrite, quartz, hematite kaolinite, muscovite, and dolomite, in a decreasing order in the amount of precipitation) precipitate in the simulation (Figure 48). The dominant mineral reactions include dissolution of calcite, pyrite, albite, illite, K-feldspar and chlorite (chamosite). Correspondingly, the components in the solution also evolve along the simulation process (Figure 49). The dominant change is increasing HCO₃ concentration with slight increases in H⁺, Ca, SO₄, SiO₂(aq), and Mg. Cl, Na, and K decreasing slightly.

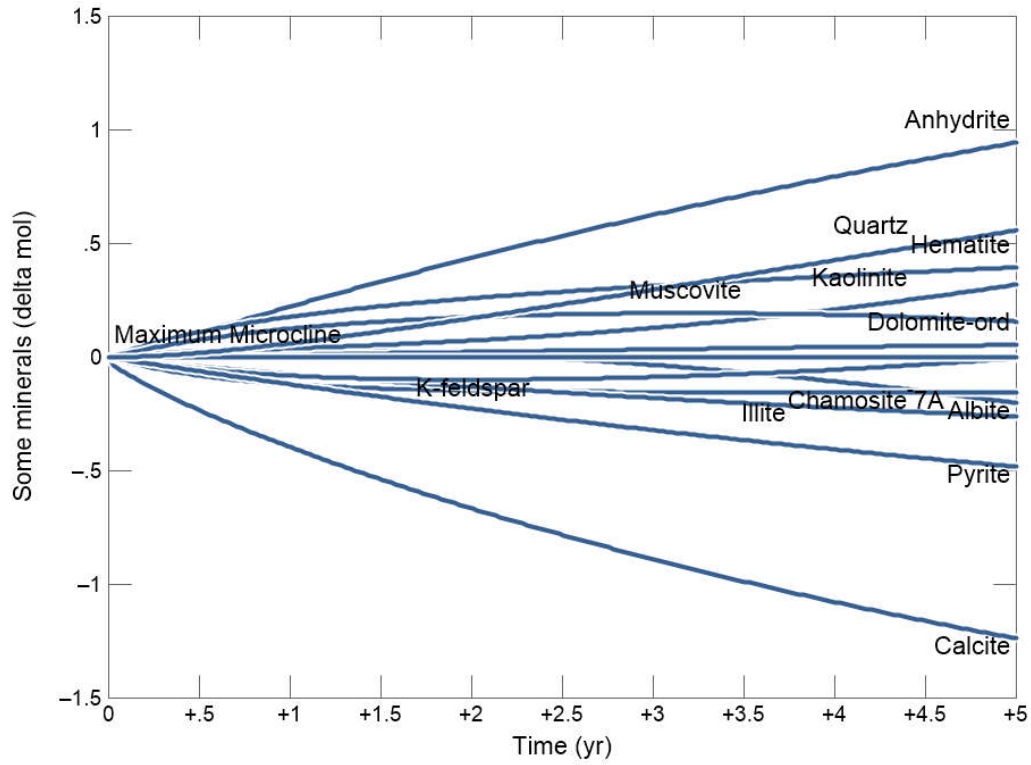


Figure 48: Changes of the amount of the minerals from the addition of CO₂ and O₂ in geochemical modeling

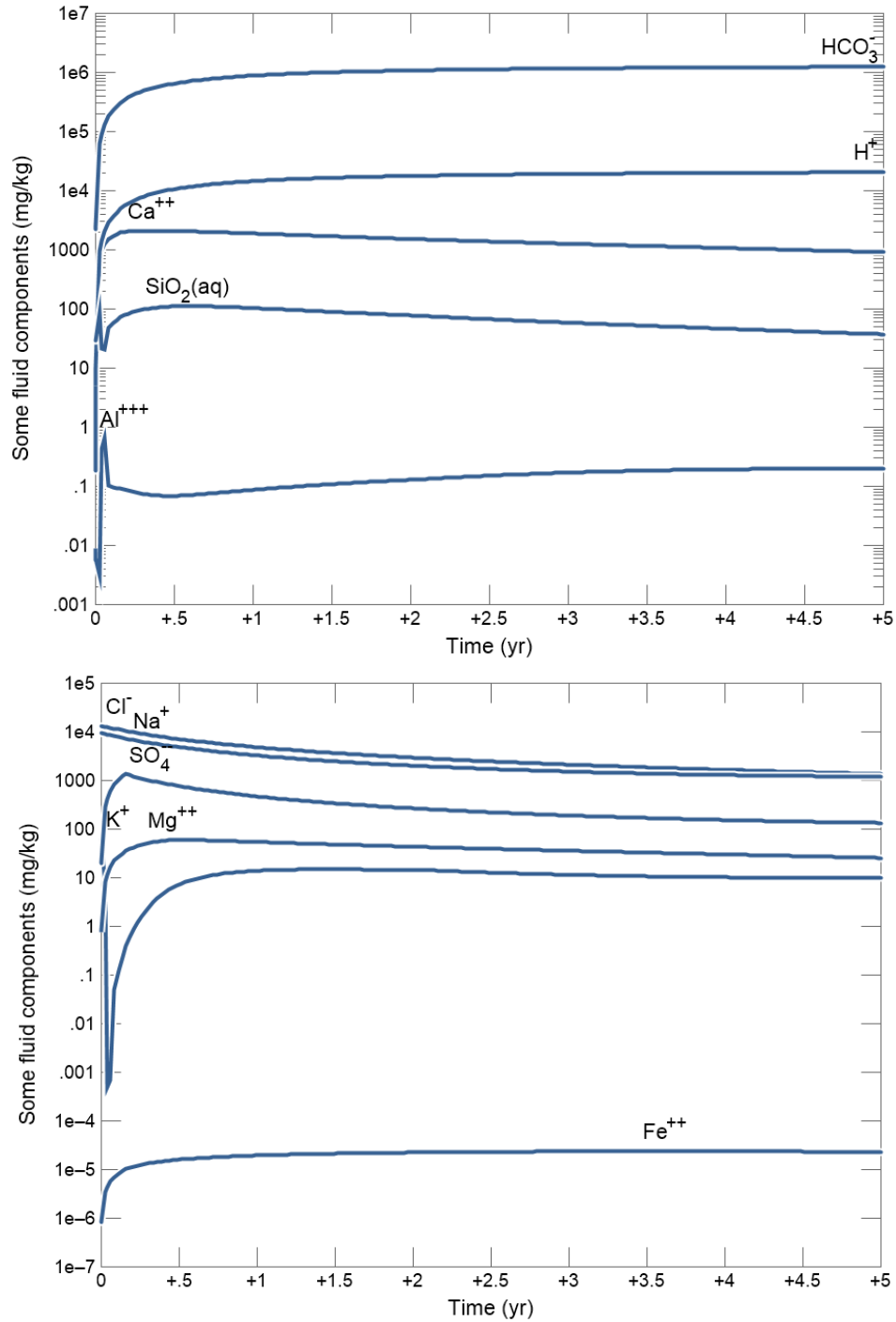
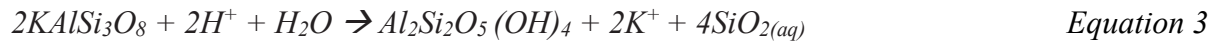
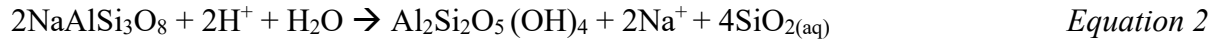


Figure 49: Aqueous composition after the addition of CO_2 and O_2 in geochemical modeling

Simulation results of the combined mineral and aqueous phases, and the major mineral reactions are listed below.



The most prominent mineral reaction initiated by the addition of CO₂ is calcite dissolution (Equation 1), which releases Ca into the solution. As a similar response to the decreasing pH, K-feldspar and albite are dissolved releasing K and Na into the solution (Equation 2 & Equation 3). Silica and kaolinite are the probable products of feldspar dissolution.

The co-injected O₂ as an impurity will have an impact if both redox-sensitive mineral species and ferrous iron-bearing minerals (pyrite, Fe-bearing carbonates, and possibly glauconite, which contains mostly ferric Fe but also some ferrous Fe) are present in the overlying formation. Specifically, pyrite, a common mineral phase in sedimentary rocks, is oxidized to release ferrous iron and sulfate (Equation 4). Ferrous iron is further oxidized into ferric iron and precipitate as hematite (Equation 5). Both reactions will further reduce pH. The increasing SO₄ concentration from pyrite oxidation may lead to formation of anhydrite (Equation 6), gypsum, and/ or barite when sufficient Ca and Ba are present in the solution.

Overall, the amounts of mineral reactions are limited by the availability of the reactive mineral phases and the extent of the space and time where the injectate and water co-exist. The latter is controlled by flow properties and injection dynamics. Sedimentary texture is also an important factor which determines specific surface area of each mineral component and it is exposed to the pore water. The contact area of between the reactants and solution determines the reaction rate.

The simulation results show net reduction of the rock mass and volume (Figure 50), indicating increased porosity. However, predicting permeability change is difficult because it is also affected by the morphology and site of the precipitated material. For example, the newly formed iron oxides may preferentially block the pore throat which will reduce permeability even if there is a net increase of porosity from mineral dissolution. Autoclave experiments of rock-water-CO₂ interaction can provide information on this issue.

Generally, pyrite and other redox sensitive minerals are not abundant in sandstones, which limits the extent of precipitation of iron oxide and sulfate minerals. Calcite dissolution usually increases porosity and permeability, which is beneficial for injection operation. The framework grains of the sandstones are predominantly quartz which is not as reactive and will preserve the geomechanical strength of the formation.

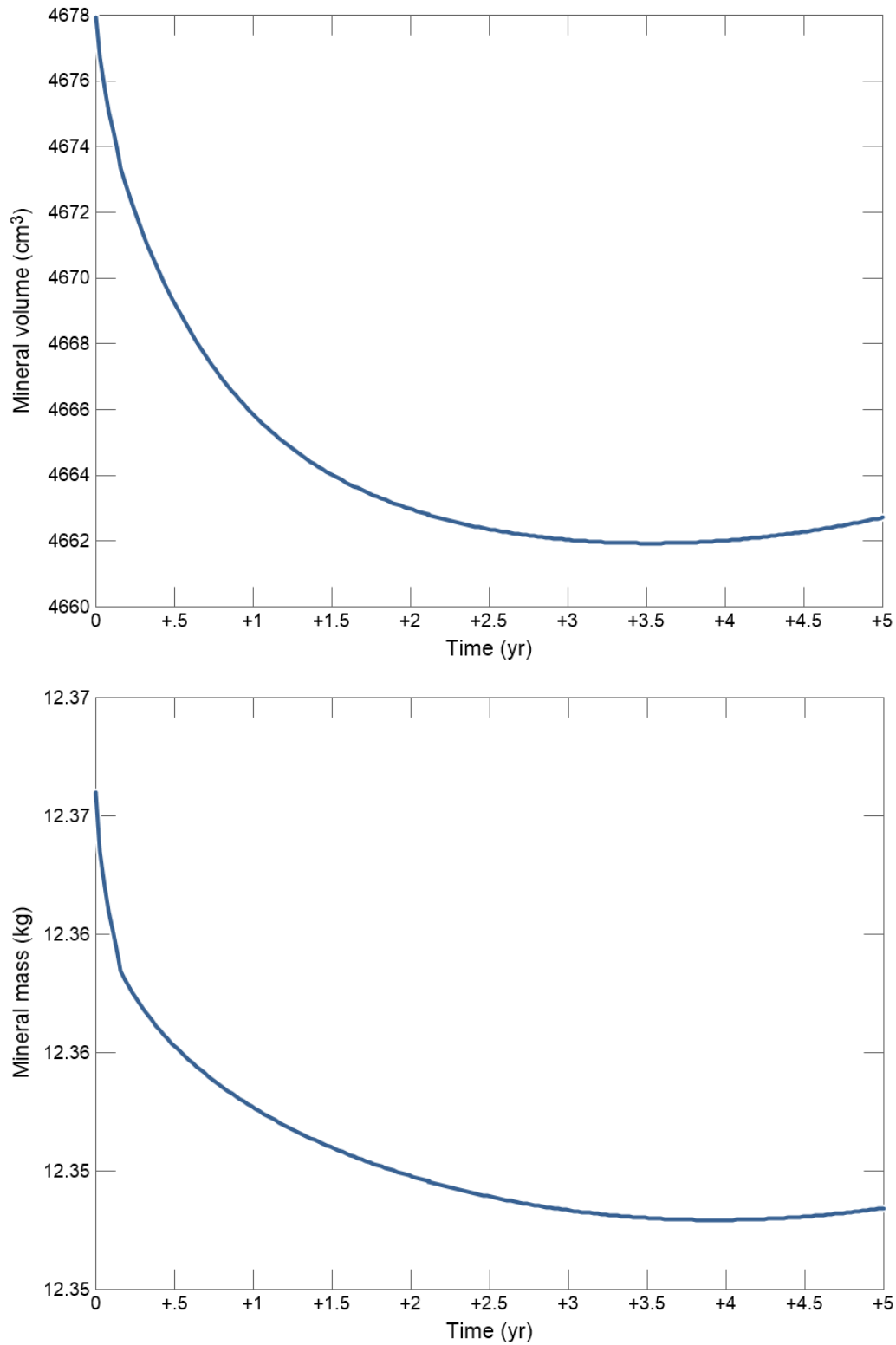


Figure 50: Mineral volume and mass after the addition of CO₂ and O₂ in the geochemical modeling

2.9. Other Information (Including Surface Air and/or Soil Gas Data, if Applicable)

At the time of this pre-construction application surface air and soil gas data have not been collected. Baseline data will be designed in future phases of this project.

2.10. Site Suitability [40 CFR 146.83]

The location of the Mendota_INJ_1 well is in a favorable setting for a CO₂ sequestration project based on the initial site characterization during this pre-construction phase.

Based on the interpretation of well tops and 2D seismic, the distribution of the sandstones of the Second Panoche injection zone is interpreted to be relatively continuous within the AoR (Section 2.2). The regional dip of this and other formations is to the northeast; this implies that the injected CO₂ will migrate approximately 2 miles to the northeast (Section 3).

The gas stream for injection contains 96.78% CO₂ with some impurities. O₂ is the most notable impurity at 1.15% because it is reactive when redox sensitive minerals are present in the formation (Section 2.8). Generally, pyrite and other redox sensitive minerals are not abundant in sandstones, which limits the extent of precipitation of iron oxide and sulfate minerals. Calcite dissolution usually increases porosity and permeability, which is beneficial for injection operation. The framework grains of the sandstones are predominantly quartz which is not as reactive and will preserve the geomechanical strength of the formation. The injection and monitoring wells are planned to be constructed with CO₂ resistant materials, which include casing, cement, packers, safety valves etc. and will consider gas stream impurities.

Reservoir simulations show that the injected CO₂ will be confined to the Second Panoche injection zone by the low permeable shales of the First Panoche Shale. Above this, the Moreno Shale will act as a thick secondary containment zone. There are only two wells in or near the AoR which penetrate the Moreno Shale. Attachment B (Schlumberger, Attachment B: Area of Review and Corrective Action Plan, 2020) details the corrective action for all nearby wells near the AoR.

The total pore volume of the Second Panoche injection zone is calculated by using the 3D geocellular model with a 5-mile radius of the proposed Mendota_INJ_1; the total pore volume is calculated to be 3.74×10^{11} ft³. Given the high porosity and permeability of the Second Panoche, this formation is suitable to receive the forecasted 350,000 tons/year of CO₂ for the proposed 20 year injection period.

Currently there are no potential concerns regarding the confining zone integrity. The zones are relatively continuous, and the faults identified around Mendota_INJ_1 show only minor displacement; furthermore, fault seal analysis completed shows that the faults in the area are sealing faults (Section 2.3).

The deepest USDW (calculated at ~1,609 ft bgs) is 5,700 ft above the Moreno Shale which is the secondary confining zone (Schlumberger, Attachment E: Post-Injection Site Care and Site Closure Plan, 2020). The Moreno Shale thickness (~1,100 ft Figure 13), lateral extent, and

relatively low porosity and permeability (Figure 28 and Figure 31) will provide very low risk to the much shallower USDW.

During future phases of this project, if approved by the EPA, additional data will be gathered and assimilated into an updated reservoir characterization. The site structural geology will be accurately delineated when there is a 3D seismic survey available. Once a characterization well is drilled (Mendota_INJ_1), petrophysical, geomechanical, fracture and geochemical properties will be much better understood. Baseline monitoring of groundwater, soil and air will also be completed in future phases of the project.

3. AoR and Corrective Action

AoR and Corrective Action GSDT Submissions

GSDT Module: AoR and Corrective Action

Tab(s): All applicable tabs

Please use the checkbox(es) to verify the following information was submitted to the GSDT:

Tabulation of all wells within AoR that penetrate confining zone *[40 CFR 146.82(a)(4)]*

AoR and Corrective Action Plan *[40 CFR 146.82(a)(13) and 146.84(b)]*

Computational modeling details *[40 CFR 146.84(c)]*

The above requested documents have been included in the file submission (Schlumberger, Attachment B: Area of Review and Corrective Action Plan, 2020). These documents address the rule requirements for the above EPA citations.

4. Financial Responsibility

Financial Responsibility GSDT Submissions

GSDT Module: Financial Responsibility Demonstration

Tab(s): Cost Estimate tab and all applicable financial instrument tabs

Please use the checkbox(es) to verify the following information was submitted to the GSDT:

Demonstration of financial responsibility *[40 CFR 146.82(a)(14) and 146.85]*

The above requested documents have been included in the file submission (Schlumberger, Attachment H: Financial Assurance Demonstration, 2020). These documents address the rule requirements for the above EPA citations.

5. Injection Well Construction

The proposed injection well (Mendota_INJ_1) design is presented in. This will be a new vertical well that will be drilled with inclination of less than 5 degrees. The conductor will be driven if soil samples permit but if not, a 26 in. diameter hole will be drilled to a depth of 86 ft. A 22 in., 197.4 lb/ft conductor pipe will be inserted and cemented to surface. A 20 in. diameter hole will be drilled to a depth of 1800 ft. The well will be logged from 86 to 1800 ft. and a 16 in. 84 lb/ft casing will be run into the hole, cemented to surface and cased hole cement evaluation logging suite run. A 14-3/4 in. diameter hole will be drilled to a depth of about 7432 ft. which should be 100 ft into the top of the Moreno Shale main seal. Well logs to provide formation properties and any needed formation sampling will be run from 7432 ft. to 1800 ft. A 10-3/4 in. 55.5 lb/ft, N-80 string of casing will be run into the hole, cemented to surface. Cement and casing evaluation logs will be run. A 9-5/8 in. diameter hole will be drilled to a depth of about 10412 ft. which should be 100 ft. into the top of the Third Panoche Shale with whole cores taken over the Moreno Shale, and First and Second Panoche sands and shales. If a competent formation to set casing is found above the Third Panoche Shale, then the 9-5/8" hole may not be drilled to 10,412 ft. The well will have extensive logging and sampling suites run from 10412 ft. to 7432 ft. to fully evaluate the Panoche Sands for injection and shales for seals. A 7 in. 38 lb/ft, L-80 from 0-7332 ft and then 7 in. 38 lb/ft L-80 13Cr casing from 7332 ft. To 10412 ft will be run into the hole, cemented to surface. Cement and casing evaluation logs will be run along with baseline monitoring logs. After the cased hole logs are run, the well will be perforated and completed with an injection packer and 3-1/2 in. L-80 13Cr tubing string. The perforation interval will be selected based on the log analysis but is anticipated to be within the depth interval from about 9600 ft. to 9820 ft. Figure 52 and Figure 53 show the pore pressure, fracture and temperature gradients used for the well construction planning.

The USDW aquifers are expected to extend to a depth of 1615 ft gbs. The surface casing planned depth is 1800 ft. The 16 in. 84 lb/ft N-80 casing with watertight connections in a generous 20 in fully cemented hole to surface provides sufficient protection and coverage of the USDW aquifers.

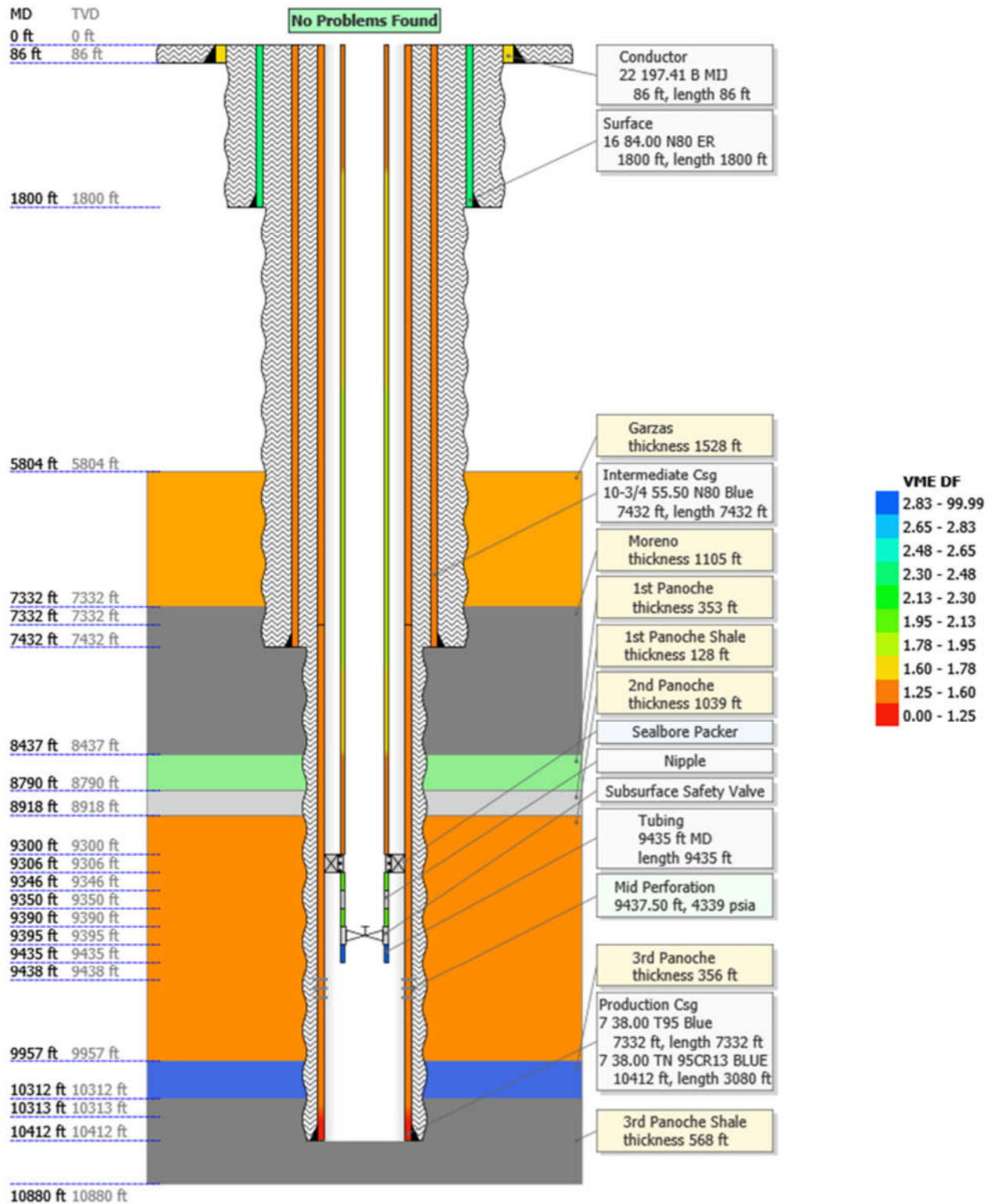


Figure 51: Mendota_INJ_1 well construction diagram

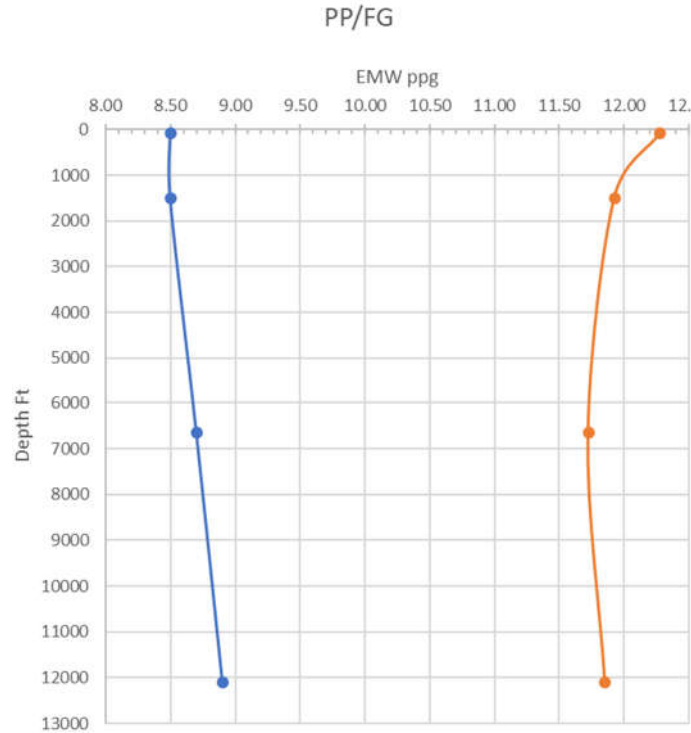


Figure 52: Pore and fracture gradients used for well construction

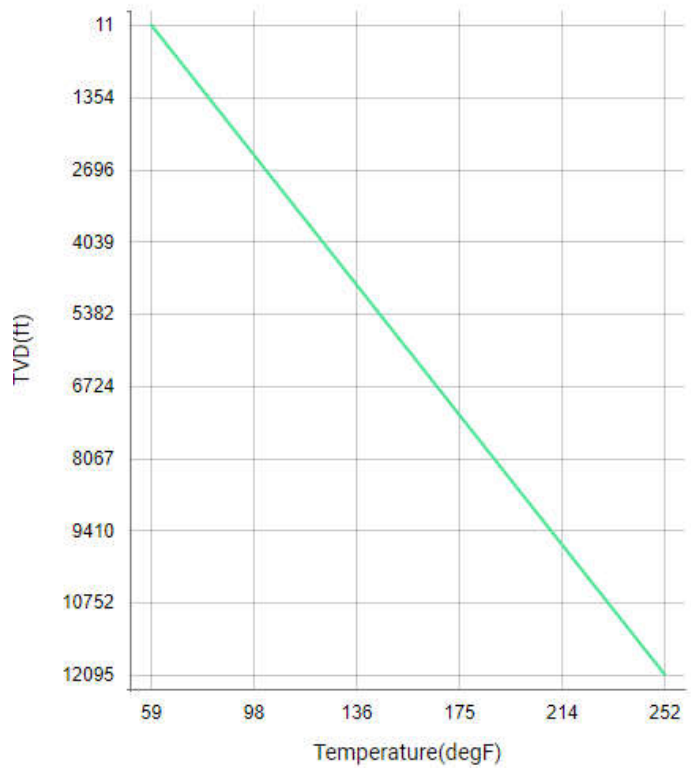


Figure 53: Temperature gradient used for well construction

5.1. Proposed Stimulation Program [40 CFR 146.82(a)(9)]

Currently, there are no plans for stimulation at Mendota_INJ_1.

5.2. Construction Procedures [40 CFR 146.82(a)(12)]

5.2.1. Surface Well Head Configuration

Surface well head will be configured for appropriate CO₂ service for those flowpath that will have interaction with the CO₂ injection stream or during well maintenance (Figure 54).

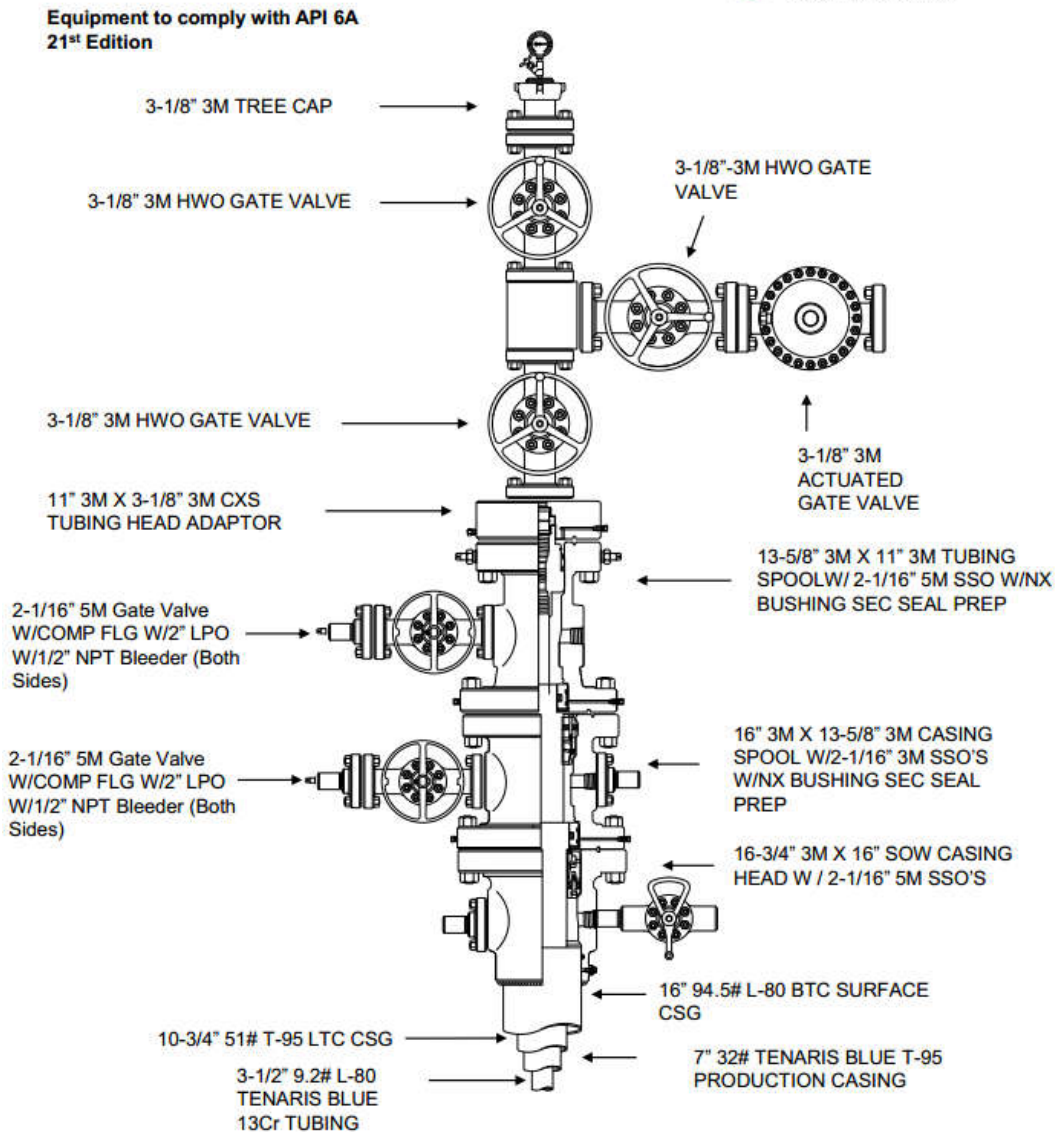


Figure 54: Surface well head configuration

5.2.2. Casing

Casing selection has been evaluated against industry standard worst case loads to determine if selected casing sizes, material thickness and grade are suitable for the environment in terms of pressure and temperature they will be subjected too (Table 10, Table 11 and Table 12). Where applicable special loads were created to determine if the casing could handle a load not covered by current standards. Areas evaluated are casing/tubing burst, collapse, axial and compressive strengths in unilateral, bilateral and triaxial (Von Mises) load scenarios.

Table 10: Casing design factors

Burst	Collapse	Tension	Compression	VME
1.10	1.10	1.60	1.20	1.25

Table 11: Casing design loads

String	Burst	Collapse	Tension	Compression	Von Mises
22" Conductor	1.63	52.26	6.98	>100	1.75
16" Surface	2.16	1.23	9.65	11.91	2.30
10-3/4" Intermediate	1.34	1.84	3.00	3.58	1.34
7" Long	1.25	2.00	2.23	3.44	1.25
3-1/2" Tubing	1.94	1.65	2.41	3.71	1.41

Figure 51 shows the position of the various casing, tubing and perforations to be implemented in the Mendota_INJ_1 injection well. Correlation of the formations covered with casing and cement as well as gradient indication of the VME Design Factor of the casing design is included.

Table 12: Mendota_INJ_1 open hole diameters and intervals

Name	Depth Interval (feet)	Open Hole Diameter (inches)	Comment
Conductor	86	26	Will try to drive conductor (reason for 1" wall thickness) but need to get soil samples to determine if viable if not viable will drill 26 in hole
Surface	1800	20	1800 ft will cover any potential freshwater aquifers and provide sufficient kick tolerance for the intermediate string. Length may vary slightly in locating a formation with sufficient strength to provide a competent casing shoe.
Intermediate	8387	14.75	This string will be set 100 ft in the Moreno shale at 7432 ft.
Long-string	10412	9.625	Will drill across the 1 st , 2 nd and 3 rd Panoche sands and have casing shoe below the 3 rd Panoche Shale (may be set in the above the 3 rd Panoche Shale if the formation is found suitable to set casing).

Table 13: Mendota_INJ_1 casing specifications

Name	Depth Interval (feet)	Outside Diameter (inches)	Inside Diameter (inches)	Weight (lb/ft)	Grade (API)	Design Coupling (Short or Long Threaded)	Thermal Conductivity @ 77°F (BTU/ft hr, °F)	Burst Strength (psi)	Collapse Strength (psi)
Conductor	86	22	21	197.41	B	Welded	26.13	2440	1950
Surface	1800	16	15.01	84	N80	Long	26.13	4330	1480
Intermediate	7432	10.75	9.760	55.5	N80	Long	26.13	6450	4020
Long-string	7332	7	5.920	38	T-95 Type 1	Long	26.13	12830	13430
Long-string	10412	7	5.920	38	TN 95Cr13	Long	14.92	12830	13430

Table 14: Mendota_INJ_1 casing details.

Casing String	Casing Depth	Borehole Diameter	Wall Thickness	External Diameter	Casing Material	String Weight
Conductor	86 ft	26 in	1 in	22 in	197.41ppf Grade: B Connection: Welded	16997 lbs
Surface	1800 ft	20 in	0.875in	16 in	84 ppf Grade: L80 Connection: Tenaris ER	151200 lbs
Intermediate String	7432 ft	14.75 in	0.495 in	10.75 in	55.5 ppf Grade: T95 Connection: Tenaris Blue	412476 lbs
Long String	7332	9.625 in	0.590 in	7.0 in	38 ppf Grade: T-95 Type1 Connection: Tenaris Blue	422792 lbs
	10412	9.625 in	0.590 in	7.0 in	38 ppf Grade:T95-13Cr Connection: Tenaris Blue	

5.2.1. Discussion on Well Construction

Well construction will provide 3 casing barriers with generously cemented annuluses covering the USDW from Surface to 1800 ft. Covering the USDW will be the 16", 10-¾" and 7" casings.

A removable 3-½" tubing string with a retrievable seal bore packer will be used to facilitate easy movement and changeout of the tubing string and allow for fluid movement and pressure testing as needed. The tubing string will be fitted with nipple profiles to facilitate testing of the tubing, packers and tubing annulus. Pressure and temperature monitors will be installed downhole as well as at surface on the various annular ports for the casing wellhead and tubing to keep track of variations of those parameters.

While the offset wells did not indicate any major drilling issues in their available drilling logs, it is always good to be prepared with contingencies. Water based muds (NaCl Gelled) will be used for drilling the whole well so there will be limited contamination in any aquifers from the drilling mud. Loss circulation will be addressed with materials such as fibers, hulls and calcium carbonate. The nature of loss circulation material is not to penetrate the formation with any significant depth (< 3 feet but depends on porosity, surface fractures along wellbore and size of lost circulation material) so damage to aquifers and other formations from loss circulation material will be very limited if at all.

This is a vertical well and risk for any fishing job for loss drillpipe or other fish in the hole will be minimal. In the event a fish has to be left in the hole after a reasonable amount of time is dedicated to retrieve the fish, a cement plug will be placed above the fish and sidetrack will be executed to go around the fish and back to vertical.

There are plans to take frequent deviation checks. It will be desirable to keep the wellbore as vertical as possible. Plan is to keep the well ≤ 5.0 degrees inclination. If MWD (Measurement While Drilling) tools are not in the drilling assembly then a drift indicator will be used with surveys taken every 300 ft minimum. If MWD are not used to drill a well section then a magnetic multishot will be dropped at the end of the section and survey intervals of 100 ft will be taken as the final assembly is retrieved from the hole. At the end of the well a gyro survey will be run to confirm the wellbore profile. MWD, Magnetic Multishot and Gyro surveys all provide 3 dimensional surveys with depth, inclination and azimuth outputs. Minimum curvature will be used to calculate the wellbore path between survey points.

All components used in the well construction will adhere to API, ASTM, ANSI and NACE standards as referenced for that component. For example, casing is controlled by API 5C3, 5CT and 5CRA for basic material control and dimensioning. ANSI/NACE MR0175/ISO 15156-2015 provide guidelines for corrosion control and ASTM defines testing methods for the materials or tools.

Materials suitable for CO₂ environment are clearly specified in API, ANSI/NACE and ASTM standards. Suppliers of components will be required to demonstrate and provide certification that their equipment has been tested and evaluated against these standards and that they are suitable for purpose in the environment defined.

5.2.2. Tubing and Packer

The below tables summarize the expected tubing and packer specifications for Mendota_INJ_1 (Table 15 and Table 16).

Table 15: Mendota_INJ_1 tubing specifications

Name	Depth Interval (feet)	Outside Diameter (inches)	Inside Diameter (inches)	Weight (lb/ft)	Grade (API)	Design Coupling (Short or Long Thread)	Burst strength (psi)	Collapse strength (psi)
Injection tubing	9430	3.5	2.992	9.2	L80Cr13	Long	10160	10540

Table 16: Mendota_INJ_1 packer specifications

Packer Type and Material	Packer Setting Depth (feet bgs)	Length (inches)	Nominal Casing Weight (lbs/ft)	Packer Main Body Outer Diameter (inches)	Packer Inner Diameter (inches)
Seal Bore Packer in N80 13Cr	9300	64	38	5.685	4.0

Tensile Rating (lbs)	Burst Rating (psi)	Collapse Rating (psi)	Max. Casing Inner Diameter (inches)	Min. Casing Inner Diameter (inches)
133.12@250degF	5000	5000	6000	5.949

Material	Setting Depth	Tensile Strength	Burst Strength	Collapse Strength	Material
3-1/2" Tubing	10135	80000 psi	10016 psi	10540 psi	9.2ppf Grade:L80-13Cr Connection: Tenaris Blue
Packer	9300	80000 psi	5000	5000	N80 13Cr 38ppf

5.2.3. Cement

All casings will be cemented to surface. There are currently no known conditions preventing bringing cement to surface without a stage collar on the Surface, Intermediate and Long strings. All cement recipes will be evaluated with respect to properties and curing times in a laboratory before job is started and test samples from the actual slurry pumped will be evaluated. Coverage of the annulus and cement strength estimates will be achieved via pumping schedule and associated pressures along evaluated with wireline CBL and ultra-sonic cement evaluation logs.

5.2.3.1. Conductor

The conductor is expected to be driven but a provision has been allowed to drill a hole and cement the casing if soil conditions do not permit driving the casing to 86 ft.

5.2.3.2. Surface Section

The surface casing will cover the USDW aquifers at a maximum depth of 1,615 ft TVD. Surface casing depth is expected to be 1,800 ft. This is needed to provide a good kick tolerance for the intermediate section. Type II/V cement meets ASTM Specification C 150. It is a low alkali Portland cement for general use and where high sulfate resistance is required (Table 17).

Table 17: Surface section fluid placement in annulus

Fluid Name	Top MD ft	Bottom MD ft	Length ft	Volume bbl	Cement Sacks	Surface Density lb/gal
Drilling Fluid	0.0	0.0	0.0	0.0		9.00
Fresh Water	0.0	0.0	0.0	40.0		8.32
12.4 ppg Lead Type II/V Cement	0.0	1300.0	1300.0	266.8	689	12.40
13.5 ppg Tail Type II/V Cement	1300.0	1800.0	500.0	69.9	286	13.50

5.2.3.3. Intermediate Section

The Intermediate casing will be set 100 ft into the top of the capping formation for the Panoche sand which is the Moreno Shales. Cement will be brought back to surface from 7,432 ft TVD. Class G cement is an API grade cement with specifications defined in various API standards, primarily API Spec 10A. Pozzolan is an additive to allow reinforce the cement slurry (Table 18).

Table 18: Intermediate section fluid placement in annulus

Fluid Name	Top MD ft	Bottom MD ft	Length ft	Volume bbl	Cement Sacks	Surface Density lb/gal
9.2 ppg Drilling Mud	0.0	0.0	0.0	0.0		10.00
CW100	0.0	0.0	0.0	60.0		8.32
11.5 ppg Lead Class G/Pozzolan	0.0	6437.0	6437.0	637.8	1558	11.50
15.8 ppg Tail Class G	6437.0	7432.0	1000.0	99.1	391	15.80

5.2.3.4. Long String Section

The long casing string will be set 100 ft into the 3rd Panoche Shale but may be set higher if an appropriate formation can be found. Cement will be brought back to surface from 10,412 ft

TVD without a need for staging equipment. The CO₂ resistant EverCRETE* will only be taken to above the Moreno Shale capping formation with a top of 7,332 ft to 7,000 ft.

Class G cement is an API grade cement with specifications defined in various API standards, primarily API Spec 10A. Pozzolan is an additive to allow reinforce the cement slurry.

The latest wellbore isolation technology for carbon dioxide geological storage, the EverCRETE* system provides an enduring solution for zonal isolation during injection, storage, monitoring, and after abandonment. This technology can be applied for carbon capture and storage as well as CO₂ enhanced oil recovery (EOR) projects.

EverCRETE* CO₂-resistant cement system has proved highly resistant to CO₂ attack in the most extreme laboratory conditions, including environments with wet supercritical CO₂ and CO₂ water saturation in downhole conditions. The system reduces the risk of CO₂-induced degradation of the cement sheath that could lead to leakage. It can be incorporated into standard primary cementing operations for zonal isolation of new CO₂ injection wells. The system can also be used to plug and abandon existing wells drilled through the storage zone to reestablish long-term well integrity (Table 19).

Table 19: Long string section fluid placement in annulus

Fluid Name	Top MD ft	Bottom MD ft	Length ft	Volume bbl	Cement Sacks	Surface Density lb/gal
Drilling Fluid	0.0	0.0	0.0	0.0		9.40
10.5 MPE w Surfactant	0.0	0.0	0.0	5.1		10.50
10.5 MPE w Surfactant	0.0	0.0	0.0	44.9		10.50
10.5 MRF	0.0	0.0	0.	224.7		10.50
11.6 ppg Lead Class G/Pozzolan	0.0	7000.0	7000.0	296.8		11.60
12.5 ppg EverCRETE	7000.0	10412.0	3412.0	170.6		12.53

6. Pre-Operational Logging and Testing

Pre-Operational Logging and Testing GSDT Submissions

GSDT Module: Pre-Operational Testing

Tab(s): Welcome tab

Please use the checkbox(es) to verify the following information was submitted to the GSDT:
Proposed pre-operational testing program [40 CFR 146.82(a)(8) and 146.87]

These data are not available at this time because the characterization wells have not yet been drilled. These data will be submitted in future phases of this project.

7. Well Operation

Well operations will be monitored at all times for pressure and temperature with surface and downhole sensor along with surface mass flow sensors. Periodic assessment of the chemical and physical characteristics of the injectorate will also be done. More details on this can be found in the (Schlumberger, Attachment C: Testing and Monitoring Plan, 2020) document. The plan is to have the pressure, temperature and mass flow information systems connected to automated controls to assist with shut down or flow controls if certain critical parameters are reached such as Maximum Flow Rate, or Pressures and Temperatures at surface and downhole as well as Minimum Maximum Flow Rate, or Pressures and Temperatures. This system is currently not defined as more details are needed to properly implement.

For the pre-construction phase the fracture pressure at the center of perforations is estimated to be 6,308 psi at 9,705 ft bgs using a gradient of 0.65 psi/ft. A safe formation injection pressure of 90% of the fracture gradient would be 5,677 psi. The surface injection pressure equivalent for the safe formation injection pressure assuming a 0.376 psi/ft gas gradient (more accurate information will be gained during operation with comparison of downhole and surface sensors) would be 2,026 psi. injection pressure to reach the 90% fracture gradient of 5,677 psi at the perforations downhole. This may change as more information is gained during the evaluation phase of the well's geophysical properties during the drilling of the characterization well.

The expected composition of the injected fluids can be found at Table 8: Composition of the injectate (Mass Fractions). However, samples of the injected fluids will be evaluated per the (Schlumberger, Attachment C: Testing and Monitoring Plan, 2020) as part of the continuous monitoring plan during the injection period.

Protection of the USDWs are the forefront of the well design. There will be 3 casing and cement barriers between the injected fluids and the USDWs at 1615 ft. TVD GL. Cement barriers are designed to be overly thick to reduce the risk of cement channeling and ensure coverage is complete and through. In addition to multiple barriers there will be pressure gauges on the wellhead of the outer annulus to monitor for pressure to make sure there is no breakdown in the cement integrity. With UIC Program Director approval, the annulus between the tubing and long string will be filled with an estimated 9.4 ppg NaCl brine to provide corrosion and scaling

resistance, oxygen sequestering, and microbial growth inhibition. A pressure system will be applied at the well head to fulfill the requirement of the tubing annulus pressure be greater than the injection pressure. This will also assist in determining if fluid levels in the tubing annulus are being maintained and if the packer seals are functioning properly.

Strict guidelines for well maintenance will be enforced with sufficient preplanning of the operations to be done to insure well integrity will be maintained before a job is started. During well maintenance, daily logs will be kept of processes completed and issues encountered so a review process can be done to improve operations.

In the event a loss of well integrity or operational control is encountered an immediate investigate to identify as expeditiously as possible the cause of the shutoff. If, upon such investigation, the well appears to be lacking mechanical integrity, or if otherwise indicates that the well may be lacking mechanical integrity, the following will occur:

1. Immediately cease injection;
2. Take all steps reasonably necessary to determine whether there may have been a release of the injected carbon dioxide stream or formation fluids into any unauthorized zone;
3. Notify the Director within 24 hours;
4. Restore and demonstrate mechanical integrity to the satisfaction of the Director prior to resuming injection; and
5. Notify the Director when injection can be expected to resume.

Additional details are in the (Schlumberger, Attachment F: Emergency and Remedial Response Plan, 2020).

7.1. Operational Procedures [40 CFR 146.82(a)(10)]

To achieve the target injection rate, the injection pressure must be greater than the minimum bottom-hole pressure required to drive the CO₂ into the reservoir formation, but the injection pressure must be maintained below the maximum safe pressure to avoid fracturing. The minimum bottom-hole pressure to provide the required flow rate into the Panoche Sandstone was determined by subsurface reservoir modeling. The maximum safe bottom-hole pressure was specified as 90 percent of the rock's fracture pressure ($0.9 \times 0.65 \text{ psi/ft} = 0.585 \text{ psi/ft}$) at the depth where the CO₂ is injected. For conservatism, the required injection pressure was calculated based on the assumption that the required bottom-hole pressure is equal to the maximum safe bottom-hole pressure. Maximum bottom-hole injection pressure (injection depth $\times 0.585 \text{ psi/ft}$).

A steady-state, one-dimensional flow model was used to calculate the pressure drop along a series of segments of the well. Pressure changes from frictional loss, gravity head, and acceleration of the flow are included in the model. The CO₂ density is calculated from the pressure and temperature using the CO₂ state equation of Peng-Robinson (1976). The CO₂ is assumed to be a liquid or supercritical fluid and the calculation stops if two-phase conditions occur. The internal energy at the end of a pipe segment was calculated from the energy equation accounting for the heat transfer from or into the CO₂ stream from the surrounding soil or rock, change in potential energy due to pressure and elevation, and kinetic energy of the flow.

Changes in the internal energy and temperature of the CO₂ with depth cause gradual changes in density, which in turn change the velocity and pressure drop. If the friction pressure drop is large (e.g., high velocity flow through small injection tubing), fluid expansion is significant as it moves down the pressure gradient. The resulting cooling effect can potentially have a greater impact on the CO₂ temperature than heat transfer to the surroundings.

Part of the bottom-hole pressure required to support the necessary flow into the rock is provided by hydrostatic head associated with the weight of the column of fluid in the well. This depends upon the fluid density, which varies with pressure and temperature because of the compressibility of CO₂. Lower temperature at the wellhead increases the fluid density and decreases the wellhead pressure required to provide the necessary bottom-hole pressure. Frictional pressure drop in the injection tubing must also be overcome. High frictional losses associated with undersized tubing would make high wellhead pressures necessary to support a given flow rate. Larger tubing sizes require lower injection pressures but larger wells. Conversely, smaller well and tubing sizes require higher injection pressures.

Wellhead injection pressures were calculated for the following conditions: a flow rate of 958.0 T/d (i.e., assuming 100 percent of the CO₂ is injected), Injection tubing of 3.5 in and 4.5 in. diameter and one surface CO₂ temperatures (60.8°F) to represent the range of anticipated CO₂ temperatures at the injection. Required injection pressures will be higher in summer than winter due to lower density, leading to less hydrostatic in the fluid column and higher frictional losses because of higher fluid velocities.

7.2. Proposed Carbon Dioxide Stream [40 CFR 146.82(a)(7)(iii) and (iv)]

CES Carbon Negative Energy (CNE) plants use biomass as feedstock to produce syngas which passes through a gas separation unit to produce hydrogen for transportation fuel. The hydrogen depleted syngas then passes through a CES proprietary gas generator to produce a pure stream of high-pressure CO₂. CES plans to compress this CO₂ to a supercritical state and inject it deep into the subsurface for geologic sequestration (GS).

The gas stream for injection contains 96.78% CO₂ with some impurities. O₂ is the most notable impurity at 1.15% because it is reactive when redox sensitive minerals are present in the formation. It also requires surface and well components which are resistant to that environment. To understand its effect, O₂ is included in the geochemical models. The current estimate of the gas stream composition is listed in Table 8: Composition of the injectate (Mass Fractions).

In the pre-construction phase the exact measurement as to composition, properties and corrosiveness have not been tested. Well construction materials described in (Schlumberger, Attachment G: Construction Details Clean Energy Systems Mendota, 2020) will be reviewed following these tests as well as the (Schlumberger, Attachment C: Testing and Monitoring Plan, 2020) and Quality Assurance and Surveillance Plan.

Table 20: Proposed operational procedures.

Parameters/Conditions	Limit or Permitted Value	Unit
Maximum Injection Pressure		
Surface	2026	psi
Downhole	5677	psi
Average Injection Pressure		
Surface	1042	psi
Downhole	4212	psi
Maximum Injection Rate	958.9	tons/day
Average Injection Rate	958.9	tons/day
Maximum Injection Volume and/or Mass	350000	tons/year
Average Injection Volume and/or Mass	350000	tons/year
Annulus Pressure	1142	psi
Annulus Pressure/Tubing Differential	100	psi

8. Testing and Monitoring

Testing and Monitoring GSDT Submissions

GSDT Module: Project Plan Submissions

Tab(s): Testing and Monitoring tab

Please use the checkbox(es) to verify the following information was submitted to the GSDT:
Testing and Monitoring Plan *[40 CFR 146.82(a)(15) and 146.90]*

The above requested documents have been included in the file submission (Schlumberger, Attachment C: Testing and Monitoring Plan, 2020). These documents address the rule requirements for the above EPA citations.

9. Injection Well Plugging

Injection Well Plugging GSDT Submissions

GSDT Module: Project Plan Submissions

Tab(s): Injection Well Plugging tab

Please use the checkbox(es) to verify the following information was submitted to the GSDT:
Injection Well Plugging Plan *[40 CFR 146.82(a)(16) and 146.92(b)]*

The above requested documents have been included in the file submission (Schlumberger, Attachment D: Injection Well Plugging Plan, 2020). These documents address the rule requirements for the above EPA citations.

10. Post-Injection Site Care (PISC) and Site Closure

PISC and Site Closure GSDT Submissions

GSDT Module: Project Plan Submissions

Tab(s): PISC and Site Closure tab

Please use the checkbox(es) to verify the following information was submitted to the GSDT:
PISC and Site Closure Plan *[40 CFR 146.82(a)(17) and 146.93(a)]*

GSDT Module: Alternative PISC Timeframe Demonstration

Tab(s): All tabs (only if an alternative PISC timeframe is requested)

Please use the checkbox(es) to verify the following information was submitted to the GSDT:
Alternative PISC timeframe demonstration *[40 CFR 146.82(a)(18) and 146.93(c)]*

The above requested documents have been included in the file submission (Schlumberger, Attachment E: Post-Injection Site Care and Site Closure Plan, 2020). These documents address the rule requirements for the above EPA citations. CES is not requesting an Alternative PISC timeframe.

11. Emergency and Remedial Response

Emergency and Remedial Response GSDT Submissions

GSDT Module: Project Plan Submissions

Tab(s): Emergency and Remedial Response tab

Please use the checkbox(es) to verify the following information was submitted to the GSDT:
Emergency and Remedial Response Plan [40 CFR 146.82(a)(19) and 146.94(a)]

The above requested documents have been included in the file submission (Schlumberger, Attachment F: Emergency and Remedial Response Plan, 2020). These documents address the rule requirements for the above EPA citations.

12. Injection Depth Waiver and Aquifer Exemption Expansion

Injection Depth Waiver and Aquifer Exemption Expansion GSDT Submissions

GSDT Module: Injection Depth Waivers and Aquifer Exemption Expansions

Tab(s): All applicable tabs

Please use the checkbox(es) to verify the following information was submitted to the GSDT:
Injection Depth Waiver supplemental report [40 CFR 146.82(d) and 146.95(a)]
Aquifer exemption expansion request and data [40 CFR 146.4(d) and 144.7(d)]

CES is not requesting an Injection Depth Waiver or Aquifer Exemption Expansion.

13. Other Information


There is no additional information that is not specifically requested/required useful for the permit application.

14. Approval

This pre-construction application and the associated attachment documents were prepared by a multi-disciplinary team at Schlumberger and approved by Schlumberger technical leads (Table 21). This document and attachments were delivered to CES.

- (Schlumberger, Attachment A: Summary of Requirements Class VI Operating, 2020)
- (Schlumberger, Attachment B: Area of Review and Corrective Action Plan, 2020)
- (Schlumberger, Attachment C: Testing and Monitoring Plan, 2020)
- (Schlumberger, Attachment D: Injection Well Plugging Plan, 2020)
- (Schlumberger, Attachment E: Post-Injection Site Care and Site Closure Plan, 2020)
- (Schlumberger, Attachment F: Emergency and Remedial Response Plan, 2020)
- (Schlumberger, Attachment G: Construction Details Clean Energy Systems Mendota, 2020)
- (Schlumberger, Attachment H: Financial Assurance Demonstration, 2020)
- (Schlumberger, Class VI Permit Application Narrative, 2020)
- (Schlumberger Quality Assurance and Surveillance Plan, 2020)

Table 21: Approval

Name	Title	Signature	Date
Randal Utech	Advisor Geoscientist		January 31, 2020

15. References

- Bartow, A. J. (1990). *1990 Bartow and Nilsen USGS Review of the Great Valley Sequence, eastern Diablo Range and northern San Joaquin Valley, central California*. USGS.
- California Department of Conservation, D. o. (1998). *CALIFORNIA OIL & GAS FIELDS Volumes I, II, & III*.
- California Department of Water Resources. (n.d.). Retrieved from water.ca.gov/Library/Other-DWR-Portals
- CEMA. (2010). *Central Coast ShakeOut Area - Historical Epicenters*. Retrieved from https://www.shakeout.org/california/images/Central_Coast_epicenters_map.jpg
- Chanchani, S. Z. (2003). A case study of hydrocarbon transport along active faults and production-related stress changes in the Monterey formation, California. *Geological Society, London, Special Publications*, 17-26.
- Chiaramonte, L. Z. (2008). Seal integrity and feasibility of CO₂ sequestration in the Teapot Dome EOR pilot: Geomechanical site characterization. *Environmental Geology*, 1667-1675.
- DOGGR. (2019). <https://www.conservation.ca.gov/dog>. Retrieved from Division of Oil, Gas, and Geothermal Resources.
- EPA. (2018). *Geologic Sequestration of Carbon Dioxide Underground Injection Control (UIC) Program Class VI Implementation Manual for UIC Program Directors*.
- EPA. (2019). *Class VI Guidance Documents*. Retrieved from Class VI Guidance Documents: <https://www.epa.gov/uic/class-vi-guidance-documents>
- EPA. (2019). *Underground Injection Control*. Retrieved from <https://www.epa.gov/uic/class-ii-permit-application-checklist>
- Gillespie, J. (2017). *Groundwater salinity in the southern San Joaquin Valley*. AAPG Bulletin, v. 101, no. 8 (August 2017), pp. 1239–1261.
- Han, D. N. (1986). Effects of porosity and clay content on wave velocities in sandstone. *Geophysics*, 2093-2107.
- Herron, M. M. (1987). Estimating the Intrinsic Permeability of Clastic Sediments from Geochemical Data. *SPWLA 28th Annual Logging Symposium*.
- Herron, M. M. (June 29-July 2, 1987). Estimating the Intrinsic Permeability of Clastic Sediments from Geochemical Data. *SPWLA Twenty-Eighth Annual Logging Symposium*.
- IHS. (2019). *IHS Markit*. Retrieved from Enerdeq, Lognet: <https://ihsmarkit.com/index.html>

- McGuire, D. (1988). Depositional framework of the Upper Cretaceous-lower Tertiary Moreno Formation, central San Joaquin basin, California. *SPEM*.
- Peng, D. Y., & Robinson, D. B. (1976). A New Two-Constant Equation of State. *Industrial and Engineering Chemistry: Fundamentals*, 15: 59–64.
- Scheirer, A. H. (2003). Winters-Domengine Total Petroleum System - Northern Nonassociated Gas Assessment Unit of the San Joaquin Basin Providence. In U. S. Team, *Petroleum Systems and Geologic Assessment of Oil and Gas in the San Joaquin*.
- Schlumberger Quality Assurance and Surveillance Plan. (2020). *Quality Assurance and Surveillance Plan*.
- Schlumberger, Attachment A: Summary of Requirements Class VI Operating. (2020). *Attachment A: Summary of Requirements Class VI Operating and Reporting Conditions*.
- Schlumberger, Attachment B: Area of Review and Corrective Action Plan. (2020). *Attachment B: Area of Review and Corrective Action Plan 40 CFR 146.84(b) Clean Energy Systems Mendota*.
- Schlumberger, Attachment C: Testing and Monitoring Plan. (2020). *Attachment C: Testing and Monitoring Plan 40 CFR 146.90 Clean Energy Systems Mendota*.
- Schlumberger, Attachment D: Injection Well Plugging Plan. (2020). *Attachment D: Injection Well Plugging Plan 40 CFR 146.92(B) Clean Energy Systems Mendota*.
- Schlumberger, Attachment E: Post-Injection Site Care and Site Closure Plan. (2020). *Attachment E: Post-Injection Site Care and Site Closure Plan 40 CFR 146.93(A) Clean Energy Systems Mendota*.
- Schlumberger, Attachment F: Emergency and Remedial Response Plan. (2020). *Attachment F: Emergency and Remedial Response Plan 40 CFR 146.94(A) Clean energy Systems Mendota*.
- Schlumberger, Attachment G: Construction Details Clean Energy Systems Mendota. (2020). *Attachment G: Construction Details Clean Energy Systems Mendota*.
- Schlumberger, Attachment H: Financial Assurance Demonstration. (2020). *Attachment H: Financial Assurance Demonstration 40 CFR 146.85 Clean Energy Systems Mendota*.
- Schlumberger, Class VI Permit Application Narrative. (2020). *Class VI Permit Application Narrative 40 CFR 146.82(A) Clean Energy Systems Mendota*.
- SEI. (2019). Seismic Exchange Inc.
- Suchsland, R. J. (1997). *Exploration and Development of the Blewett Trend, Northern San Joaquin Basin, California*. AAPG Pacific Section.

- TGS. (2019). TGS-NOPEC Geophysical Company ASA.
- USGS. (1983). *The Coalinga, California, Earthquake of May 2, 1983*. USGS. Retrieved from <https://pubs.usgs.gov/pp/1487/report.pdf>
- USGS. (2003). In *Petroleum Systems and Geologic Assessment of Oil and Gas in the San Joaquin*.
- USGS. (2005). *National Assessment of Oil and Gas Project - San Joaquin Basin Province (010) Boundary*. (C. R. Team, Producer) Retrieved from <https://catalog.data.gov/dataset/national-assessment-of-oil-and-gas-project-san-joaquin-basin-province-010-boundary>
- USGS. (2019). *Earthquake Hazards Program*. Retrieved from <https://earthquake.usgs.gov/>
- USGS. (2019). *U.S. Quarternary Faults*. Retrieved from USGS Geologic Hazard Science Center: <https://usgs.maps.arcgis.com/apps/webappviewer/index.html?id=5a6038b3a1684561a9b0aadf88412fcf>
- USGS. (2019). *USGS Mineral Resources*. Retrieved from <https://mrdata.usgs.gov/geology/state/state.php?state=CA>
- Vernik, L. a. (1989). Effects of rock elastic and strength properties in estimation of the state of stress at depth. *ISRM International Symposium*.
- Winters, W. W. (1987). Roller bit model with rock ductility and cone offset. *SPE*.
- Yielding. (2002). Shale Gouge Ratio - calibration by geohistory. *Norwegian Petroluem Society Special Publications*, 1-15.
- Yielding, e. a. (1997). Quantitative Fault Seal Prediction. *AAPG*, 897-917.
- Zoback, M. B. (2003). Determination of stress orientation and magnitude in deep wells. *International Journal of Rock Mechanics and Mining Sciences*, 1049-1076.